2019

Implications of Groundwater Plume Transport and Analysis of Karst Aquifer Characteristics in Central Florida

Daljit Sandhu
University of Central Florida, dsandhu@knights.ucf.edu

IMPLICATIONS OF GROUNDWATER PLUME TRANSPORT AND ANALYSIS OF KARST AQUIFER CHARACTERISTICS IN CENTRAL FLORIDA

by

DALJIT SANDHU
B.S. University of Central Florida, 2014
M.S. University of Central Florida, 2016

A dissertation submitted in partial fulfillment of the requirements
for the degree of Doctor of Philosophy
in the Department of Civil, Environmental, and Construction Engineering
in the College of Engineering and Computer Science
at the University of Central Florida
Orlando, Florida

Summer Term
2019

Major Professors: Arvind Singh, Dingbao Wang

ABSTRACT

Groundwater aquifers make up the primary source of drinking water in Florida. It is imperative to protect and maintain water quality to ensure optimal drinking water conditions. Florida is known for being prone to sinkholes due to karst features. One sinkhole event occurred beneath a phosphogypsum stack, and leaked a large amount of radioactive waste in the Floridan aquifer, raising water quality concerns. To study the behavior of contaminant transport, the radioactive waste plume was modeled by coupling hydraulic and chemistry concepts. Adsorption was studied to see if it can serve as a potential remediation solution to the contaminant waste, using available adsorption knowledge and data from previous studies. Results suggest that simulating mineral adsorption helped limit how far the waste stack would travel in the aquifer, however it would still pose risk in water quality, as drinking water wells are situated along the path of the contaminant plume. Implementation of treatment wells and monitoring would ensure drinking water criteria are met.

Acknowledging that the Floridan aquifer contains karst features that consist of limestone fractures and the rock matrix, groundwater flow patterns may be influenced over time. For instance, fractures (or conduits) can conduct larger amounts of groundwater at higher conductivities, which could have implications on groundwater/contaminant transport. To model this process, a karst evolution model utilizing hydraulic and chemistry concepts are applied in a basin in Florida. Results indicate the karst model reproduces head profiles and estimates the age of several conduits. A sensitivity analysis was conducted to investigate how karst evolution is influenced by hydraulic and chemistry parameters. Results show that fracture length has more influence on karst evolution, however other physical parameters show some influence as well.

A karst conduit network was simulated for the Silver Springs springshed, based on obtained potentiometric head data. Implementing information on aquifer chemistry and fracture geometry resulted in a unique realization of a karst network. During this process, flow rates change direction, inducing backflow, which can have implications on groundwater resources. Overall, an improved understanding of karst processes can aid in better characterizing conduit flow patterns and improve water resources management.

ACKNOWLEDGMENTS

I would like to take this opportunity to thank all the people who have helped me complete my graduate studies. I could not have done this without the support of all these people. I would also like to extend my thanks to my advisers, Dr. Arvind Singh, and Dr. Dingbao Wang for presenting me this unique opportunity to take on this research study, and for allowing me to be a part of the Center for Hydroscience Analysis, Modeling and Predictive Simulations (CHAMPS) Lab. I want to thank Dr. Boo Hyun Nam and Dr. Qipeng Zheng for serving on my committee, for helping me in my research and providing helpful feedback and suggestions. I gained a lot of knowledge in my graduate programs. I am also grateful to all the other professors I have taken in the past that helped contribute to my understanding of civil engineering, particularly water resources.

In addition, I would like to thank all members, past and present, of the CHAMPS Lab for being supportive and positive. I have served as an officer for the International Association for Hydro-Environment Engineering and Research (IAHR). Through this experience, I have participated in seminars and led some workshops related to engineering. Also, I have been able to attend various conferences to present my research.

TABLE OF CONTENTS

LIST OF FIGURES ix

LIST OF TABLES xv

CHAPTER 1: INTRODUCTION 1

1.1 Transport of radioactive water into the Floridan aquifer 1

1.2 Modeling karst dissolution and evolution 3

1.3 Karst conduit network simulation 5

1.4 Dissertation structure 7

CHAPTER 2: TRANSPORT OF RADIOACTIVE WATER AND IMPLICATIONS TO DRINKING WATER SUPPLIES 8

2.1 Introduction 8

2.2 Methods 16

2.2.1 Study area description 17

2.2.2 Model description and data collection 18

2.3 Results and Discussion 25

2.3.1 Ferrihydrite cases 26

2.3.2 Carbonate cases 27

2.4 Summary and Conclusions 34

2.5 Acknowledgements 36

CHAPTER 3: INFERRING CONDUIT AGE FROM A KARST CONDUIT EVOLUTION MODEL 37

3.1 Introduction 37

3.2 Methods 39

3.2.1 Model Description: Karst evolution model (K-model) 39

3.2.2 Model Description: One-dimensional groundwater leakage model (L-model) 41

3.2.3 Data and site description 42

3.3 Results and Discussion 48

3.4 Summary and Conclusions 55

3.5 Acknowledgments 56

CHAPTER 4: PARAMETER INFLUENCE ON KARST EVOLUTION 57

4.1 Introduction 57

4.2 Methods 58

4.3 Results and Discussion 61

4.3.1 Examining conduit feedback 61

4.3.2 Sensitivity observations 62

4.4 Conclusion 68

CHAPTER 5: MODELING KARST CONDUIT NETWORKS 70

5.1 Introduction 70

5.2 Data and methods 72

5.3 Results and Discussion 73

5.3.1 Broader impacts 75

5.4 Conclusion 85

CHAPER 6: CONCLUSION 86

6.1 General conclusions 86

6.2 Future research 88

LIST OF REFERENCES 89

LIST OF FIGURES

Figure 1 – List of reported sinkholes up to 2015 (Florida Geological Survey / Florida Department of Environmental Protection). 10

Figure 2 – Location of the sinkhole as depicted by the blue star, and the general direction of groundwater flow shown by the yellow arrow. The area circled in black represent approximate well locations. The dashed area in purple is a conceptual representation of the zone of influence of the plume after 20 years, based on advection, diffusion, and adsorption. The zone of influence would be smaller if any wells in the region are active. (Figure created using ESRI ArcGIS 10.0 software, https://www.esri.com/en-us/arcgis/about-arcgis/overview. World Imagery basemap is included in ArcGIS 10.0 and is attributed to ESRI, DigitalGlobe, GeoEye, Earthstar Geographics, CNES/Airbus DS, USDA, USGS, AEX, Getmapping, Aerogrid, IGN, IGP, swisstopo, and the GIS User Community). 11

Figure 3 – Sample photo by Tampa Bay Times of the sinkhole formation on top of the phosphogypsum stack (O'Donnell, 2016). 12

Figure 4 – Sample aerial view by Tampa Bay Times of the same sinkhole formation shown in Figure 3 (O'Donnell, 2016). 13

Figure 5 – Sensitivity of radionuclide concentration to cell size. The initial concentration used was 2.93 Bq/L. 22

Figure 6 – Sample output graph of radium concentration vs. distance, considering advection and diffusion for a) a time instant and b) the complete simulation time. Cooler colors and warmer colors represent breakthrough curves near the initial and final simulation times,

respectively. The black line shows the radium concentration limit whereas the lower dark red curve shows the plume concentration at the end of the simulation. The constant dark red portion represents background conditions. 29

Figure 7 – Output plots of radium transport with weak surface ferrihydrite at leaks of a) 2.93 Bq/L and b) 3.70 Bq/L. As expected, a longer distance is needed to dilute the concentration of 3.70 Bq/L. In both cases, accounting for adsorption reduces the distance needed for dilution. 30

Figure 8 – Output plots of radium transport with strong surface ferrihydrite for leaks of a) 2.93 Bq/L and b) 3.70 Bq/L. Similar to the previous plot, adsorption (red dots) slightly reduces radium concentrations. 31

Figure 9 – Output plots of radium transport with carbonate using leaks of a) 2.93 Bq/L and b) 3.70 Bq/L. In general, the higher the specific surface area is, the faster (i.e., shorter distance) the dilution of the plume. 32

Figure 10 – Silver Springs discharge and flow rate evolution from karst simulation. a) Streamflow time series at the Silver Springs near Ocala, FL. Note the sudden change in mean due to groundwater pumping (Shoemaker et al., 2004). b) Flow evolution sensitivity using conditions from *Kaufmann* (2009) (in black, referred to as Reference in the legend), and flow evolution curves after modifying a specific parameter (i.e., increasing conduit length, denoted as *L*, by a factor of 1.5; increasing conduit diameter, denoted as *d*, by a factor of 2; and decreasing hydraulic gradient, denoted as *i*, to 60%) while keeping reference conditions constant. As seen, increasing *L*, increasing *d*, and decreasing *i* shift their respective curves from the reference curve to the right, left, and

right, respectively, emphasizing conduit evolution sensitivity. The colored vertical dashed lines indicate where breakthrough occurs for each flow evolution curve, indicating the times where the flow regime changes from laminar to turbulent, due to continuous dissolution. c) Flow evolution for cross-section SS' (Figure 11b) near Silver Springs. The flow rate of the filled-in dot closely matches the average flow rate (22.48 m^3/s) in Figure 10a and would imply a conduit age of ~45 Myrs, assuming an initial fracture size of 1.2 mm. Although Figure 10c shows a similar flow evolution shape, the time scales and discharge magnitudes can vary significantly, due to different initial parameters..... 44

Figure 11 – Study area. a) Springshed boundary for Silver Springs in Ocala, Florida, and its location in relation to Florida, United States shown in the inset. The water-level contour map was generated via kriging based on observation wells. b) Upper confining unit thickness variation across Silver Springs with sample cross-sections shown. c) Karst map indicating where the carbonate rock is at or near the land surface or buried. d) Sample cross-sections from which head profiles were extracted based on previous fracture maps. 45

Figure 12 – Flow evolution verification using inputs from *Kaufmann* (2009) (blue) and *Kaufmann and Braun* (1999) (orange). The black dashed lines indicate where breakthrough occurs for each study, indicating the point where the flow regime becomes turbulent, due to continuous dissolution. 46

Figure 13 – Estimated transmissivity values within the Silver Springs springshed (Kuniansky et al., 2012). 47

Figure 14 – Observed and simulated head profiles. a) Head profiles of the cross-sections in Figure 11b-d. b) Normalized plots of a) with respect to their maximum potentiometric head. The linear black dashed line is plotted for visual curvature comparison purposes. c) Sample plot of various head profiles at different times from the K-model. These plots correspond to cross-section AA' (shown in Figure 11b). As expected, the head profiles change as a function of time, due to the propagating karst dissolution along the conduit. This plot predicts the age of this conduit segment to be 54 Myrs (dashed black curve), when it overlaps the observed profile curve (solid blue curve). 53

Figure 15 – Observed and modeled head profiles based on karst dissolution (K-model) and groundwater leakage (L-model) for cross-sections a) AA', b) BB', c) CC', d) DD', e) EE', and f) FF'. For the most part, as can be seen, the K-model produces a smaller RMSE than the L-model, and in some cases, almost an order of magnitude smaller. These observations suggest the K-model fits the observed head profiles more accurately, which can be seen visually, particularly for cross-sections AA' and DD'. 54

Figure 16 – Flow rate evolution over time for the reference simulation. Note that breakthrough time is 20 kyrs. 60

Figure 17 – Reynold's number as a function of time for the Reference conditions. The flow pattern becomes turbulent at a breakthrough time of 20 kyrs (see Figure 16). 65

Figure 18 – Conduit diameter profile over time using the Reference parameters. The bottom and top plot represent $\Delta t = 0$ and 50.0 kyrs, respectively. Note the bottom plot is straight, indicating a linear, uniform conduit. Subsequent nonlinear plots indicate non-uniform

conduits. The sudden jump in diameter represents breakthrough, which occurs at $\Delta t = 20$ kyrs (see Figure 16). 66

Figure 19 – Breakthrough sensitivity analysis as a function of a) hydraulic gradient, *i*, b) calcium equilibrium concentration, C_{eq}, c) low order kinetic rate, k_0, d) initial conduit radius, e) conduit length, *L*, and f) diffusion coefficient, *D*. A range of initial conduit diameters in a) were also tested along with hydraulic gradient values. 67

Figure 20 – Sample plot of observed potentiometric head within the Silver Springs springshed. 76

Figure 21 – Contour plot of initial potentiometric head seen in Figure 20..... 77

Figure 22 – Surface view of the observed (hence, time = 0) potentiometric head field shown in Figure 20. 78

Figure 23 – Initial conduit network with initial diameter of 0.010 cm for all segments. 79

Figure 24 – Potentiometric head field at the onset of turbulent flow. 80

Figure 25 – Contour plot of potentiometric head at the end of simulation (see Figure 24)..... 81

Figure 26 – Surface view of potentiometric head of the simulated karst network at the onset of turbulent flow. Note the nonlinear behavior of the head surface as a result of non-uniform conduit network. 82

Figure 27 – Diameter thickness of the karst network at the onset of turbulent flow. Based on aquifer conditions, preferential flow paths begin to emerge. Thinner and thicker segments indicate smaller and larger conduits respectively. 83

Figure 28 – Flow rate thickness at the end of simulation. Thinner and thicker segments indicate smaller and larger flow rates respectively. The black color indicates the positive direction

(right and down directions), whereas the red color indicates the negative direction (left and up directions)..... 84

LIST OF TABLES

Table 1 – Chemical reactions simulating surface adsorption, where '≡' denotes a surface. 17

Table 2 – Conditions and solution composition at sinkhole. 23

Table 3 – Solution composition for background conditions (in which maximum values are used), and conditions in close proximity to the flow path. A well density of 1.02 g/cm^3 is used for the model simulations..... 24

Table 4 – List of distances (km) and times (yrs) in which radium concentrations would meet drinking water criteria for all simulations shown. 33

Table 5 – List of hydraulic and chemistry properties used in this study. 48

Table 6 – RMSE values for the K and L models, and the parameters associated with the L-model. Note that the RMSEs for the K-model are on average lower than the RMSEs for the L-model. Associated age obtained from the K-model is also shown for the considered cross-sections..... 55

Table 7 – Summary of values used for analysis. 59

Table 8 – List of power law slopes from Figure 19. 68

CHAPTER 1: INTRODUCTION

1.1 Transport of radioactive water into the Floridan aquifer

Groundwater aquifers are an essential source of drinking water in Florida. It is estimated that about 93% of Florida relied on groundwater for drinking water demands in 1995 (Marella, 1999), and consequently, aquifers should be protected against any source of contamination, such as waste from industrial processes. In Florida, for example, phosphate rock is processed industrially for fertilizer, and its byproducts are discarded as phosphogypsum stockpiles, known as stacks (Rutherford et al., 1994), which are situated across various sites around Florida (Hull and Burnett, 1996; Burnett and Elzerman, 2001). These stacks contain trace amounts of radionuclides, such as radium, from the processing of phosphate rock, which could pose a threat to drinking water quality and water resources should contaminants leak into the Floridan aquifer (Rutherford et al., 1994; Tihansky, 1999). The radium is part of the uranium-238 decay series, and is the major source of radioactivity in phosphogypsum, due to its long half-life (about 1620 years). Radon gas (^{222}Rn), a decay product of ^{226}Ra, is known to cause health problems (Rutherford et al., 1995), highlighting waste management issues regarding gypsum stacks.

In addition, Florida is known for its karst terrain, due to the presence of carbonates and limestones. As a result, Florida is prone to many sinkhole formations, primarily due to dissolution, cover-subsidence, and cover-collapse mechanisms (Tihansky, 1999; Spechler and Kroening, 2007). Percolating water (i.e., rainfall) enters the sediments and makes its way to the carbonates. Given the water is acidic, carbonate dissolution takes place forming voids, cavities and caverns in the carbonate rock, which induces sinkhole formation over time (Sinclair, 1982;

Spechler and Kroening, 2007). A study in Orlando observed that the combination of downward groundwater recharge and the decline of potentiometric head in confined aquifers contributed to more frequent sinkhole formations (Wilson and Beck, 1992). These potentiometric head declines may be attributed to increased human activity, such as groundwater pumping, which eventually induces new sinkholes (Sinclair, 1982; Newton, 1986; Tihansky, 1999; Shoemaker et al., 2004). In some cases, these sinkhole occurrences can lead to the formation of several lakes, which creates additional flow and recharge paths for surficial water, as seen in Florida (Spechler and Kroening, 2007).

Sinkholes can form in many sizes, and are known to cause significant damage to infrastructure, such as buildings, bridges, homes, and roadways, which can lead to financial losses. Financial losses due to sinkholes have been estimated to be about $1.4 billion from 2006 to 2009 in Florida (Floir, 2010). In addition, sinkholes can also have adverse impacts to environmental and water resources (Tihansky, 1999). For instance, a sinkhole forming beneath a gypsum stack would cause the stacks to leak radioactive contamination into the aquifers. It is suggested that sinkhole formations affect 15% of the global land area (Wilson and Beck, 1992). Thus, there is an interest in understanding and characterizing radioactive contaminant behavior in groundwater settings to observe if natural water resources are being harmed. To explore this further, a recent sinkhole formation in Florida was studied.

In 2016, a sinkhole located precisely beneath an acidic phosphogypsum stack formed under central Florida's karst terrain, leaking the waste into the Floridan aquifer, which is mostly confined. This raised immediate concern over water quality in and around surrounding areas. The Floridan aquifer naturally contains small amounts of radioactive materials (Miller and

Sutcliffe, 1985; Szabo et al., 2012), therefore, continuous monitoring and modeling the transport of the contaminated waste is vital to ensure drinking water criteria (i.e., maximum contaminant levels, MCL) are met and to better manage treatment practices. According to the Florida Department of Environmental Protection (FDEP) and the United States Environmental Protection Agency (USEPA), the MCL of radium (including ^{226}Ra and ^{228}Ra) for drinking water is 0.185 Bq/L (5 pCi/L). Recovery wells can be used to pump and discard contaminant waste from aquifers, that way, pre-sinkhole conditions are restored. However, the solution may be expensive (e.g., $6.8 million), and several years may be required to remove aquifer contamination (Fuleihan et al., 1997).

The transport behavior of contaminant plumes, in the absence of karst conduits, can be modeled using geochemical software, based on hydraulic and hydrologic conditions of the site (Sandhu et al., 2018). The chemical process adsorption can then be mimicked as a potential measure to help remediate the radioactive contamination. Previous studies indicate adsorption to be a potential remediation solution to contamination problems (Clifford et al., 1988; Mishra and Tiwary, 1999), and can be simulated by using sorption data of natural minerals (Jambor and Dutrizac, 1998; Jones et al., 2011; Sajih et al., 2014). Here, adsorption is focused more in detail, although other conventional water treatment processes include reverse osmosis, sodium cation exchange, lime soda ash softening, and iron removal (Miller and Sutcliffe, 1985).

1.2 Modeling karst dissolution and evolution

However, recognizing that the Floridan aquifer contains karst features that consist of limestone fractures and the rock matrix, groundwater flow patterns may be influenced over time.

In addition, these flow patterns may change with changing climate and anthropogenic activities (Sandhu et al., 2016; Tahsin et al., 2016; 2018). Due to the high presence of carbonate rock (i.e., karst limestone) in the aquifer, dissolution is propagated continuously. As time progresses, this can lead to the formation and evolution of conduits (Hanna and Rajaram, 1998; Andre and Rajaram, 2005). Fractures (or conduits) can conduct larger amounts of groundwater at higher conductivities, which could have implications on groundwater/contaminant transport, and also seawater intrusion (Xu et al., 2016). Thus, understanding and characterizing karst features are of interest as they comprise about 20% of the Earth's surface (Palmer, 1991; Ford and Williams, 2007; Ronayne, 2013).

Previous studies have applied dissolution chemistry along with hydraulics to simulate karst evolution in groundwater settings, in the form of numerical models (Dreybrodt, 1996; Kaufmann and Braun, 1999; Kaufmann, 2009). The dissolution mechanism implemented in these models were based from prior chemistry experiments, which suggested modeling fast low-order and slow high-order reaction kinetics to accurately represent fracture enlargement (Dreybrodt, 1990; Palmer, 1991).

Furthermore, the head profiles from these conduits can be computed and plotted over time as conduits expand, to see if the head profiles match observed profiles. Interestingly, matching a modeled head profile with an observed head profile would provide information on a conduit's age. In this study, the karst model is applied to the Silver Springs springshed in Ocala, Florida to investigate how conduits emerge from initial fractures. In addition, the head profiles of these conduits will be computed and matched with observed profiles to see if a conduit's age can be inferred.

As karst evolution employs various chemistry and hydraulic parameters, a sensitivity analysis is conducted to study which parameter(s) influences karst evolution the most. Karst features evolve depending on the initial conditions specified in the model. Thus, the evolution of karst features in Florida may vary from karst features elsewhere. Prior studies show karst conduits evolving at different rates based on initial values (see e.g., Dreybrodt, 1996; Kaufmann and Braun, 1999). As conduits enlarge, flow patterns change. In other words, flow is initially laminar, then a conduit enlarges to a point such that flow becomes turbulent. This point is commonly referred to as the breakthrough (Dreybrodt, 1996; Clemens et al., 1996; Dreybrodt and Gabrovsek, 2000; Perne et al., 2014). Essentially, this transition in flow regime is a function of chemistry and hydraulic variables and can dictate how karst evolves in aquifer environments.

1.3 Karst conduit network simulation

Models that simulate karst conduit evolution in one-dimension can be expanded to simulate a collection of conduits representing a karst network in two-dimensional space. To improve the understanding of cave systems, early studies conducted cave explorations to study cave morphology and to collect data (White, 2002; Florea et al., 2003). Over time, comprehensive field studies concluded that cave systems originate from initial fractures and experience limestone rock dissolution from flowing water. In addition, several patterns of cave formations have been observed and categorized (Palmer, 1991). Later, studies focused on defining dissolution rate laws that govern limestone dissolution, which would be later incorporated into models. These kinetic rate laws are based from natural limestone systems (Dreybrodt, 1990; Palmer, 1991).

This knowledge paved the way to models that simulate karst conduit network evolution. Due to the time scales in which karst aquifers evolve (which can range from tens or hundreds of thousands of years) (White, 2002); and given that early, smaller cave systems are difficult to characterize physically, simulating and modeling karst networks received greater interest. Karst conduit network evolution under laminar flow conditions revealed that preferential flow paths emerge along a pre-defined network (Groves and Howard, 1994), which implies that those flow paths are least resistant to flow (Groves and Howard, 1994; Howard and Groves, 1995; Siemers and Dreybrodt, 1998). Depending on aquifer characteristics, karst conduits within a network evolve at different rates, due to the high heterogeneity of karst aquifers (Pardo-Igúzquiza et al., 2012). In the case of turbulent flow, network flow paths become less preferential and more distributed within the network. Over time, this can lead to the development of distinct cave formations. Recent studies attempt to reproduce karst networks based on stochastic methods to improve accuracy (Pardo-Igúzquiza et al., 2012), while other studies suggest that conduit network formation can govern solute transport (Ronayne, 2013). Observing how potentiometric head levels change during conduit network simulation is a key aspect since head changes can influence flow directions (Shoemaker et al., 2008). Changing flow directions can have implications on groundwater resources (Gulley et al., 2011). Thus, exploring the response of hydraulic head with evolving karst conduit networks can improve better water resources management practices.

1.4 Dissertation structure

This dissertation research focuses mainly on two topics. The first topic is to model the extent of contaminant migration and to explore adsorption as a possible remediation solution concerning gypsum waste stacks. Then, to further study the karstic nature of Florida, the next topic is to implement a karst evolution model in a springshed in Florida to study how karst features evolve under surrounding conditions to possibly infer conduit age and to discuss the impacts it would have on physical processes. Finally, a karst conduit network is modeled in central Florida to observe its dynamic nature and discuss some implications based on results. The dissertation is structured as follows: Chapter 2 focuses on the fate and transport of radioactive stack water following a sinkhole formation, Chapter 3 discusses the application of a karst evolution model in a springshed in Florida and focuses on estimating conduit age based on head profiles, Chapter 4 studies the sensitivity of karst evolution as function of several parameters. Chapter 5 explores the simulation of karst conduit networks, and their implications, and Chapter 6 provides conclusions and discusses potential areas for further research.

CHAPTER 2: TRANSPORT OF RADIOACTIVE WATER AND IMPLICATIONS TO DRINKING WATER SUPPLIES

2.1 Introduction

The presence of phosphogypsum stacks can be harmful to natural aquifers, potentially contaminating and degrading groundwater below that may serve as a source of drinking water. The gypsum in phosphogypsum stacks is created as a by-product after phosphorous acid is obtained from natural phosphate rock deposits and processed in industrial facilities, and these stacks contain radionuclide amounts, in the form of radium (Burnett and Elzerman, 2001). Central Florida is home to numerous gypsum stacks and is also prone to sinkholes due to karst geology (Fuleihan et al., 1997; Spechler and Kroening, 2007). In fact, Figure 1 shows the number of reported sinkholes, which mostly occur in west and central Florida. In September 2016, a sinkhole spanning 13.7 m (45 ft) in diameter damaged the liner system at the base of a phosphogypsum stack, causing an opening that allowed an estimated 813,000 cubic meters (215 million gallons) of waste fluids to leak into the Floridan aquifer (location shown in Figure 2), immediately raising concerns over the extent of radionuclide contamination to the area's drinking water supply. A sample photo of the sinkhole formed in the phosphogypsum stack is shown in Figure 3 (O'Donnell, 2016). As can be seen, the gypsum stack water, containing trace amounts of radionuclides leaked into the Floridan aquifer. A direct aerial view of the same sinkhole is shown in Figure 4 (O'Donnell, 2016).

The owner of the phosphate fertilizer facility, Mosaic Company, near the area of Mulberry, Florida, acted promptly to prevent further migration of byproducts from the phosphate rock into the aquifer. The FDEP and the USEPA define the maximum contaminant level of

radium (^{226}Ra and ^{228}Ra) for drinking water as 0.185 Bq/L (5 pCi/L). Naturally occurring amounts of radium in soils may vary by location and terrain configuration. For example, observed radioactive quantities in the nation's aquifers vary from 0.037 to 0.185 Bq/L (1-5 pCi/L) (Szabo et al., 2012). However, it has been observed that water samples from wells in Sarasota County, Florida, contained high levels of radioactivity (as high as 110 pCi/L), in the form of ^{226}Ra (Miller and Sutcliffe, 1985).

In general, gypsum stacks, which include phosphogypsum stacks, are acidic with pH levels varying from 1.5 to 2.0. They also contain high concentrations of fluoride, sulfate, phosphate, and sodium (Fuleihan et al., 1997). Therefore, a sinkhole occurrence beneath a waste stack may cause radionuclides to leak and migrate in the aquifer. It is necessary to monitor and sample total radium contamination in potentially affected aquifers to ensure safe drinking water requirements are met.

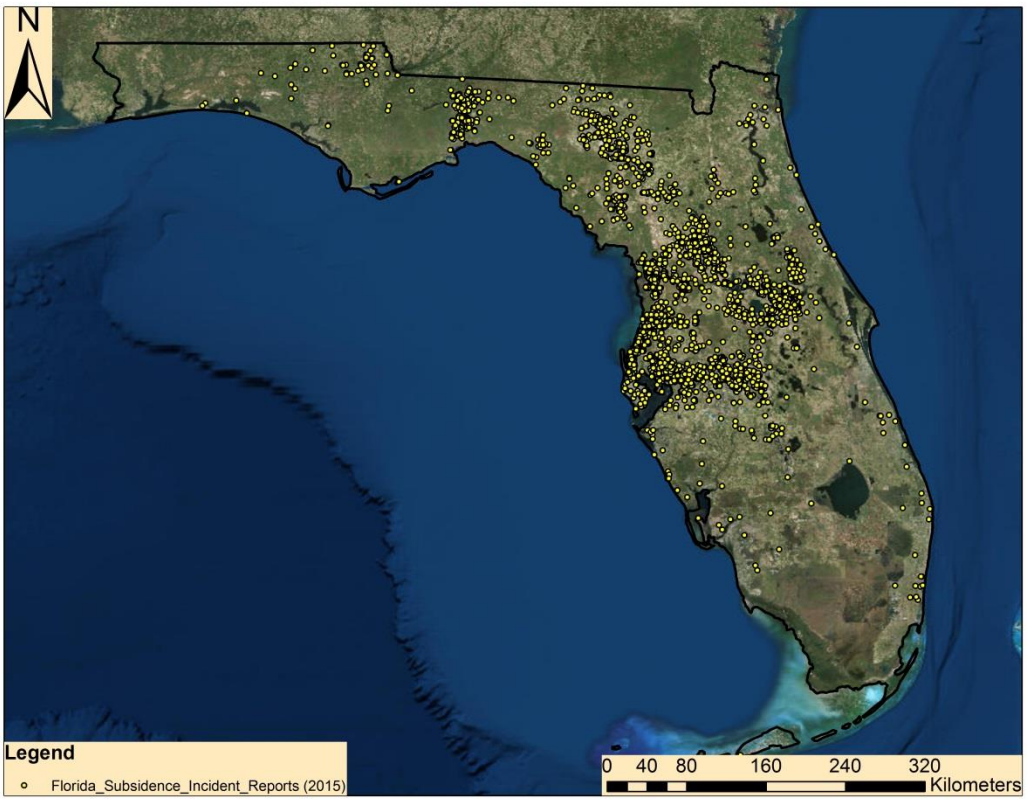

Figure 1 – List of reported sinkholes up to 2015 (Florida Geological Survey / Florida Department of Environmental Protection).

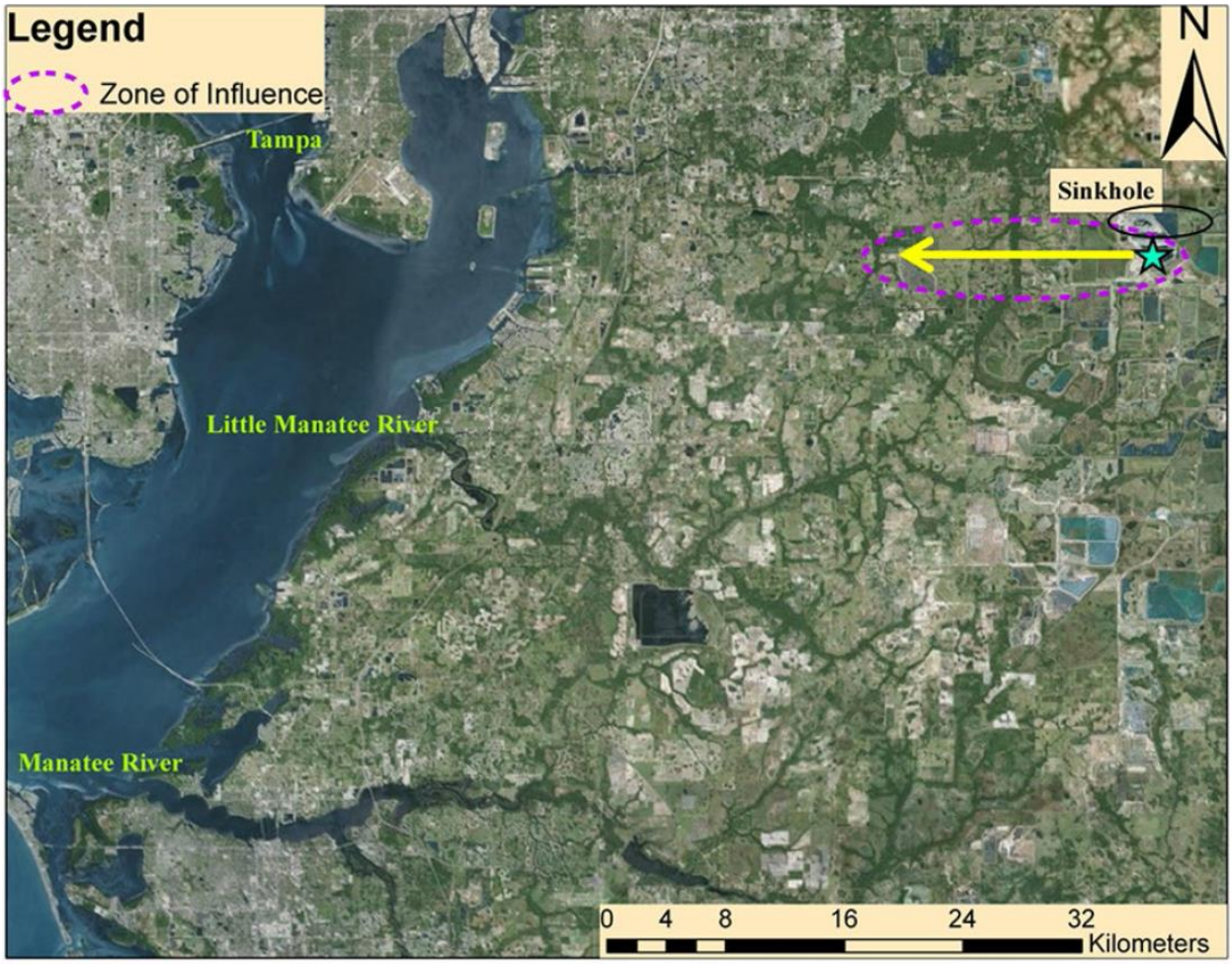

Figure 2 – Location of the sinkhole as depicted by the blue star, and the general direction of groundwater flow shown by the yellow arrow. The area circled in black represent approximate well locations. The dashed area in purple is a conceptual representation of the zone of influence of the plume after 20 years, based on advection, diffusion, and adsorption. The zone of influence would be smaller if any wells in the region are active. (Figure created using ESRI ArcGIS 10.0 software, https://www.esri.com/en-us/arcgis/about-arcgis/overview. World Imagery basemap is included in ArcGIS 10.0 and is attributed to ESRI, DigitalGlobe, GeoEye, Earthstar Geographics, CNES/Airbus DS, USDA, USGS, AEX, Getmapping, Aerogrid, IGN, IGP, swisstopo, and the GIS User Community).

Figure 3 – Sample photo by Tampa Bay Times of the sinkhole formation on top of the phosphogypsum stack (O'Donnell, 2016).

Figure 4 – Sample aerial view by Tampa Bay Times of the same sinkhole formation shown in Figure 3 (O'Donnell, 2016).

A prior incident, also in central Florida, happened in 1994, in which a sinkhole collapse occurred near a phosphogypsum stack. At that time, to ensure the Floridan aquifer was protected from contamination, angle drilling and cement grouting injection at the throat of the sinkhole ahead of the aquifer were conducted. Also, surrounding recovery wells were utilized to extract and discard contaminated water flowing in the aquifer. *Fuleihan et al.* (1997) argued that the contaminated water was contained on site and pre-sinkhole conditions were restored (with an estimated cost of $6.8 million, which translates to $10.5 million in 2018), however they noted the production wells may take additional years to remove the contaminants from the aquifer (Fuleihan et al., 1997). Some other conventional water treatment methods include reverse osmosis, sodium cation exchange, lime soda ash softening, and iron removal (Miller and Sutcliffe, 1985).

It has been suggested that the geology and associated minerals of Florida can enhance the understanding of contaminant behavior in soils (Jones et al., 2011; McCartan et al., 1988). For instance, knowing the distribution of minerals is needed to predict the transport behavior of radionuclides, in particular, radium. Minerals can be characterized by geochemical reactions that explain processes such as adsorption, precipitation, and complexation, which can play a part in their advective and diffusive transport. It has been previously noted that the adsorption process governs radium dissolution at small concentrations (Jones et al., 2011). Adsorption can be simulated by modeling the reactions and transport behaviors of the radionuclides with the minerals. The minerology of southwest central Florida, within the general vicinity of the study area, has been studied. According to X-ray diffractions (XRD) from core samples, the

mineralogy is comprised of mostly calcite and dolomite, with some clay minerals in between (McCartan et al., 1988).

Various models have been developed and used to quantify the geochemistry and transport of elements in groundwater systems. Some examples are WATEQ4F, pH-REdox-EQulibrium (PHREEQC) (from the United States Geological Survey, USGS) (Parkhurst and Appelo, 1999), the Geochemist's Workbench, and Metal Speciation Equilibrium for Surface and Ground Water Model (MINTEQA2) (from USEPA). The PHREEQC model is of interest for this study because of its common use and extensive transport modeling capabilities. Data from *Dzombak and Morel* (1990) is incorporated by PHREEQC to model surface complexation. Their database contains sorption reactions for the mineral hydrous ferric oxide (Dzombak and Morel, 1990; Zhu and Anderson, 2002). The PHREEQC transport module is governed by the one-dimensional advection-diffusion equation (Thyne, 2007; Parkhurst and Appelo, 2013). Previous studies have used the PHREEQC model to study the behavior or radionuclides in coastal Brazil (Almeida, et al., 2004; Lauria et al., 2004), geochemistry in Mexico (Gonneea et al., 2014), and radionuclide transport in Germany (Nitzsche and Merkel, 1999). For example, *Navarro and Carbonell* (2008) investigated aquifer contamination due to waste dumping by using PHREEQC to simulate reactions, speciation, and transport in Spain (Navarro and Carbonell, 2008). PHREEQC was also used to investigate the geochemical factors that led to radium activity levels in excess of the USEPA limit of 0.185 Bq/L in Wisconsin. From that study, it was determined that it was determined that sorption reactions that are assumed to control radium can also control barite (Grundl and Cape, 2006), the precipitation of multicomponent solids can also have an impact on contaminant remediation (Grundl and Cape, 2006), though not studied here. *Zhu et al.* (2001)

constructed a transport model using PHREEQC to study groundwater plume attenuation in a pond. Essentially, PHREEQC has the ability to model water and contaminant transport processes and establish a connection with real world physical hydrogeochemistry (Appelo and Postma, 2005). In some cases, during the drinking water monitoring process, it may be necessary to consider a sinkhole collapse event beneath radioactive gypsum stacks and the resulting transport of radium in the aquifer due to both advection-diffusion and adsorption, since advection-diffusion alone may not always be enough to explain radium concentration dilution. For this study, we use the PHREEQC program to model the transport of radioactive material through the groundwater aquifer system in central Florida.

2.2 Methods

Radium transport is modeled by considering the effects of advection, diffusion, and adsorption using the PHREEQC model. In general, PHREEQC simulates one-dimensional transport of contaminants by accounting for the element concentrations, which can be measured from well samples. In addition, PHREEQC defines surface reactions that can mimic the adsorption effect. In this study, several simulations are considered based on various possible ways adsorption can occur in the Floridan aquifer, and the concentration of radionuclides is monitored near the sinkhole site.

Table 1 lists the chemical reactions used for adsorption simulations. Specifically, the concentration of radium is modeled to determine whether it exceeds the USEPA MCL. This is accomplished by assessing how the radium concentration changes due to the effects of advection, diffusion, and adsorption.

Table 1 – Chemical reactions simulating surface adsorption, where '≡' denotes a surface.

Mineral case	Reaction	Log K
Carbonate	$Ra^{+2} + CO_3^{-2} = RaCO_3$	2.50
Ferrihydrite (weak surfaces)	$\equiv OH + Ra^{+2} = \equiv ORa^{+} + H^{+}$	-5.67
Ferrihydrite (strong surfaces)	$\equiv OH + Ra^{+2} = \equiv OHRa^{+2}$	6.66

2.2.1 Study area description

The sinkhole occurred in Mulberry, Florida, approximately 30 miles outside Tampa. According to Tampa Bay Times (O'Donnell, 2016), it was estimated that the sinkhole was 45 ft (~14 m) wide and 300 ft (~91 m) deep. The sinkhole caused roughly 215 million gallons (900 million L) of gypsum to be dumped into the upper Floridan aquifer, the major source of drinking water for the state.

The Floridan aquifer is mostly confined in central Florida (Miller, 1990), and consists of carbonate karst terrain, which is prone to sinkholes. At roughly 300 ft (~91 m) below ground level, the aquifer is comprised of Suwannee and Ocala limestone (Williams and Kuniansky, 2015). The soil within the property is primarily made up of fine sand and also clay, though to a lesser extent. However, from this soil configuration, the carbonate minerals are relevant for this study. Florida has a fairly flat topography, however as observed from the study site, groundwater tends to flow in the west direction, towards Tampa Bay (see Figure 2).

In the general case for adsorption, the ferrihydrite mineral can serve to adsorb pollutants in natural systems (Jambor and Dutrizac, 1998). In addition to advection and diffusion, this can further help reduce concentrations of radium in aquifers. Furthermore, from previous studies, iron oxyhydroxides are other common adsorbents found in nature due to their high surface areas

and sorption capacities (Jambor and Dutrizac, 1998; Mishra and Tiwary, 1999). However, in the southwest Florida vicinity, carbonate minerals, such as calcite and dolomite, are quite common, and can be seen in the X-ray diffractogram (McCartan et al., 1988). Consequently, reactions of radium with ferrihydrite, using available data, and carbonate were relied on to simulate adsorption in this study.

2.2.2 Model description and data collection

PHREEQC simulates advection and diffusion as follows:

$$\frac{\partial C}{\partial t} = -v\frac{\partial C}{\partial x} + D_L\frac{\partial^2 C}{\partial x^2} - \frac{\partial q}{\partial t} \qquad (2.1)$$

where C is concentration in water, t is time, v is pore water flow velocity, x is the distance, q is the concentration of the solid phase, and D_L refers to the hydrodynamic dispersion coefficient ($D_L = D_e + \alpha_L v$), where D_e is the diffusion coefficient, v is the pore water flow velocity, and α_L is the dispersivity (Parkhurst and Appelo, 1999).

In the PHREEQC model, the contaminant source is modeled as an instantaneous leak into the aquifer through the sinkhole, followed by background groundwater flushing the contaminant plume along the flow path. The exact amount of radionuclide waste that leaked into the aquifer is unknown, but the normal stack condition concentration as reported by Mosaic to the *FDEP* (2017) was 2.93 Bq/L as combined radium. To simulate a worst-case scenario, 3.70 Bq/L of leakage is simulated. These values are used as the input concentrations at the sinkhole. The model structure itself consists of a one-dimensional (1D) grid, discretized into a number of cells. Each cell has a user defined length and time step. Before deciding on an adequate number of

cells, a sensitivity analysis was performed to quantify the effect of different cell sizes on model output, under the same chemical compositions. Figure 5 shows the concentration output from the model as a function of cell size. As can be seen from Figure 5, the output concentration is dependent on cell size when cell size is greater than 75 m, but is not sensitive to cell size when cell size is reduced to 50 m. Therefore, a cell size of 25 m is used in this study. The corresponding time step for a 25 m cell size is 1,644,737 sec, or roughly 19 days. This value is important because should the plume approach the nearest well, the well may need to be shut down. Also, the Little Manatee and Manatee Rivers are positioned in the path of the groundwater flow, therefore it is important to know if and when the contaminant plume would hit the rivers.

Next, the chemical concentrations and properties of well samples were provided as inputs to the model. In addition, existing data of constituents from active wells surrounding the site analyzed by FDEP as well as additional well samples were used in the PHREEQC model. To be consistent across all data, radium concentration (pCi/L) was converted into mg/L. Table 2 shows the solution composition and properties at the sinkhole. As the leak was mostly acidic water, a pH value of 2 was used for the gypsum stack, which was near the value reported by *FDEP* (2017). In addition, the density of the phosphogypsum leak was assumed to be 2.45 g/cm^3, as the waste was heavily concentrated. This value was near the range reported in *SENES* (1987).

Well data for the background and flow path conditions were collected for the transport simulations. The sampled wells are operated by Polk County Utilities and Tampa Bay Water to analyze the water quality post-spill. Data collection was carried out in agreement with *Standard Methods* (2017), Table 3 shows the well data in the vicinity of the sinkhole (Myers, 2016; Baird et al., 2017). The pH, temperature, ^{226}Ra, sulfate, fluoride, barium, calcium, and sodium

descriptions were used as inputs to PHREEQC. In the aquifer, the groundwater density was assumed to be 1.02 g/cm^3, a conservative estimate (Halley and Schmoker, 1983). Upon mixing, the plume density in the aquifer was assumed to be 1.75 g/cm^3. For the simulations, different well data were applied throughout the model. The cell dispersivity was assumed to be 2 m, due to the low hydraulic gradient and based on the data by *Gelhar* (1986), and the diffusion coefficient representative of the study area was assumed to be $9.9 * 10^{-11}$ m^2/s (Yobbi, 1996). Simulations were run with the llnl.dat database, a file that contains specific thermodynamic data (Parkhurst and Appelo, 2013).

Langmuir and Reese (1985) provided thermodynamic properties and reaction parameters of radium, which can be input into the PHREEQC model. In addition, adsorption reactions of radium onto ferrihydrite for both weak and strong binding surfaces along with their equilibrium constants (log K) have been defined, which are used in this study (Sajih et al., 2014). Table 2 summarizes the chemical reactions used for adsorption simulation. The values from *Dzombak and Morel* (1990) and the reactions derived from *Sajih et al.* (2014) were applied to the study area. Here, the specific surface area of hydrous ferric oxide was assumed to be 600 m^2/g (Dzombak and Morel, 1990). The site densities of weak and strong binding sites were assumed to be 0.2 and 0.005 sites per mol Fe, respectively based on the same database (Dzombak and Morel, 1990).

Furthermore, since the study area is mostly calcite, the reaction of radium with carbonate was also considered as this would occur in alkaline aquifers. The reaction and equilibrium constant were based on the work of *Langmuir and Reese* (1985). The approximate specific surface area of carbonate ranges from ~2–22 m^2/g, according to the Rossendorf Expert System

for Surface and Sorption Thermodynamics (RES^3T) database. In general, site density values may range from 1–20 sites/nm^2 (Turner, 1993).

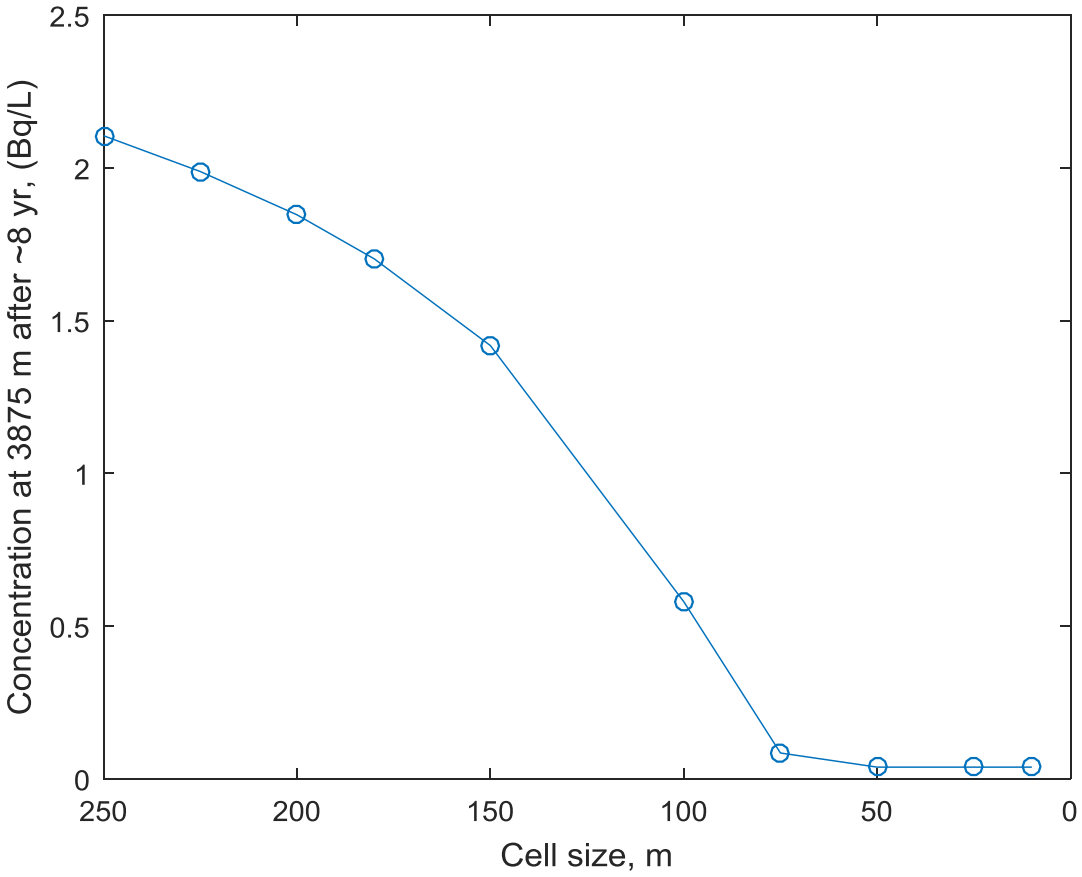

Figure 5 – Sensitivity of radionuclide concentration to cell size. The initial concentration used was 2.93 Bq/L.

Table 2 – Conditions and solution composition at sinkhole.

Constituent	Units	Value
pH		2
Temperature	C	22
Density	g/cm^3	2.45
Aluminum	mg/L	241
Calcium	mg/L	1962
Chloride	mg/L	190
Fluoride	mg/L	13207
Iron	mg/L	233
Magnesium	mg/L	616
Manganese	mg/L	11.1
Ammonia Nitrogen	mg/L	872
Potassium	mg/L	295
Phosphorous	mg/L	9207
Radium	Bq/L	2.93, 3.70
Sodium	mg/L	2109
Sulfate	mg/L	8024

Table 3 – Solution composition for background conditions (in which maximum values are used), and conditions in close proximity to the flow path. A well density of 1.02 g/cm^3 is used for the model simulations.

Sample Description	Unit	Background	Well 16	Well 17	SCHM 5D	SCH17	SCH16
Conductivity	uS					526	411
pH		7.65	7.5	7.56	7.59	7.56	7.59
Temp	C	26.1	24.2	27.3	25.9	27.3	25.9
Turbidity						0.4	0.41
H2S						2.50	2.10
Gross alpha	Bq/L (pCi/L)		0.08 (2.2)	0.21 (5.7)	0.06 (1.6U)	0.10 (2.60)	0.13 (3.60)
Ra-226	Bq/L (pCi/L)	0.02 (0.6)	0.02 (0.5)	0.04 (1)	0.02 (0.6)	0.03 (0.90)	0.03 (0.70)
Ra-228	Bq/L (pCi/L)		0.03 (0.8U)	0.03 (0.8U)	0.03 (0.8U)	0.04 (1.10)	U
Uranium	Bq/L (pCi/L)		0.01 (0.4U)	0.02 (0.6U)	0.02 (0.5U)	U	U
Sulfate	mg/L	58.2	13.6	66.2	70.6	69.5	11.9
Fluoride	mg/L	0.29	0.14	0.18	0.24	0.38	0.33
TDS	mg/L		181	260	259	254	174
Barium	mg/L	0.01	0.017	0.023	0.012	0.025	0.022
Calcium	mg/L	54.1	39.3	54.5	54.5	53.7	40.3
Sodium	mg/L	7.01	7.4	7.71	6.88	9.07	8.67

2.3 Results and Discussion

PHREEQC was used to model one-dimensional radium transport across a range of distances and conditions. PHREEQC internally computes the velocity of a plume as the cell length divided by the time step. This velocity (1.31 m/day) for 1 unit hydraulic gradient is estimated based on the reported hydraulic conductivity (~392 m/day) and porosity (0.20) (Ardaman and Associates, Inc, 2017). This is utilized to mimic the contaminant plume being transported along the hydraulic gradient. A well for limited public use is situated at just over 4 km west from the sinkhole, according to the FDEP. Thus, 4 km was chosen as the length of the cell domain as an initial conservative, worst-case scenario to determine whether the radioactive plume will hit the nearest active well. If concentration levels are too high, the model would be extended to see at what distances the concentrations will be adequately reduced. This distance is referred to as the "safe distance." Plotting results in Bq/L allows one to compare the radium transport concentration with the USEPA drinking water limit of 0.185 Bq/L ($\approx 5 * 10^{-9}$ mg/L) and then assess whether the radium is below this threshold. A sample output plot of radium transport vs. distance with the breakthrough curves is shown in Figure 6. The inset in Figure 6 shows a sample plot of a breakthrough curve at an instant in the simulation. For each scenario, the maximum value of the modeled breakthrough curves at each cell is plotted separately as an upper envelope. Figure 6 presents a case for advection and diffusion at distances less than ~5.2 km, hence the content is above the threshold concentration (Figure 6). Distances greater than ~5.2 km indicate that the quantities are below the threshold concentration.

According to the FDEP, the radium activity at the gypsum stack under normal condition is 79 pCi/L (2.93 Bq/L) (FDEP, 2017); thus, the radioactive transport of radium was modeled

using this value with and without adsorption. Then, as a severe case, in an attempt to represent the sinkhole collapse, a value of 100 pCi/L (3.70 Bq/L) of radium was simulated with and without adsorption to study the differences in the plume transport.

2.3.1 Ferrihydrite cases

In this section, we explore the radium transport with ferrihydrite. Ferrihydrite can be represented as a weak or a strong binding surface type. For this case, adsorption is simulated using ferrihydrite only, and is modeled with the well data. The simulation with 0 mol sites represents advection and diffusion only. Using a value greater than 0 mol sites will enable the adsorption effect. Here, a value of 0.2 mol sites was used for weak ferrihydrite, based on the data from *Dzombak and Morel* (1990). Figure 7 shows the behavior of radium transport reacting with weak surface binding ferrihydrite using leaks of 2.93 Bq/L and 3.70 Bq/L. In this case, the ferrihydrite reacting without adsorption requires a longer distance to reduce radium concentrations for both the 2.93 and 3.70 Bq/L scenarios; whereas with adsorption, these distances are reduced. For example from Figure 7a it can be observed that the safe distances after a 2.93 Bq/L leak are 5.24 km and 5.06 km without and with adsorption, respectively. The contaminant plume would reach those distances at times of 11 and 10.6 years, respectively. For the case of 3.70 Bq/L, the safe distances without and with adsorption are 8.35 km and 7.79 km, respectively (Figure 7b). The associated times for the plume to reach those distances are 17.4 and 16.3 years (see Table 4). Figure 8 shows the radium behavior with strong surface binding ferrihydrite, again for leaks of 2.93 Bq/L and 3.70 Bq/L. To simulate adsorption for the strong surface ferrihydrite, 0.005 mol sites are used for the surface, again based on data from *Dzombak and Morel* (1990). Although not easily seen, the strong binding ferrihydrite performed slightly

better in terms of reducing concentrations. However, the influence of ferrihydrite on contaminant binding is minor. Figure 8a indicates safe distances without and with adsorption of 5.24 km and 5.01 km, after just 11 and 10.5 yrs, respectively, for the case of 2.93 Bq/L, whereas for 3.70 Bq/L (Figure 8b) the safe distances without and with adsorption are 8.35 km and 7.74 km, after 17.4 and 16.2 yrs, respectively. These results suggest that the strong surface binding ferrihydrite is capable of greater adsorption. Previous studies also suggest that other constituents in the solution may compete with each other to bond with the mineral, which could minimize its impact (Almeida et al., 2004; Sajih et al., 2014). From other studies, a low pH in the solution may hinder adsorption capacity (Almeida et al., 2004). A summary of these values is listed in Table 4.

2.3.2 Carbonate cases

Figure 9 shows the radium transport with carbonate for the case of 2.93 Bq/L and 3.70 Bq/L as a function of distance. For these scenarios, a site density of 5 sites/nm^2 was used, which has been used previously according to the RES^{3}T database. Two scenarios of specific surface area of calcite are used, i.e., 10 m^2/g and 22 m^2/g, also obtained from the RES^{3}T database. This range of known surface areas from the RES^{3}T database was assumed to apply to the study area due to the presence of carbonate rock in Florida. As can be seen from Figure 9a, the safe distance without considering adsorption is about 5.24 km, which corresponds to about 11 yrs. Adsorption with a specific surface area of 10 m^2/g reduced the safe distance to 4.96 km, which would take the plume about 10.3 yrs to reach. As expected, the higher the specific surface area, the higher the adsorption, which would imply that larger carbonate minerals (i.e., specific surface area) would have the potential to reduce the contaminant plume in the central Florida area via adsorption. Increasing the surface area to 22 m^2/g further reduced the safe distance to 4.36 km,

after 9.1 yrs. Similarly, this effect can be seen for the 3.70 Bq/L scenario, in Figure 9b. Without adsorption, the safe distance would be 8.35 km, or 17.4 yrs. At 10 m^2/g surface area, the safe distance is reduced to 7.79 km, 16.3 yrs, and at 22 m^2/g, the safe distance is further reduced to 6.51 km, or 13.6 yrs. These values are also listed in Table 4. Due to the frequent presence of calcite (i.e. limestone) in the Floridan aquifer, it appears that the calcite would be capable of resisting the flow of contamination, but the time scale is too large to observe this. If there was an abundant mass amount of mineral, perhaps that would further reduce concentration levels, but that would not significantly reduce the risk associated with this event, regardless of how much radium leaked into the aquifer.

Overall, for the observed cases, the results suggest that there is a risk of drinking water contamination due to radionuclide transport. Although both the weak and strong binding ferrihydrite mineral performed similarly, the result can change depending on the competitive nature of the constituents in the soil, which can be seen in past analyses (Chen and Kocar, 2018). A previous study showed that radium levels in Tampa Bay are low. Our analysis would appear to follow the same trend (Swarzenski, et al., 2007). The carbonate performed better than the ferrihydrite minerals, but since the time scale is long, i.e. on the order of tens of years, and due to drinking water processing regulations, additional external resources should be leveraged to safely contain the contaminated waste. This further reinforces the importance of safely containing phosphogypsum stack wastes that may threaten natural resources, such as drinking water.

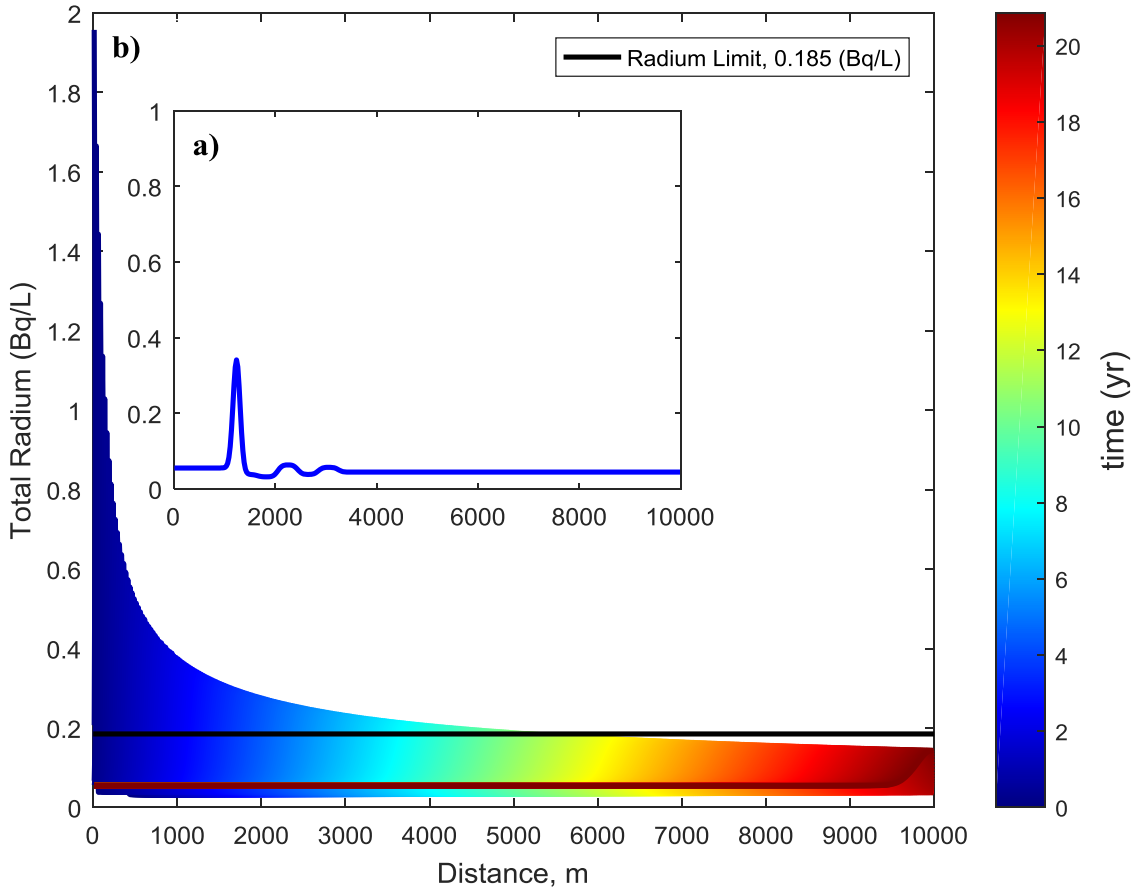

Figure 6 – Sample output graph of radium concentration vs. distance, considering advection and diffusion for a) a time instant and b) the complete simulation time. Cooler colors and warmer colors represent breakthrough curves near the initial and final simulation times, respectively. The black line shows the radium concentration limit whereas the lower dark red curve shows the plume concentration at the end of the simulation. The constant dark red portion represents background conditions.

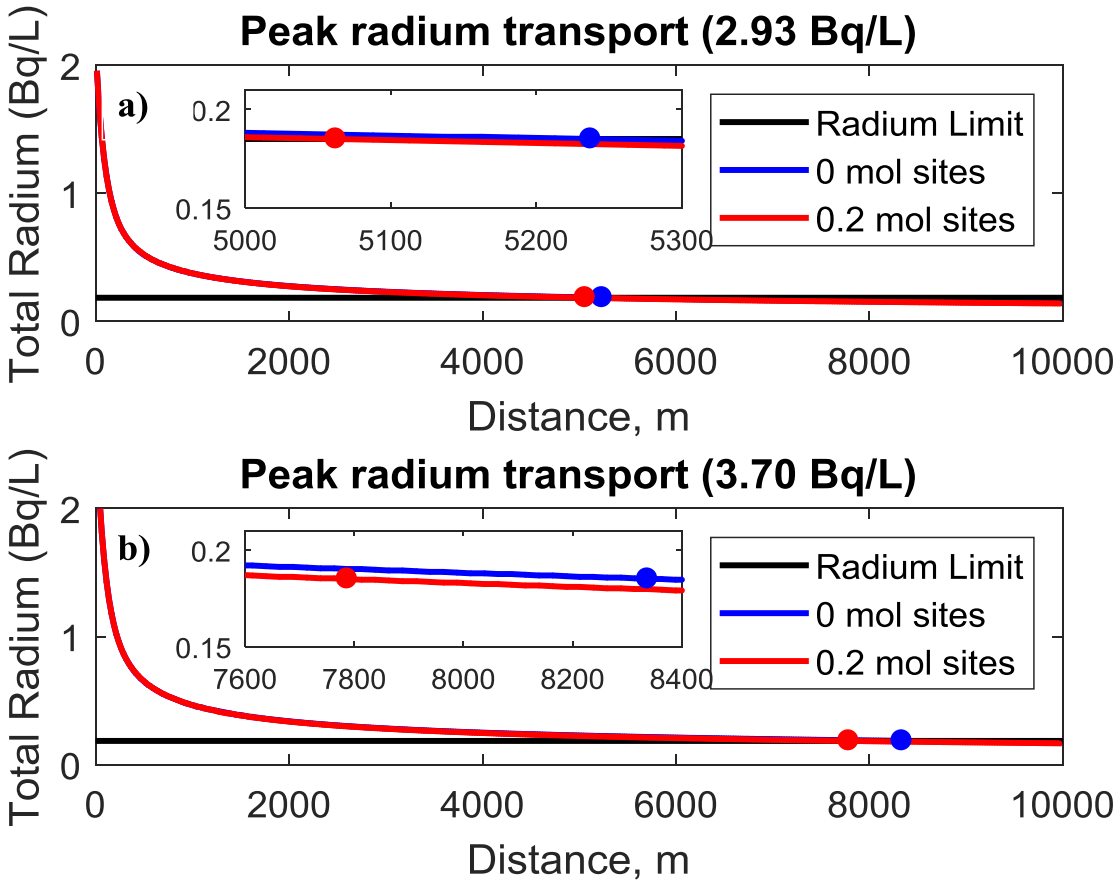

Figure 7 – Output plots of radium transport with weak surface ferrihydrite at leaks of a) 2.93 Bq/L and b) 3.70 Bq/L. As expected, a longer distance is needed to dilute the concentration of 3.70 Bq/L. In both cases, accounting for adsorption reduces the distance needed for dilution.

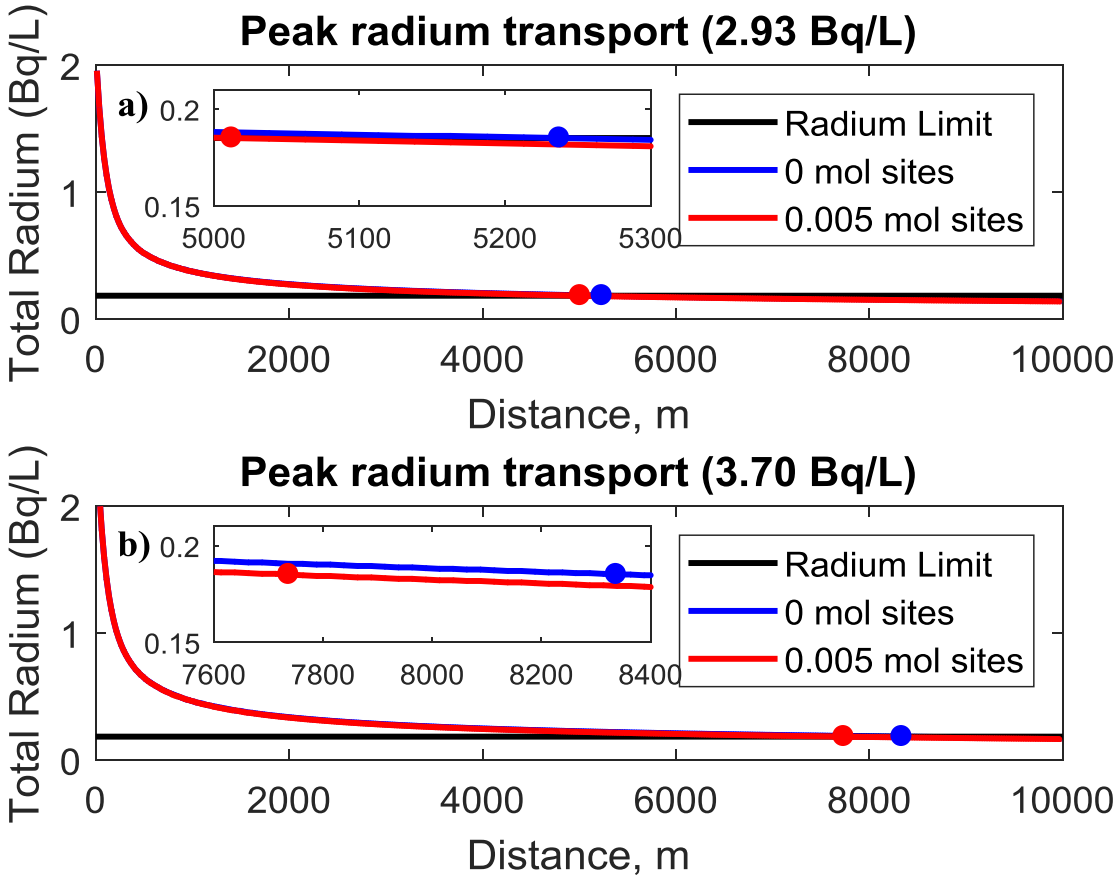

Figure 8 – Output plots of radium transport with strong surface ferrihydrite for leaks of a) 2.93 Bq/L and b) 3.70 Bq/L. Similar to the previous plot, adsorption (red dots) slightly reduces radium concentrations.

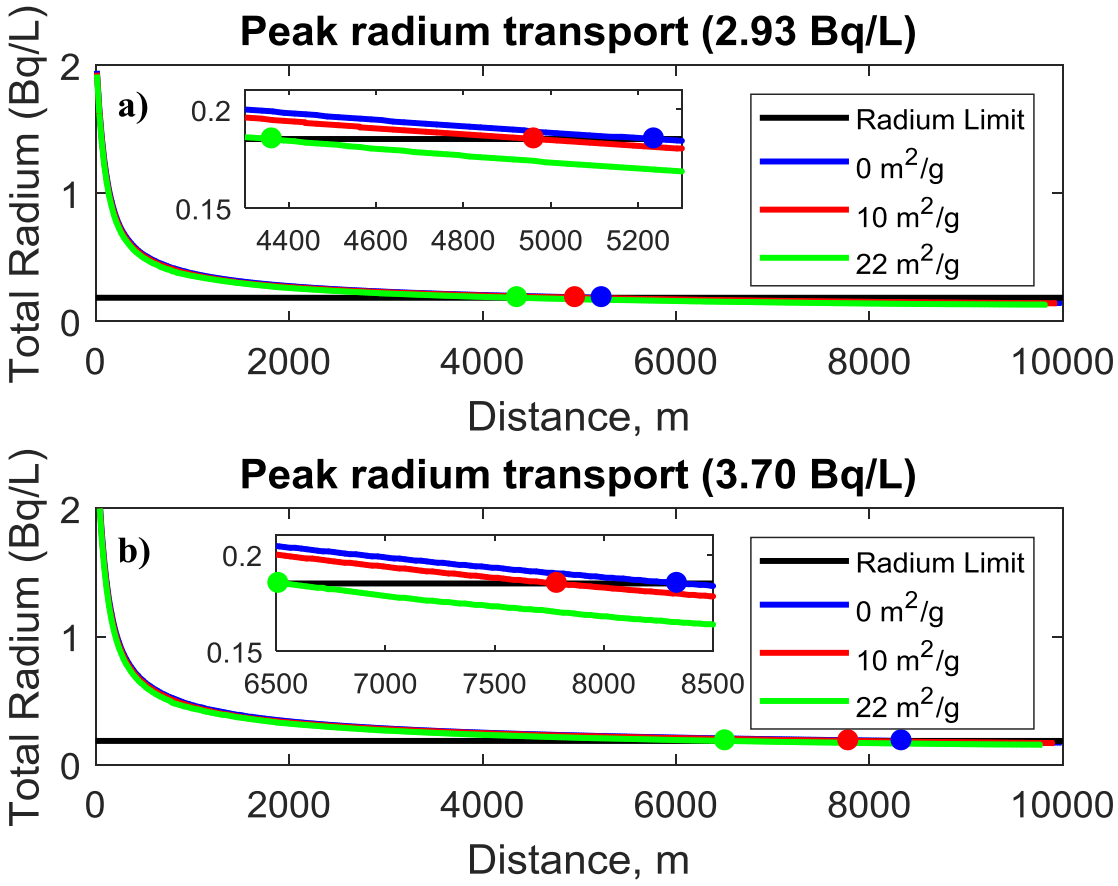

Figure 9 – Output plots of radium transport with carbonate using leaks of a) 2.93 Bq/L and b) 3.70 Bq/L. In general, the higher the specific surface area is, the faster (i.e., shorter distance) the dilution of the plume.

Table 4 – List of distances (km) and times (yrs) in which radium concentrations would meet drinking water criteria for all simulations shown.

Weak Ferrihydrite			
Bq/L	mol sites	Distance, km	Time, yrs
2.93	0	5.24	11
	0.2	5.06	10.6
3.70	0	8.34	17.4
	0.2	7.79	16.3
Strong Ferrihydrite			
Bq/L	mol sites	Distance, km	Time, yrs
2.93	0	5.24	11
	0.005	5.01	10.5
3.70	0	8.34	17.4
	0.005	7.74	16.2
Carbonate (5 sites/nm^2)			
Bq/L	Specific Surface Area (m^2/g)	Distance, km	Time, yrs
2.93	0	5.24	11
	10	4.96	10.3
	22	4.36	9.1
3.70	0	8.34	17.4
	10	7.79	16.3
	22	6.51	13.6

2.4 Summary and Conclusions

In this study we simulated the transport of radioactive contaminant waste in the Floridan aquifer. To model the reduction of the concentration of radium, advection, diffusion, and adsorption were simulated using the PHREEQC transport model. Based on the hydrogeological nature of Florida, our results suggest that it would take between 11-17 years and about 5.2 km to 8.4 km from the sinkhole leak to naturally reduce concentrations at or below the drinking water threshold of 0.185 Bq/L. Including the adsorption effect using entities like ferrihydrite (with either weak or strong binding surfaces) and carbonate may help to moderately reduce the time needed to lower concentrations, i.e. to 9-16 years. The safe distances associated with these times range from 4.4 km to 7.8 km.

Although ferrihydrite is commonly occurring in nature, it is likely not as frequent as calcite in central Florida. Despite that, ferrihydrite was simulated based on the available data by *Dzombak and Morel* (1990) and *Sajih et al.* (2014). Based on the simulations, ferrihydrite can treat the contaminant waste, however a long time period is needed to ensure that radium concentrations reach levels below the threshold determined by the USEPA. For weak ferrihydrite minerals and a 2.93 Bq/L leak, it would take a distance of more than 5 km and about 10-11 years for the concentration to be attenuated. A leak of 3.70 Bq/L would require distances from 7.8 to 8.4 km and 16-17 years for remediation. For strong ferrihydrite minerals, results were slightly different. For a 2.93 Bq/L leak, it would take over 5 km and under 11 years to remediate the plume. For the 3.70 Bq/L case, 7.4 to 8.4 km and 16-17 years would be necessary to attenuate the waste. For the carbonate case, distances from 4.4 to 5.2 km and 9-11 years are sufficient for a 2.93 Bq/L scenario, and distances from 6.5 to 8.4 km and 13-17 years would be sufficient for a

3.70 Bq/L leak. From the observations, it appears that calcite may be the best mineral to counteract the radioactive plume. Although calcite may be commonly occurring in the study area, additional efforts (i.e., barriers or cement injection) may be needed to contain and treat the contaminant waste to meet the drinking water criterion (0.185 Bq/L) before potentially hitting a pumping well. The amount of abundant minerals in the aquifer can affect the overall remediation process; however it is complex to quantify the amount of potential adsorbents in the soil. From previous studies, a low pH and the presence of other elements and compounds in the solution may induce competition among them, which may then in turn affect the potential of adsorption occurring in the soils (Sajih et al., 2014; Chen and Kocar, 2018).

Based on the cases presented, there is uncertainty in the fate of the contaminant waste after the sinkhole collapse. Several factors, hydrological and chemical, play roles on influencing how radionuclides are transported. The large-scale nature of this event alone poses considerable risk. Perhaps if the sinkhole event was small-scale, the outlook may have been favorable. Due to difficulties and complexities in knowing the exact conditions in the aquifer, a range of possibilities must be analyzed to aid in developing potential solutions. This stresses the importance of safely containing contaminant waste before natural resources, such as drinking water, are harmed. It is probable that carbonate, calcite, and ferrihydrite are present and significant to adsorption processes; several of these processes are simulated to increase the likelihood that the actual behavior of the plume transport falls within the cases.

While characterizing aquifer and chemical conditions may be complex, it is essential to providing a basic understanding of contaminant transport following natural hazardous events

through observation and simulation. Thus, this is a necessary step in identifying potential threats imposed on surrounding systems, and ultimately improving best management practices.

2.5 Acknowledgements

This research was funded in part under award CBET-1665343 from the National Science Foundation. The authors would like to acknowledge Jason Hopp from Polk County Utilities, Chris Owen, Philip Matthews from Tampa Bay Water, the Florida Department of Environmental Protection, and University of Central Florida (UCF) graduate student Ms. Maria Arenas for providing water quality data.

CHAPTER 3: INFERRING CONDUIT AGE FROM A KARST CONDUIT EVOLUTION MODEL

3.1 Introduction

Karst aquifers are distinct groundwater systems in nature where physical processes behave differently as compared to non-karstic systems. In the Floridan aquifer system, there is a high presence of carbonate rock (i.e., karst limestone), which is subjected to dissolution continuously. Over time, this can lead to the formation and evolution of conduits (Hanna and Rajaram, 1998; Andre and Rajaram, 2005). This dynamic shaping of the Floridan aquifer system can have implications on certain processes, such as groundwater flow, contaminant transport, and even seawater intrusion (Xu et al., 2016). It is documented that karst landscapes are present in about 20% of Earth's surface (Palmer, 1991; Ford and Williams, 2007; Ronayne, 2013); therefore, there is an interest in characterizing karst features, as karsts themselves may vary depending on geographic locations (Florea and Vacher, 2006b).

For modeling karst system processes and dynamics, one has to consider dynamic karst conduits coupled with the rock matrix. Several models, especially numerical models, have been used to simulate the evolution of conduits in karst aquifers (Clemens et al., 1996; Dreybrodt, 1996; Kaufmann and Braun, 1999; Kaufmann, 2009). These karst evolution models employ dissolution chemistry along a fracture to simulate conduit enlargement, followed by hydraulics to model flow patterns. Early studies advocated the use of dissolution mechanisms in karst initiation and evolution to understand how fast low-order and slow high-order kinetics are necessary to model the initial karst evolution (Dreybrodt, 1990; Palmer, 1991).

The Floridan aquifer system consists of the soil and rock matrix and evolving karst fractures (fractures are commonly referred to as conduits once they reach a diameter of 1 cm, (White, 2002)), which can differ considerably in terms of hydraulic conductivities. Slug tests for the Upper Floridan Aquifer (UFA) in the north-central Florida area revealed matrix hydraulic conductivity values between 1.74×10^{-5} m/s and 2.20×10^{-4} m/s (Langston et al., 2012); whereas, core samples have indicated an average matrix conductivity of 10^{-6} m/s (Florea and Vacher, 2007). Hydraulic conductivities in fractures (or conduits) are in general several orders of magnitude greater than matrix conductivities. For example, a conduit diameter of 1 cm can correspond to a conductivity of about 10 m/s (Kaufmann, 2016).

The UFA aquifer is mostly confined in southern areas, yet slowly becomes thinly confined and unconfined towards the northwest direction, indicating a certain degree of heterogeneity (Williams and Kuniansky, 2015). According to the survey data on the hydraulic nature of the UFA, the karst conduits are spaced out and disconnected from one another with segments of varying lengths, particularly near the Ocala area in Florida, and are mostly oriented in the northeast-southwest and northwest-southeast directions (Vernon, 1951; Phelps, 1994; Florea and Vacher, 2006a).

One conduit property that can be difficult to quantify is the diameter, especially throughout the conduit's length. Cave exploration is one method that has been used to characterize conduit size (Florea and Vacher, 2006a). In the UFA in north Florida, the average conduit dimensions (i.e., width and height) range from 12 m to 24 m (Moore et al., 2010). For Silver Springs, the spring vent diameter was measured as 11 m (Sepúlveda, 2009), whereas in the

Santa Fe River, the average conduit diameters calculated ranged in between 22 m and 25 m (Langston et al., 2012).

In recent decades, the Silver Springs discharge has been on a decline (see Figure 10a) due to increased groundwater pumping for growing population demands (Shoemaker et al., 2004), and only recently there has been an effort to restore discharge levels back to natural conditions. Given the area's susceptibility to sinkholes and the increase of human activities (e.g., groundwater pumping) in recent years, there is an interest in understanding and characterizing the complex karst features in the UFA (see e.g., Figure 10). To gain such an understanding, this study aims to model karst conduit evolution in the Silver Springs area (Figure 11) to describe the head profiles and quantify conduit properties that would improve understanding of karst conduit flow and complex karst geology. In addition, conduit age can be predicted by simulating conduit evolution and resulting head profiles over time based on conduit properties.

3.2 Methods

3.2.1 Model Description: Karst evolution model (K-model)

A circular conduit is discretized into logarithmically equal increments to compute dissolution rates and calcium concentration along the conduit. The calcium dissolution process is modeled as (Dreybrodt, 1996; Kaufmann, Braun, 1999; Siemers and Dreybrodt, 1998):

$$F = k_i \left(1 - \frac{C(x,t)}{C_{eq}}\right)^{n_i}; i = 1, 2 \qquad (3.1)$$

where F is the dissolution rate, i refers to the kinetic behavior of the dissolution process (i.e., 1 for low-order kinetics and 2 for high-order kinetics), k is the kinetic rate, C is the calcium

concentration, C_{eq} is the calcium equilibrium concentration, and n is the kinetic exponent ($n_1 = 1$ and $n_2 = 4$). The kinetic rate, k, for low-order conditions is computed as:

$$k_1 = k_0\left(1 + \frac{k_0 d(x,t)}{6DC_{eq}}\right)^{-1} \quad (3.2)$$

where k_0 is the kinetic rate constant, d is the conduit diameter, and D is the diffusion coefficient. For high-order conditions, the kinetic rate is obtained from:

$$k_2 = k_1\left(1 - \frac{C_T}{C_{eq}}\right)^{n_1 - n_2}. \quad (3.3)$$

Here C_T is the threshold concentration where low-order kinetics transitions to high-order kinetics. As the dissolution chemistry is being simulated inside the conduit, the increase in calcium concentration in the water as it flows through the conduit can be determined. Afterwards, the growth rate of the conduit and the increase in conduit diameter can be computed by defining time steps and number of iterations (Dreybrodt, 1996; Kaufmann and Braun, 1999; Kaufmann, 2009). Using the Darcy-Weisbach equation, the head loss can be modeled as:

$$\Delta h = \frac{fLV^2}{2gd} \quad (3.4)$$

where Δh is the head loss, f is the friction factor, L is the conduit length, V is the average flow velocity, and g is the acceleration due to gravity. The Reynold's number ($Re = \frac{Vd}{\upsilon}$, where υ is kinematic viscosity) characterizes laminar and turbulent flow. Flow is laminar and turbulent for Reynold's numbers less than and greater than a critical threshold, respectively. In this study, a critical threshold of 2200 is used. For both laminar and turbulent flows, the friction factor is modeled using the following equation (Swamee and Swamee, 2007):

$$f = \left\{\left(\frac{64}{Re}\right)^8 + 9.5\left[\ln\left(\frac{\epsilon}{3.7d} + \frac{5.74}{Re^{0.9}}\right) - \left(\frac{2500}{Re}\right)^6\right]^{-16}\right\}^{0.125} \quad (3.5)$$

where ϵ is the wall roughness coefficient.

The K-model was tested using the initial conditions obtained from past studies for verification (Figure 12). Figure 10b shows flow evolution and breakthrough times in an evolving karst conduit using initial and boundary conditions assumed in *Kaufmann* (2009). As can be seen, the breakthrough is sensitive to changes in initial fracture geometry and hydraulic conditions. While holding reference conditions constant, increasing conduit length, increasing conduit diameter, and decreasing hydraulic gradient cause the respective flow evolution curves to shift to the right, left, and right, respectively, highlighting the sensitivity of karst evolution. As a result, simulated head profiles for different conditions may vary as well. Following the verification phase, the model was applied to the Florida karst system.

Figure 10c shows the modeled flow rate evolution based on initial fracture geometry and hydraulic conditions from cross-section SS' (see Figure 11b) near Silver Springs. The flow rate in the filled-in dot closely matches the average flow rate in Figure 10a. Although Figure 10b and Figure 10c show similar flow evolution shapes, due to different initial parameters, the time scales and discharge magnitudes can vary significantly.

3.2.2 Model Description: One-dimensional groundwater leakage model (L-model)

The head h at a location x for one-dimensional confined aquifer with leakage at steady state can be expressed as:

$$h(x) = h_0 - C_1 \exp\left(\frac{x}{B}\right) - C_2 \exp\left(-\frac{x}{B}\right), \qquad (3.6)$$

where h_0 is the initial head, $B = \sqrt{\frac{Tb'}{K'}}$ is the leakage factor, T is transmissivity, b' and K' are the confining layer thickness and conductivity, respectively, and C_1 and C_2 are constants.

3.2.3 Data and site description

Data on the potentiometric levels from twenty-two (22) observation wells within the springshed of Silver Springs were obtained from the St. Johns River Water Management District (SJRWMD). The springshed boundary is shown in Figure 11a. Water-levels only for the UFA, where karst features are present, are considered. For unconfined areas, the well depths range from 12 to 37 m, whereas the depths in confined areas range from 37 to 73 m. The thickness of the UFA is roughly 200 m near the Ocala area, with the top of the UFA being a few meters below ground surface (Williams and Kuniansky, 2015). The mean value of water elevation for each well was computed, from which a potentiometric surface was generated via kriging (Figure 11a) (Kitadinis, 1997).

The estimated transmissivity values for Silver Springs ranged from 4000 – 52,000 m^2/day (Figure 13); the vast range in magnitude of transmissivity values is due to the high presence of carbonate rock in the aquifer (Kuniansky et al., 2012). The upper confining thickness ranges from about 0 – 56 m (Williams and Kuniansky, 2015). These values can serve as a reference for modeling groundwater flow under confined conditions and are shown in Figure 11b. Karst maps, obtained from the United States Geological Survey (USGS) show that within the study area, carbonate rocks are present at or near the surface, as well as buried <90 m beneath sediments, which can be seen in Figure 11c. Therefore, the profiles of potentiometric levels can be

examined further to investigate whether and to what degree they follow the previously observed nonlinear relationship (concave down) seen in karst simulations (Dreybrodt and Gabrovsek, 2003; Romanov et al., 2004; Perne et al., 2014; de Rooij and Graham, 2017).

The following hydraulic and chemistry parameters were used in this study, based on *Kaufmann* (2009), ϵ = 0.002 cm, υ = 0.012 cm^2/s, and $C_T = 0.9(C_{eq})$. In addition, $k_0 = 1 \times 10^{-11}$ mol/cm^2-s, and a C_{eq} value of 3×10^{-6} mol/cm^3 was assumed, although values may range from 5×10^{-7} to 3×10^{-6} mol/cm^3 (Gabrovsek, 2007). A *D* value of 10^{-6} cm^2/s is assumed as noted in *Yobbi* (1996). These values are summarized in Table 5.

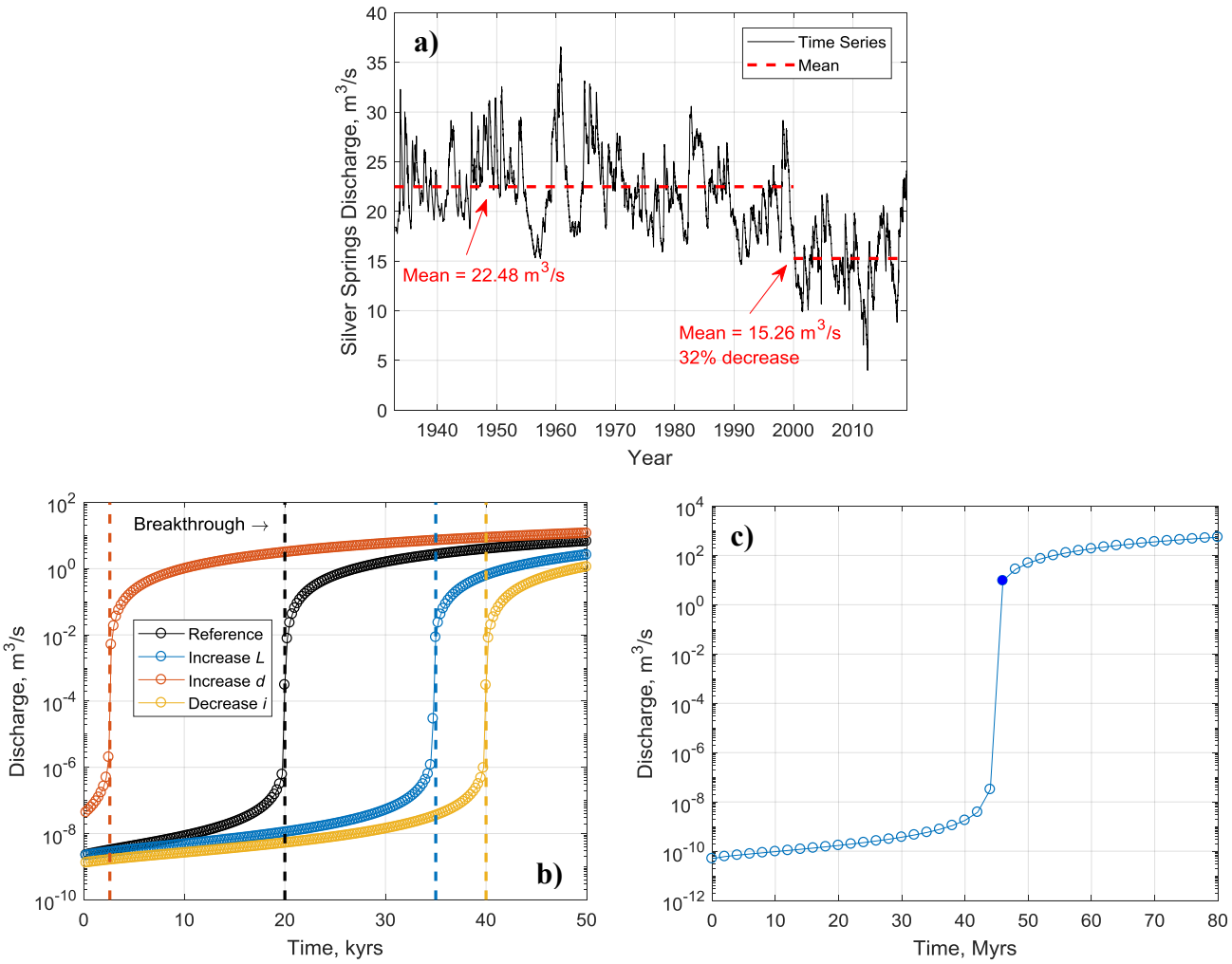

Figure 10 – Silver Springs discharge and flow rate evolution from karst simulation. a) Streamflow time series at the Silver Springs near Ocala, FL. Note the sudden change in mean due to groundwater pumping (Shoemaker et al., 2004). b) Flow evolution sensitivity using conditions from *Kaufmann* (2009) (in black, referred to as Reference in the legend), and flow evolution curves after modifying a specific parameter (i.e., increasing conduit length, denoted as *L*, by a factor of 1.5; increasing conduit diameter, denoted as *d*, by a factor of 2; and decreasing hydraulic gradient, denoted as *i*, to 60%) while keeping reference conditions constant. As seen, increasing *L*, increasing *d*, and decreasing *i* shift their respective curves from the reference curve to the right, left, and right, respectively, emphasizing conduit evolution sensitivity. The colored vertical dashed lines indicate where breakthrough occurs for each flow evolution curve, indicating the times where the flow regime changes from laminar to turbulent, due to continuous dissolution. c) Flow evolution for cross-section SS' (Figure 11b) near Silver Springs. The flow rate of the filled-in dot closely matches the average flow rate (22.48 m^3/s) in Figure 10a and would imply a conduit age of ~45 Myrs, assuming an initial fracture size of 1.2 mm. Although Figure 10c shows a similar flow evolution shape, the time scales and discharge magnitudes can vary significantly, due to different initial parameters.

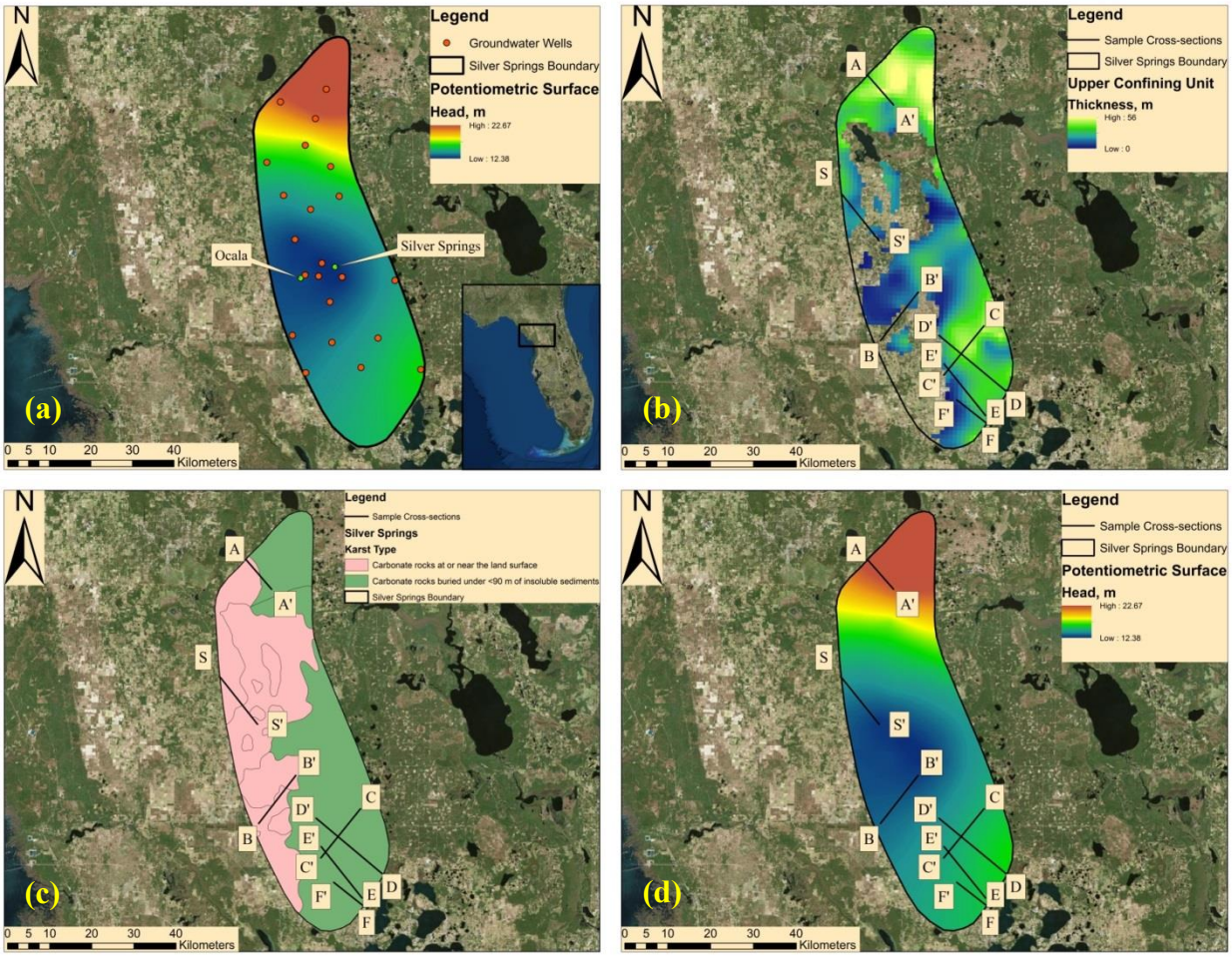

Figure 11 – Study area. a) Springshed boundary for Silver Springs in Ocala, Florida, and its location in relation to Florida, United States shown in the inset. The water-level contour map was generated via kriging based on observation wells. b) Upper confining unit thickness variation across Silver Springs with sample cross-sections shown. c) Karst map indicating where the carbonate rock is at or near the land surface or buried. d) Sample cross-sections from which head profiles were extracted based on previous fracture maps.

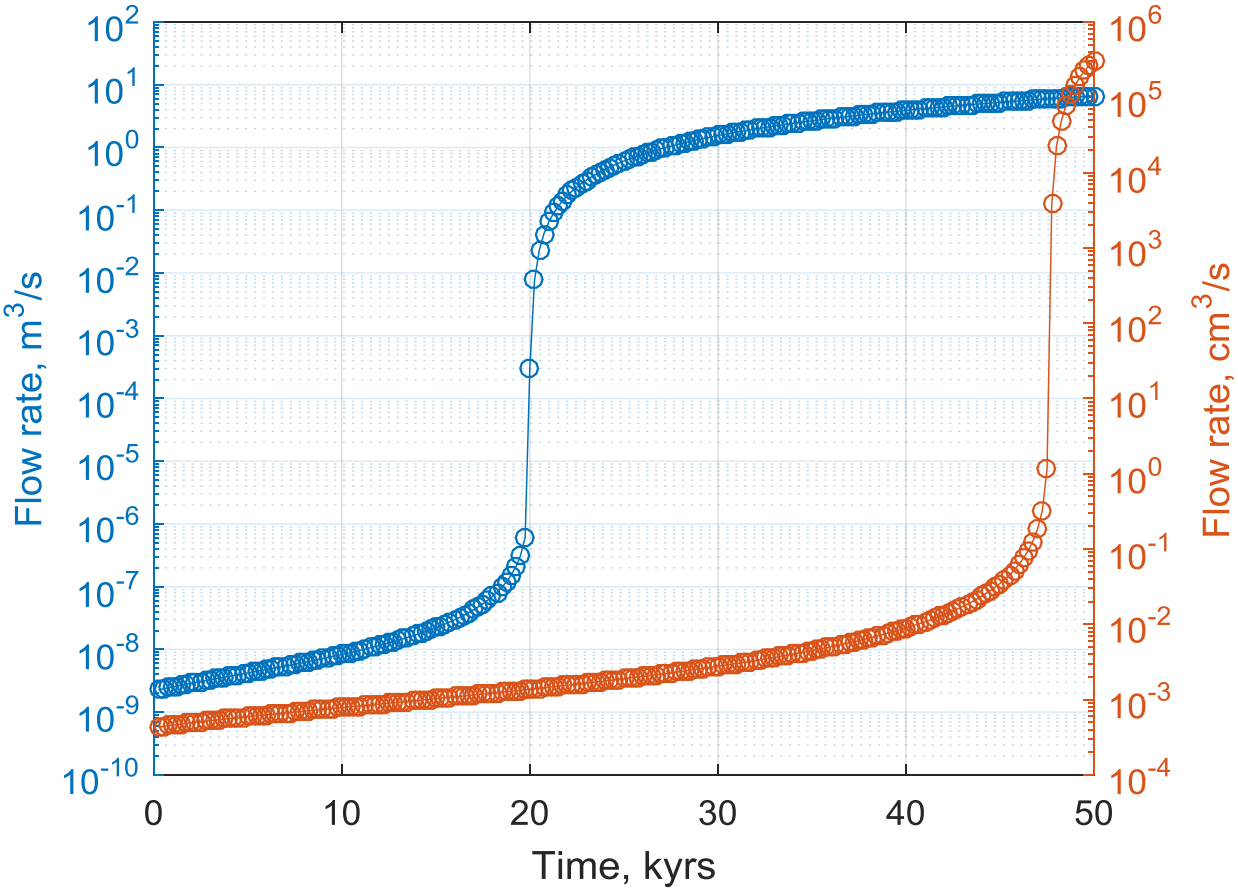

Figure 12 – Flow evolution verification using inputs from *Kaufmann* (2009) (blue) and *Kaufmann and Braun* (1999) (orange). The black dashed lines indicate where breakthrough occurs for each study, indicating the point where the flow regime becomes turbulent, due to continuous dissolution.

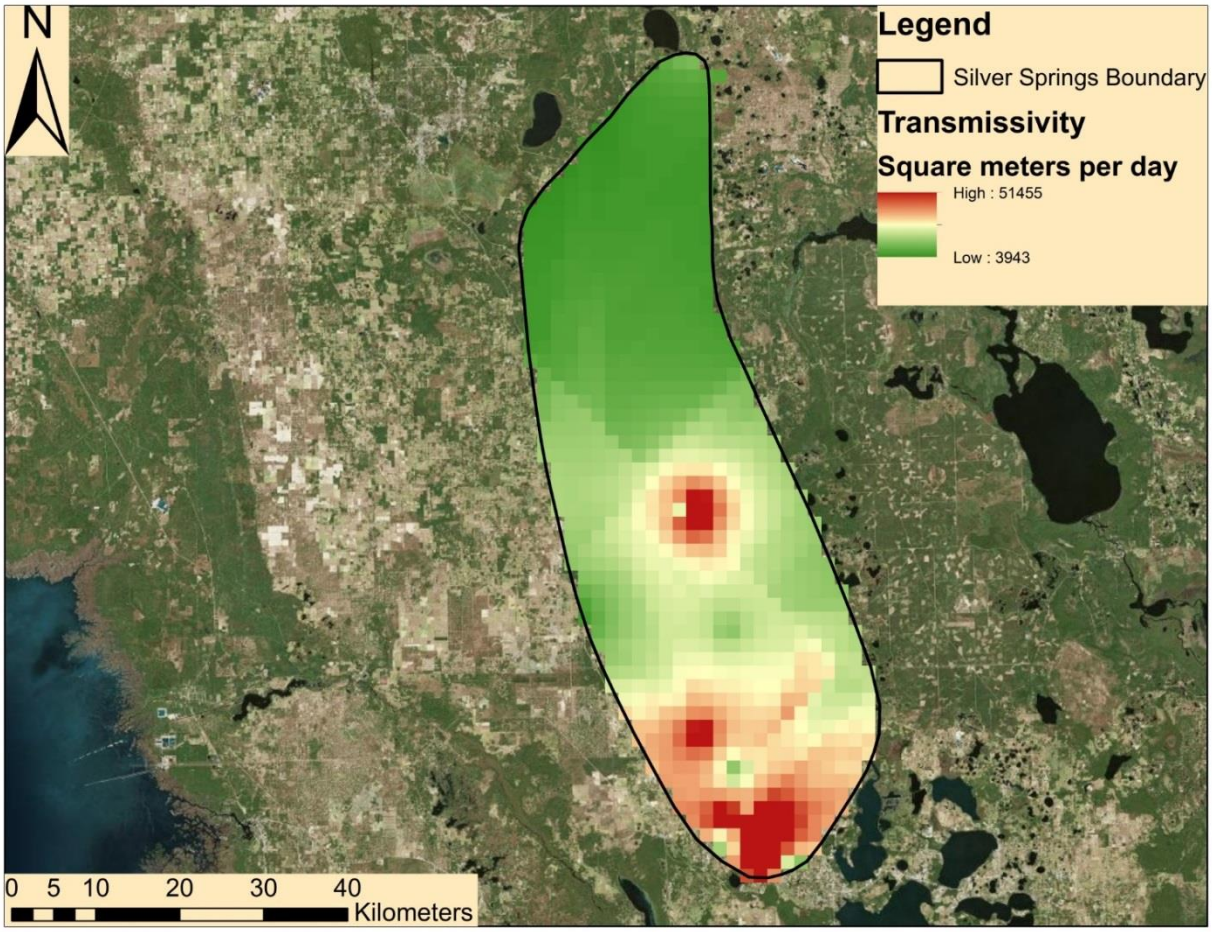

Figure 13 – Estimated transmissivity values within the Silver Springs springshed (Kuniansky et al., 2012).

Table 5 – List of hydraulic and chemistry properties used in this study.

Parameter	**Value**
Conduit roughness, ϵ	0.002 cm
Kinematic viscosity, υ	0.012 cm^2/s
Diffusion coefficient, D	1×10^{-6} cm^2/s
Calcium equilibrium concentration, C_{eq}	3×10^{-6} mol/cm^3
Low order rate constant, k_0	4×10^{-11} mol/cm^2-s
Threshold concentration, C_T	$0.9(C_{eq})$ mol/cm^3

3.3 Results and Discussion

Modeling karst conduit evolution requires knowledge of the processes that drive karst dissolution and subsequent evolution (Palmer, 1991; Dreybrodt, 1996). Aggressive water with respect to calcium entering karst conduits dissolves the surrounding limestone, slowly enlarging the conduits (i.e., increasing diameter), until the water becomes saturated, at which point further conduit dissolution no longer occurs. As a result, incoming under-saturated water (assumed to have a calcium concentration ~ 0 mol/cm^3), further dissolves the conduit, and this behavior propagates throughout the karst conduit system. The dissolution is modeled for low-order and high-order kinetics.

Figure 10b-d indicate the sample cross-sections from which the potentiometric head profiles are analyzed. These profiles correspond to fractures that have been mapped out based on aerial photographs and remote sensing of photolinears in previous studies (Vernon, 1951; Florea and Vacher, 2006a). By superimposing fracture maps to scale, various fracture cross-sections were then traced in areas where the aquifer is confined. Figure 14a shows the head profiles of the traced fracture cross-sections, whereas normalized head profiles with respect to maximum

elevation head are shown in Figure 14b. As can be seen, these profiles display nonlinear concave down behavior, therefore the karst conduit evolution model (K-model) can be appropriately employed to simulate head profiles to see if it can mimic the observed values.

Furthermore, the K-model is also able to predict the age of the conduits. This analysis is based on initial conditions for fracture geometry and dissolution chemistry. Figure 14c shows a sample output for predicting the age of cross-section AA' (Figure 11b). In the K-model, the head profile changes as a function of time, due to the continuous dissolution simulated in the conduit. For predicting the age of the conduits, the simulations were run until the modeled head profiles overlapped with the observed ones and the elapsed time was recorded (see Figure 14c). Note that for brevity we only show the age prediction for AA'; however, simulations were run for all cross-sections shown in Figures 8b-d.

In general, fractures can have varying initial aperture diameters (e.g., 10 μm – 10 mm) (While, 2007). These aperture diameter values can provide an estimate for initial fracture size. In this study, the K-model simulates the observed head profiles for each cross-section by assuming an initial fracture diameter of 1 mm and the lengths of each cross-section. The hydraulic gradient is derived from measured head levels. To compare the accuracy of the K-model with respect to the observed profile, the root mean square error (RMSE) was employed and can be calculated as: $RMSE = \sqrt{\frac{\sum_i^N (P_i - O_i)^2}{N}}$, where *P*, *O*, and *N* are the predicted value, observed value, and number of observations, respectively.

Applying the K-model, for example, for cross-section AA', we observe that it takes approximately 54 Myrs for the karst conduit to evolve and reproduce the observed head profile, with the fit having an RMSE of 0.001 m (Figure 15a). Figure 15b shows the head profiles for

cross-section BB', which can be considered thinly confined. The K-model plots a similar head profile, with an RMSE of 0.006 m. This head profile would occur after 30 Myrs. Figure 15d show the observed head for cross-sections CC' and DD', respectively. The associated RMSE and age for CC' and DD' were 0.004 m, 45 Myrs, and 0.004 m, 21 Myrs, respectively. Figure 15e shows the head profiles for cross-section EE', whereas Figure 15f shows the head profile for cross-section FF'. The corresponding RMSE and the age for EE' and FF' were 0.008 m, 30 Myrs, and 0.004 m, 9 Myrs, respectively. These RMSE values for the K-model are also listed in Table 6. Out of the six profiles, the K-model profiles for cross-sections AA' and DD' best resemble their observed profiles, whereas cross-sections BB' and CC' do not fit well enough compared to their observed profiles. For example, for cross-sections BB' and CC', at the end of the observed profiles (Figure 15b-c), the evident concave up behavior is not accurately captured by the K-model. This concavity change could be due to processes such as groundwater withdrawals that may induce lower water levels in the observed profiles than what was simulated by the K-model (Ghasemizadeh et al., 2016).

It should be noted that a nonlinear (concave down) head distribution may be also attributed to leakage flowing to the confined aquifer through a semi-confining layer (see Methods for details on L-model). The available data on transmissivity and thickness of the confining layer pertaining to each fracture cross-section is used to fit a value for K'. Modeling both karst and leakage processes can help characterize the terrain of the UFA and can also suggest which of these two processes can explain the observed profiles better.

Figure 15a also shows the modeled profile using the one-dimensional groundwater flow leakage model (L-model). This profile was fit using average rock parameters, i.e., a T value of

4.98×10^{-2} m^2/s, and a b' value of 23 m. From these values, a minimum error (RMSE between observed and L-model predicted heads) of 0.011 m is obtained when a fitted K' value of 1.3×10^{-7} m/s is used. The leakage parameter values T, b' and K', along with RMSE values for cross-sections BB' – FF' can be seen in Table 6, whereas the cross-section profiles along with the simulated head profiles are shown in Figure 15. Given, on average, that the RMSE in the case of K-model is one-order smaller than the RMSE in L-model, these results indicate K-model can reproduce the observed head with much higher accuracy, compared to the L-model.

In addition, for all the analyzed cases, the simulated head profiles using the K-model with the initial conditions occurred before breakthrough (see model description for details), yet, the continuous dynamic enlargement of the conduits would imply that turbulent flow would occur eventually. As a result, this occurrence would carry implications on flow and transport processes. For instance, there would be a greater tendency for conduits to transfer flow as compared to flow in the rock matrix.

The hydraulic conductivities modeled for the confining layers indicate aquitard behavior, as expected. For reference, aquitard conductivities range from $1.3 \times 10^{-6} – 2.4 \times 10^{-9}$ m/s (Sepúlveda, 2009), thus the values obtained here, with the exception of cross-section BB', fall within the range of estimated values. For the most part, the RMSEs from the K-model were less than the L-model with the exception of cross-sections BB' and FF', suggesting that the potentiometric head profiles can be better explained by karst dissolution. Estimates on conduit age were obtained by applying the K-model, in which the modeled head profiles indicate that it would take between 9 – 54 Myrs (see Table 5) to achieve the observed head profiles, based on the initial fracture assumptions. From earlier studies, it is suggested that the rock geology of the

UFA in the Ocala area are from the Eocene and Oligocene series (Williams and Kuniansky, 2015; Florea and Vacher, 2006a), which occurred roughly 25 – 50 Myrs ago. In fact, the aquifer age of Silver Springs is listed at 40 Myrs (Florea and Vacher, 2006b). The extracted nonlinear head profiles estimated age is reasonable in the sense that the predicted ages fall within the age range of the geologic rock (Florea and Vacher, 2006b). For the profiles exhibiting early karst evolution, to predict an older conduit age for the geologic rock in Florida, the initial fracture size would need to be smaller than initially assumed; however, other parameters may also affect conduit age simulations. For instance, simulating karst evolution with a lower C_{eq} and/or a higher k_0 value would slow down the dissolution process and prolong breakthrough. This implies that it would take more time for the simulated head profiles to overlap the observed head profiles, which would lead to overestimating the conduit age relative to prior reports.

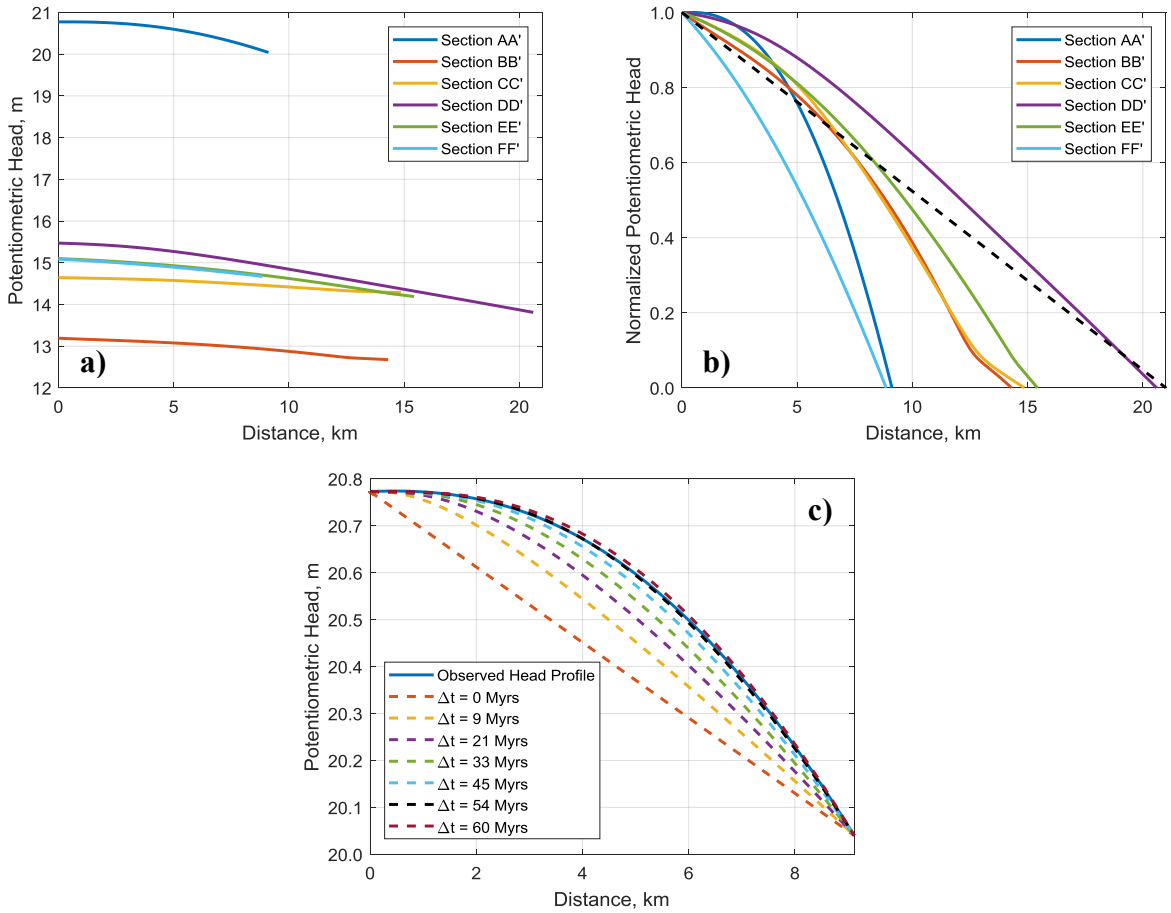

Figure 14 – Observed and simulated head profiles. a) Head profiles of the cross-sections in Figure 11b-d. b) Normalized plots of a) with respect to their maximum potentiometric head. The linear black dashed line is plotted for visual curvature comparison purposes. c) Sample plot of various head profiles at different times from the K-model. These plots correspond to cross-section AA' (shown in Figure 11b). As expected, the head profiles change as a function of time, due to the propagating karst dissolution along the conduit. This plot predicts the age of this conduit segment to be 54 Myrs (dashed black curve), when it overlaps the observed profile curve (solid blue curve).

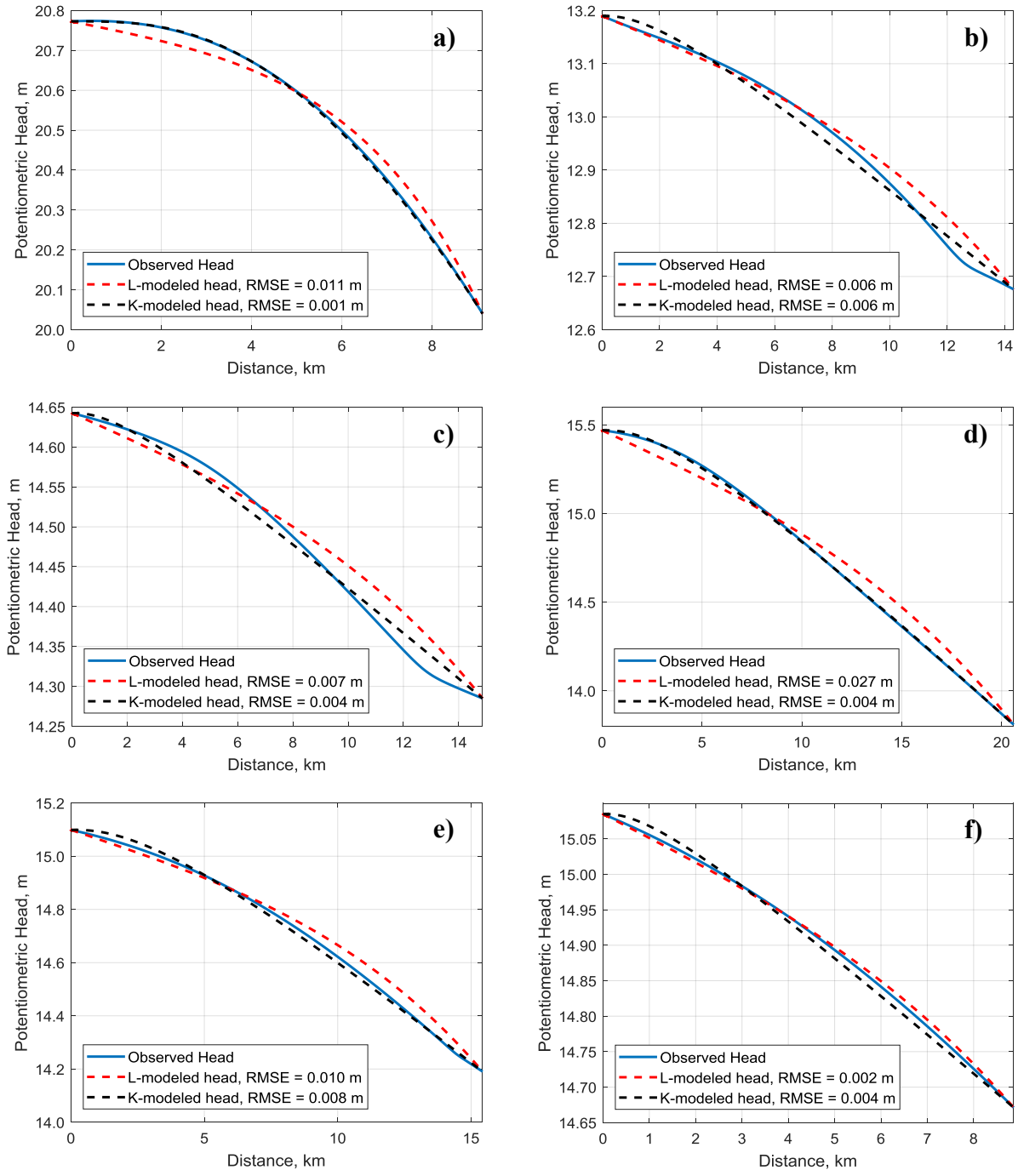

Figure 15 – Observed and modeled head profiles based on karst dissolution (K-model) and groundwater leakage (L-model) for cross-sections a) AA', b) BB', c) CC', d) DD', e) EE', and f) FF'. For the most part, as can be seen, the K-model produces a smaller RMSE than the L-model, and in some cases, almost an order of magnitude smaller. These observations suggest the K-model fits the observed head profiles more accurately, which can be seen visually, particularly for cross-sections AA' and DD'.

Table 6 – RMSE values for the K and L models, and the parameters associated with the L-model. Note that the RMSEs for the K-model are on average lower than the RMSEs for the L-model. Associated age obtained from the K-model is also shown for the considered cross-sections.

Cross Section	K-model		L-model			
	RMSE, m	Age, Myrs	T, m^2/s	b', m	K', m/s	RMSE, m
AA'	0.001	54	4.98×10^{-2}	23	1.30×10^{-7}	0.011
BB'	0.006	30	1.04×10^{-1}	6	9.33×10^{-9}	0.006
CC'	0.004	45	1.27×10^{-1}	24.4	3.98×10^{-8}	0.007
DD'	0.004	21	1.22×10^{-1}	27.4	2.18×10^{-8}	0.027
EE'	0.008	30	1.35×10^{-1}	15.2	3.19×10^{-8}	0.010
FF'	0.004	9	1.79×10^{-1}	10.7	5.13×10^{-8}	0.002

3.4 Summary and Conclusions

This study explored modeling the piezometric head profiles of the UFA in the Silver Springs area by applying karst dissolution chemistry and subsequent conduit evolution, and confined groundwater flow conditions. Piezometric head data on the UFA were obtained, in which extracted head profiles revealed nonlinear behavior. The evolution of karst conduits was simulated, and the modeled head profiles (K-model) overlapped the observed head levels, suggesting a strong presence of karstic systems. Although the modeled head profiles from the K-model were associated with laminar flow for all cross-sections, dissolution is ongoing and at some point the flow regime will become turbulent, which would imply a greater tendency for flow to pass through conduits. As for groundwater flow with leakage, modeled head profiles (L-model) also approximately matched observed head levels, with reasonable aquifer parameters, however, the RMSEs were nearly one order of magnitude larger in some cases than in the K-model. This implies that the UFA can be more accurately characterized by the K-model

compared to the L-model. In areas where karst features are present, karst dissolution shows potential in modeling conduit segments.

In addition to the K-model reproducing observed heads, the K-model can also predict the age of a conduit segment. Although initial assumptions on fracture size, length, and chemistry dissolution parameters may vary, one can compute head profiles across time and compare them with observed levels until an overlap occurs at a specific time, which would imply a current conduit's age. Based on the analyzed head profiles, the K-model predicts approximately 9 – 54 Myrs for the conduits to achieve the observed head profiles. More accurate mapping of karst conduits and their geometries would help improve conduit age prediction, relative to the geologic age of the present rock that makes up the UFA (~25 – 50 Myrs).

For an area that is karstic like the Floridan aquifer, applying dissolution chemistry to simulate karst conduit evolution allows for the modeling of the conduit geometry and head profiles over time, as well as the age of the present conduit features. Thus, there is potential in utilizing karst dissolution chemistry to model existing head profiles to characterize karst systems. This information could potentially improve decision making regarding human activities, such as, groundwater pumping, and other interactions that may indirectly induce sinkhole activity.

3.5 Acknowledgments

Simulations were done using the STOKES Advanced Research Computing Center at the University of Central Florida.

CHAPTER 4: PARAMETER INFLUENCE ON KARST EVOLUTION

4.1 Introduction

As noted from the previous Chapter, the karst evolution model can yield different results depending on the initial conditions specified in the model. Modeling complex karst aquifer evolution requires knowledge of hydraulics and chemistry, therefore quite a bit of parameters can influence the output result of a simulated karst conduit. Earlier studies have applied karst aquifer evolution models based on dissolution chemistry with different initial conditions and have yielded different results, specifically breakthrough times. Here, breakthrough times are commonly referred to as the point at which conduit flow transitions from laminar to turbulent conditions (i.e., when flow rates suddenly increase by several orders of magnitude) (Clemens et al., 1996; Dreybrodt, 1996; Dreybrodt and Gabrovsek, 2000; Perne et al., 2014).

Initial conditions used by *Dreybrodt* (1996) yielded a breakthrough time of about 17 kyrs. Later simulations done by *Kaufmann and Braun* (1999) and *Kaufmann* (2009), using their own unique conditions yielded breakthrough times of 47.5 and 20 kyrs, respectively, highlighting the variability of breakthrough transition times depending on how a representation of a karst fracture (or conduit) is initialized. *Siemers and Dreybrodt* (1998) calculated breakthrough times for conduits with differing occupation probabilities, and their results indicated that changes in breakthrough times follow a power law behavior, with differing power-law slope values. This chapter also explores how varying initial parameters can affect breakthrough times of conduit flow, which suggests that karst aquifers are spatially heterogenetic in nature. The chapter is

structured as follows: Section 4.2 discusses the methods, Section 4.3 provides the results, and Section 4.4 summarizes and concludes the chapter.

4.2 Methods

Both hydraulic and chemistry parameters are selected and tested across different ranges of reasonable values. For this analysis, these varying parameters are input into the karst evolution model which is run until the breakthrough transition is captured. The time in which breakthrough occurs is recorded and then compared with other breakthrough times for each parameter range. Here, the hydraulic gradient, i, initial conduit radius, r, calcium equilibrium concentration, C_{eq}, low order kinetic rate, k_0, and conduit length, L, and diffusion coefficient, D, are varied across a range of possible values to observe their sensitivities, and to explore how karst dissolution depends on different parameters.

As far as the ranges are concerned, possible realistic values for each parameter are considered. The ranges of parameters are as follows: i varies from 0.005 – 0.2, r ranges between 0.015 – 0.100 cm, C_{eq} varies from $5 \times 10^{-7} - 5 \times 10^{-6}$ mol/cm^3, the low-order kinetic rate changes between $2 \times 10^{-11} - 8 \times 10^{-11}$ mol/cm^2-s, L varies from 500 m – 4 km, and D is varied from $1 \times 10^{-7} - 1 \times 10^{-3}$ cm^2/s. As a reference model, the initial fracture radius (diameter) is set at 0.025 cm (0.050 cm), the gradient is set at 0.05, whereas the calcium equilibrium concentration is 2×10^{-6} mol/cm^3, kinetic rate is equal to 4×10^{-11} mol/cm^2-s, conduit length is set to 1 km, and diffusion coefficient is assumed to be 10^{-5} cm^2/s. These values are summarized in Table 7. Essentially, each parameter is varied within its specified range while holding the other parameters fixed to the reference simulation. Details on the karst evolution

model and computations can be obtained from earlier studies (Dreybrodt, 1996; Kaufmann and Braun, 1999).

Table 7 – Summary of values used for analysis.

Parameter	Values	
	Reference	Range
i	0.050	0.005 – 0.200
r	0.025 cm	0.015 – 0.100 cm
L	1 km	500 m – 4 km
k_0	4×10^{-11} mol/cm^2-s	$2 \times 10^{-11} - 8 \times 10^{-11}$ mol/cm^2-s
C_{eq}	2×10^{-6} mol/cm^3	$5 \times 10^{-7} - 5 \times 10^{-6}$ mol/cm^3
D	1×10^{-5} cm^2/s	$1 \times 10^{-7} - 1 \times 10^{-3}$ cm^2/s

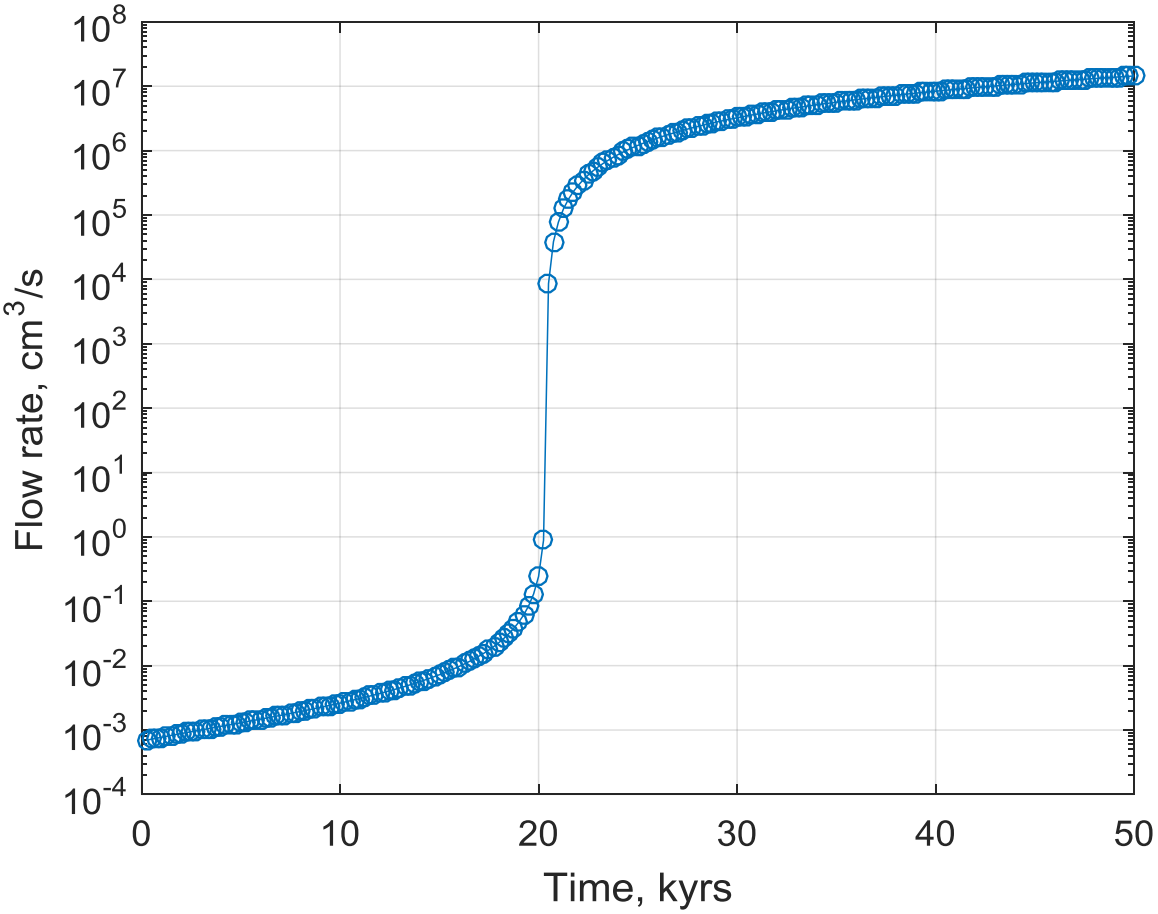

Figure 16 – Flow rate evolution over time for the reference simulation. Note that breakthrough time is 20 kyrs.

4.3 Results and Discussion

4.3.1 Examining conduit feedback

Figure 16 shows the flow rate as a function of time but does not indicate the flow regime (i.e., laminar or turbulent). The Reynold's number can be simply computed for each time step and then plotted with respect to time. Figure 17 displays how the Reynold's number varies with time, using the Reference conditions in Table 7. Note that at a time of 20 kyrs, the breakthrough transition intersects with the critical Reynold's number value of 2200. It can be seen that breakthrough is not only associated with the several orders of magnitude increase in flow rate, but also with the transition from laminar to turbulent flow conditions, which ultimately affects the conduit evolution. This breakthrough feature can also be visualized by plotting the conduit profile.

Figure 18 shows a sample plot of the conduit diameter along with its length. The different curves occur at a specific time in the simulation. The horizontal plot at the bottom corresponds to the initial simulation time, i.e., the initial condition of the fracture, here taken to be 5×10^{-4} m. As dissolution progresses, the subsequent curves at later times indicate the conduit is evolving non-uniformly in shape along its length. However, at about 20 kyrs, the conduit experiences a sudden increase in diameter. This reflects the conduit's response or feedback to changing flow conditions (from laminar to turbulent). From this point, the conduit reverts back to uniform conditions, since at this point the dissolution mechanism has progressed along the entire length of the conduit. The topmost curve corresponds to the end of simulation (50 kyrs). The breakthrough features seen in Figure 16 – Figure 18 are ultimately affected by the surrounding

aquifer hydrology and chemistry, and analyzing the sensitivity of karst evolution can explain how flow conditions respond to changes in local aquifer conditions.

4.3.2 Sensitivity observations

For brevity, only breakthrough times are plotted against parameter values (see Figure 19). However, note that breakthrough times can be inferred from plotting flow rate values with time (such as in Figure 16, from which the inferred breakthrough time is 20 kyrs), since modifying parameters would result in a unique realization of Figure 16. In Figure 19a, the hydraulic gradient was varied across a range for a specific initial conduit size. This was repeated for several initial conduit size values. For smaller initial diameters, data points were limited, due to limitations in computation. As seen, breakthrough times are longer for smaller initial diameters, which require more time and computational power to solve. However, trends show consistency across all diameters. From the figure, it is clear that for a smaller hydraulic gradient (i.e., flatter ground surface), the time required for the flow to transition from laminar to turbulent is very high, since travel times are much slower for smaller gradients, which slows down the dissolution process. The breakthrough times decrease as hydraulic gradient increases as flow travels faster and would dissolve at a quicker rate for steeper slopes. A power law regression was fit to the data, and the power law slopes range from -1.1 to -1.3.

Figure 19b shows the variation of breakthrough as a function of calcium equilibrium concentration. Similarly, the variation follows a negative power law behavior. For lower calcium equilibrium concentrations, the flowing water quickly become saturated, which limits the amount of dissolution that can occur, prolonging breakthrough. However, for higher calcium equilibrium concentrations, the opposite is observed. In addition, the flowing water can dissolve and contain

more dissolved calcium, enhancing conduit enlargement, lowering breakthrough times. The resulting regression slope is -1.2.

Figure 19c shows the change in breakthrough as a function of low order kinetic rate. As can be seen, as the kinetic rate increases, breakthrough times increase as well. For higher kinetic rates, the reaction between the calcite and the water occurs at a higher rate. This enhances the calcium flux intake, however as a result, the water becomes saturated quicker. This limits further dissolution, which slightly increases breakthrough times. Overall, the sensitivity is not relatively significant, yielding a power law slope of 0.26.

Figure 19d shows the influence of initial conduit size (i.e., radius) to breakthrough times. As expected, the smaller the conduit size is, the more dissolution (and time) it takes to achieve breakthrough. Whereas for larger initial conduit sizes, because the discharge is higher, and the flow regime is closer to turbulent conditions, not much additional dissolution is required to transition to turbulent flow, which leads to reduced breakthrough times. The power law slope is -2.75, and when compared to the other power law slopes obtained here for other parameters, suggests that the initial conduit size has some influence on breakthrough.

The conduit length is varied over a range of values and the corresponding breakthrough results can be seen in Figure 19e. In general, shorter conduits experience more dissolution as length is limited. Hence, conduits are enlarged, and breakthrough occurs relatively early. For longer conduits, the dissolution throughout a conduit is limited to the saturation point of the solution. Therefore, additional flow and dissolution is needed to further dissolve and enlarge conduits over its length, increasing breakthrough times. The slope of the power law regression is 1.3.

Lastly, the diffusion coefficient influence on breakthrough times is shown in Figure 19f. In particular, the diffusion coefficient becomes important for smaller values. After some threshold, breakthrough times do not change considerably. Here, diffusion influences how much calcium flux is being transferred from the limestone to the discharge. Conceptually, for low diffusion coefficients, the calcium flux is reduced as discharge is flowing through a conduit. Since the solution slowly approaches saturation, it is able to dissolve more calcium the further it travels downstream, which speeds up the breakthrough process. For higher diffusion, more calcium is being transferred to the solution as flow progresses. Calcium saturation is achieved earlier, which then limits the amount of the limestone to be dissolved by the solution, prolonging breakthrough times. The power law slope yielded a value of 0.232. The power law slope values for all parameters are listed in Table 8.

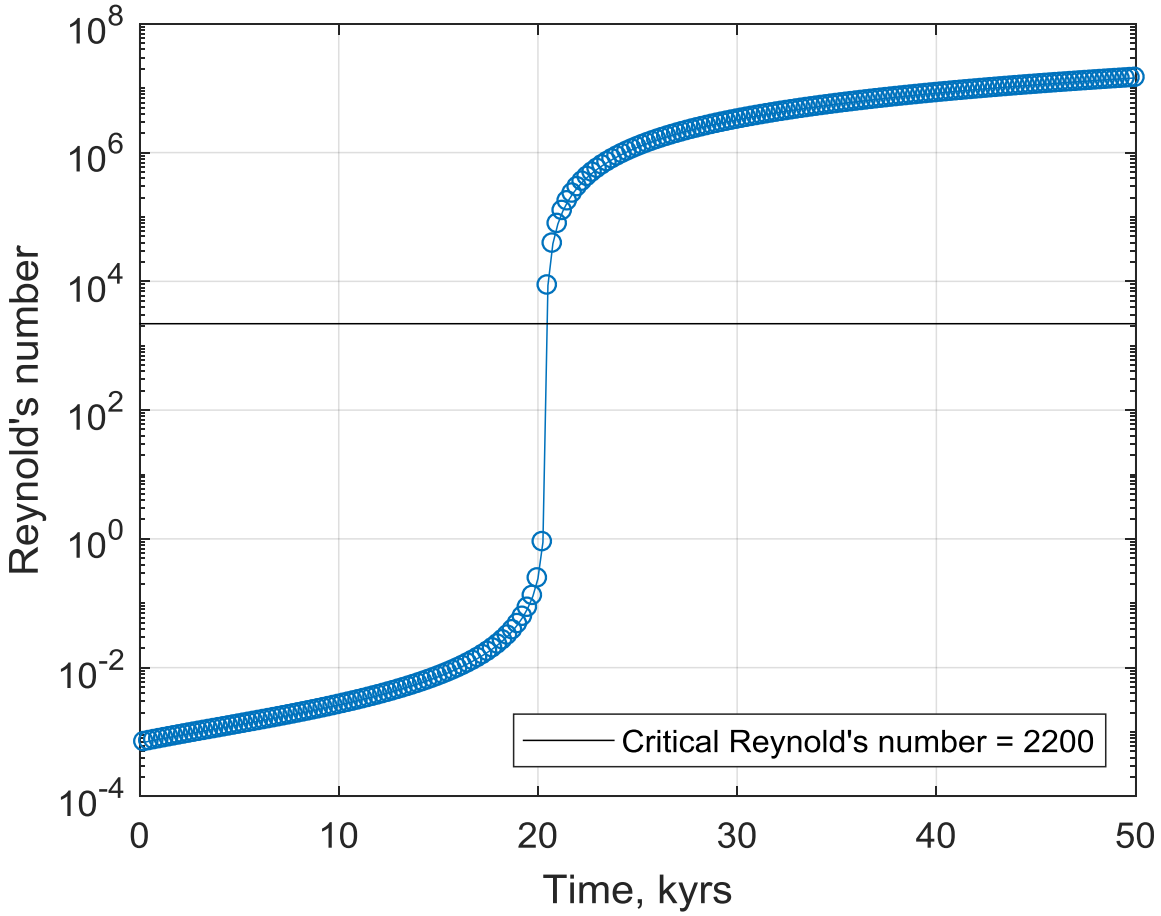

Figure 17 – Reynold's number as a function of time for the Reference conditions. The flow pattern becomes turbulent at a breakthrough time of 20 kyrs (see Figure 16).

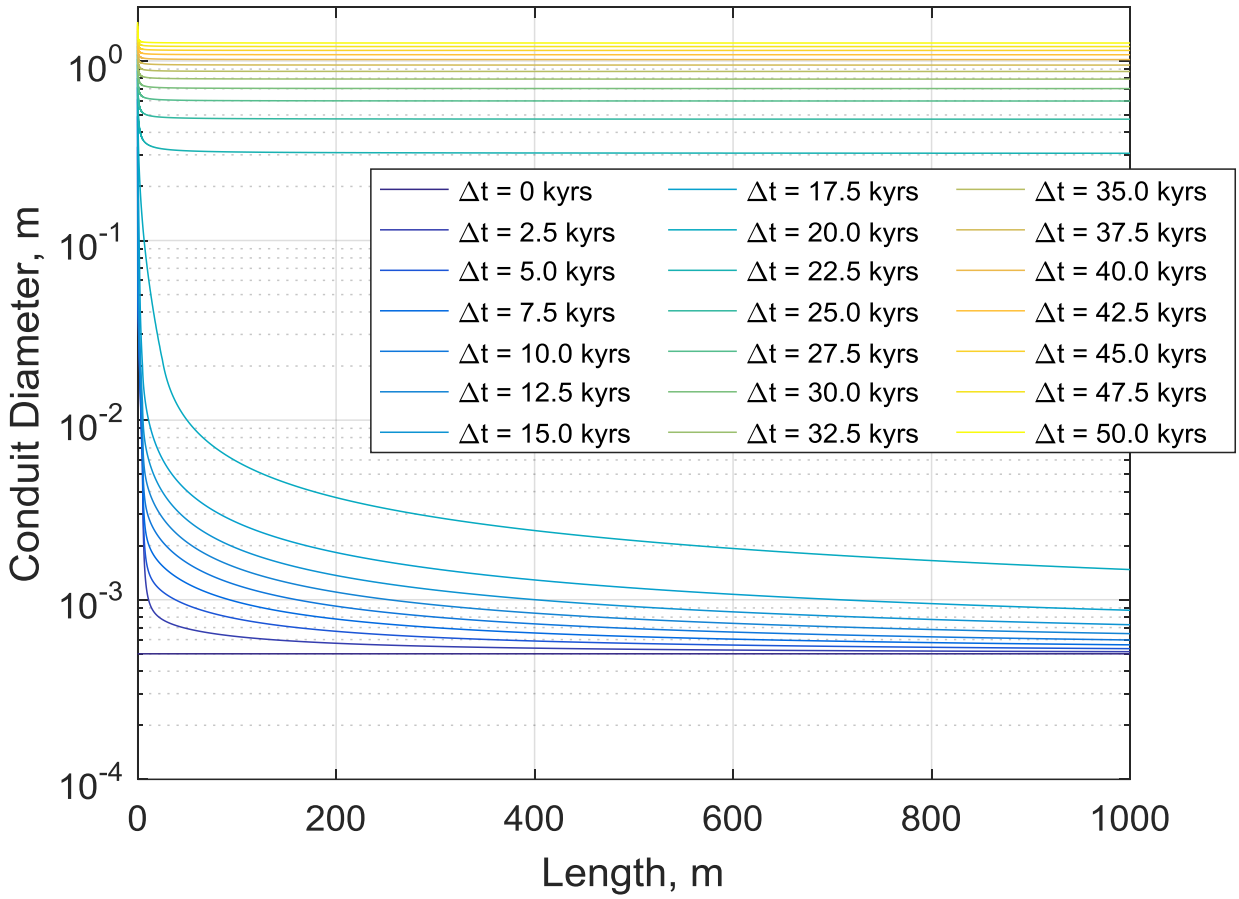

Figure 18 – Conduit diameter profile over time using the Reference parameters. The bottom and top plot represent Δt = 0 and 50.0 kyrs, respectively. Note the bottom plot is straight, indicating a linear, uniform conduit. Subsequent nonlinear plots indicate non-uniform conduits. The sudden jump in diameter represents breakthrough, which occurs at Δt = 20 kyrs (see Figure 16).

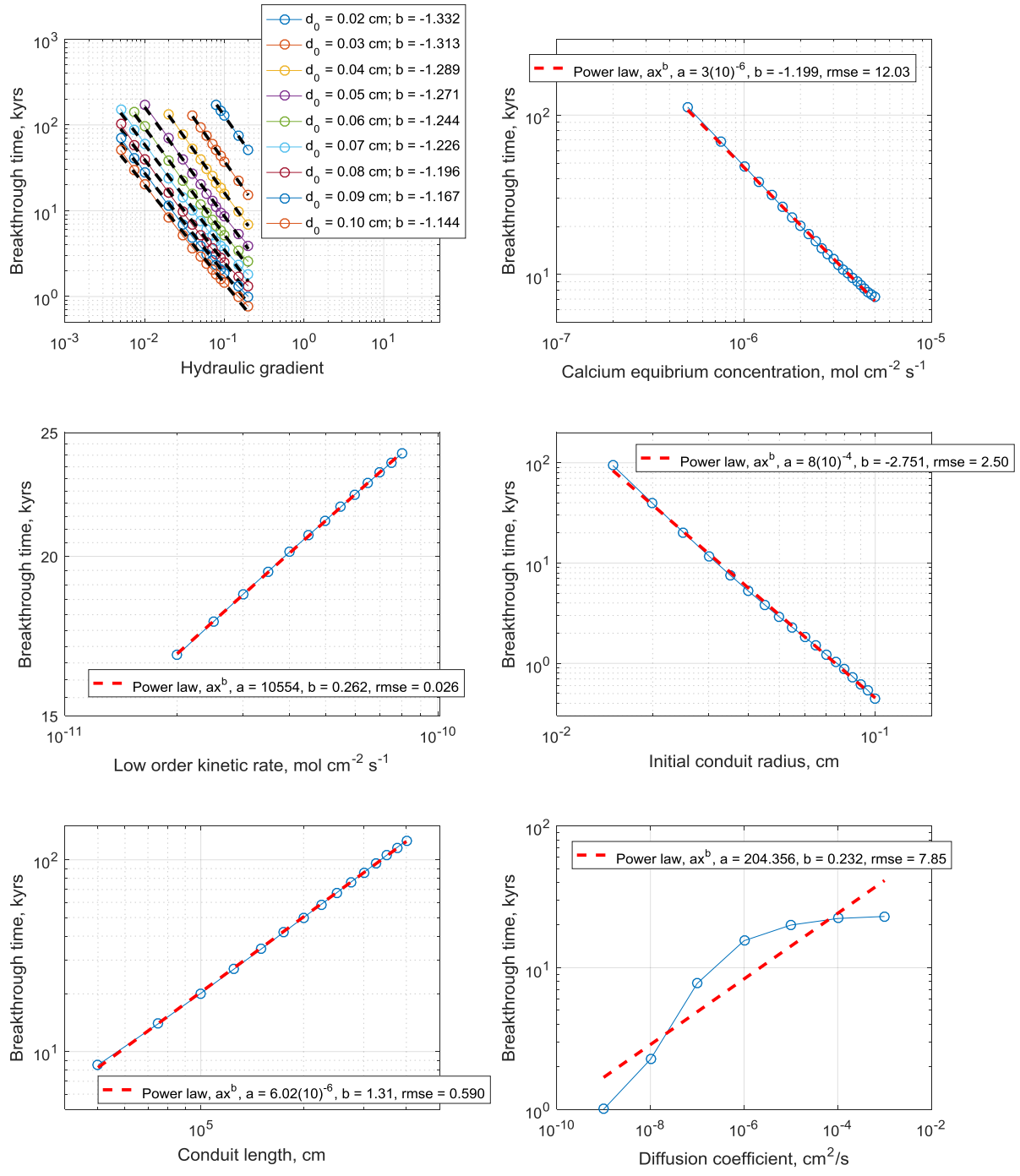

Figure 19 – Breakthrough sensitivity analysis as a function of a) hydraulic gradient, *i*, b) calcium equilibrium concentration, C_{eq}, c) low order kinetic rate, k_0, d) initial conduit radius, e) conduit length, *L*, and f) diffusion coefficient, *D*. A range of initial conduit diameters in a) were also tested along with hydraulic gradient values.

Table 8 – List of power law slopes from Figure 19.

Parameter	Power law slope
i	-1.1 to -1.3
C_{eq}	-1.2
k_0	0.262
r	-2.751
L	1.31
D	0.232

4.4 Conclusion

It is observed that karst dissolution can be influenced by several parameters, namely initial conduit size, and one can get an idea of how karst conduits would enlarge given the parameters of its surroundings. These results indicate that most of the parameters tested show a power law relationship with breakthrough time. Interestingly, some parameters are directly proportional to breakthrough times (kinetic rate, conduit length, and diffusion coefficient); whereas other parameters are inversely proportional to breakthrough time (calcium equilibrium concentration, and initial conduit radius).

Observing the power law slopes in Table 8, the kinetic rate, $k_{0,}$ and the diffusion coefficient, D, appear to have weak influence on breakthrough times, as the magnitude of their power law slopes are smaller relative to the other power law slopes obtained. Hydraulic gradient, i, calcium equilibrium concentration, C_{eq}, and initial conduit length, L, show some influence on breakthrough times through their power law slopes. Lastly, initial conduit radius, r, appears to have the most influence on breakthrough times, yielding a power law slope of -2.75. In fact, these sensitivity results, for the most part, follow the same trends compared with the results from

previous conceptual studies (see Siemers and Dreybrodt, 1998; Kaufmann et al., 2016). Furthermore, the results discussed here can apply to karst conduit networks. A karst conduit network consisting of fractures and conduits may evolve in response to its surroundings, which then suggests that karst conduit networks evolve differently in unique location settings. Subsequently, groundwater processes such as contaminant transport are influenced by the presence of karst and the dynamic karst evolution process. Therefore, the knowledge gained here can improve understanding of karst aquifer evolution, especially for different geographic locations, which can ultimately improve better management practices.

CHAPTER 5: MODELING KARST CONDUIT NETWORKS

5.1 Introduction

Karst systems consist of networks of underground conduits, which can influence groundwater processes. Over time, the dissolution process occurring in conduit networks can lead to the formation of different types of caves (Palmer, 1991). The evolution of individual conduits that make up a network depends on the initial fractures and hydrologic conditions of aquifers (Dreybrodt, 1996; Kaufmann and Braun, 1999). Moreover, certain fractures evolve faster than other fractures within a network, which can form preferential flow paths under different flow conditions. Preferential flow paths are defined as paths that are least resistant to flow (Groves and Howard, 1994; Howard and Groves, 1995; Siemers and Dreybrodt, 1998). Due to the time scales at which karst aquifers evolve (i.e., tens or hundreds of thousands of years) (White, 2002), observing and understanding karst network evolution is best done by numerical analysis (Groves and Howard, 1994; Howard and Groves, 1995; Clemens et al., 1996; Siemers and Dreybrodt, 1998; Kaufmann and Braun, 1999).

Groves and Howard (1994) observed during laminar flow that preferential flow paths tend to form along paths directly between a network entrance and exit; also, flow paths parallel with the hydraulic gradient evolve faster than paths perpendicular or at some angle with the hydraulic gradient. *Howard and Groves* (1995) concluded that during the turbulent flow regime, karst network flow paths become less preferential and more generally distributed, leading to maze-like formations. Based on these studies, a question of interest to explore when simulating karst networks is understanding how the conduit size evolution propagates throughout a network,

and how boundary conditions affect the overall development of a karst conduit network. Another aspect that can be studied is the evolution of a conduit's potentiometric head over time. Observing the head evolution may provide information about a conduit's development stage (i.e., early development, before breakthrough; or later development, after breakthrough).

In this chapter, a karst conduit network is simulated in the Silver Springs springshed near Ocala in the central Florida area. The Floridan aquifer is dominated by carbonate rock across Florida, which can impact flow patterns and processes (Miller, 1986). As a result, the central Florida karst region has been previously studied due to its distinct karst and physical features, ranging from caves and sinkholes (Florea and Vacher, 2006a; Sepúlveda, 2009; Langston et al., 2012; and Sandhu et al., 2018) to aquifer characteristics and groundwater flow (Marella, 1999; Shoemaker et al., 2004; Williams and Kuniansky, 2015; and Xu et al., 2016). Cave diving and exploration has been conducted to further study and survey mature caves (Florea and Vacher, 2006a). However, for early cave systems, surveying efforts become challenging and models can be applied to characterize cave and conduit systems. The presence of karst conduits and their temporal evolution can induce changes in potentiometric head values (Perne et al., 2014). Temporal potentiometric head changes can then have implications of groundwater processes. In addition, in central Florida, groundwater pumping has increased in recent years due to increases in drinking water demands (Shoemaker et al., 2004), which also induce reductions in hydraulic head levels (Ghasemizadeh et al., 2016). The response of potentiometric head to karst network evolution is explored further to observe head changes with respect to karst configurations.

5.2 Data and methods

To simulate a karst conduit network, observed potentiometric well data are obtained from the SJRWMD, from which a head field was generated using kriging methods (see Figure 11a) (Kitadinis, 1997). From this head field, a smaller, rectangular-shaped head field within the Silver Springs springshed was extracted for simplification purposes. Within this head field, a square grid consisting of perpendicular conduit segments is defined. The karst conduit evolution model (see e.g., Groves and Howard, 1994; Dreybrodt, 1996; Siemers and Dreybrodt, 1998; and Kaufmann and Braun, 1999 for model details) is applied to all conduit segments in the model domain to simulate conduit growth and evolution.

Karst conduit network evolution may share similar properties as other networks (e.g., river networks; Rodríguez-Iturbe and Rinaldo, 2001; Abed-Elmdoust et al., 2016; Abed-Elmdoust et al., 2017; Hooshyar et al., 2017; and Hooshyar et al., 2019) as its evolution can be governed by energy equations, and requires several criteria that need to be satisfied. The first criterion requires that flow rate, Q, entering and leaving a junction is conserved. This is achieved by applying the following continuity equation at each junction:

$$\sum Q = 0 \qquad (5.1)$$

The next criterion states that the total head loss ($\Delta h_L = KQ^n$; where K is the pipe resistance, and n is the pipe flow exponent) around any loop of conduits should equal zero. This can be done by applying the commonly known Hardy Cross method of successive iterations (Cross, 1936; Mays, 2011), by computing the flow correction, ΔQ, for each loop, and applying it to the corresponding conduit segments that make up a specific loop:

$$\Delta Q = \frac{-\sum Ksign(Q+\Delta Q)(Q+\Delta Q)^n}{n\sum |K(Q+\Delta Q)^{n-1}|} \qquad (5.2)$$

From the Darcy-Weisbach equation, for $n = 2$, K can be expressed as:

$$K = \frac{8fL}{g\pi^2 D^5} \quad (5.3)$$

These two criteria given by equations 5.2 and 5.3 are checked for and satisfied during each time step in the simulation to help validate the network generated. The convergence threshold for the flow conservation and the Hardy Cross method was set to 1×10^{-8}, which was satisfied for all calculations.

The following parameters were used in this study, ϵ = 0.002 cm, υ = 0.012 cm^2/s, C_T = 0.9(C_{eq}), $k_0 = 4 \times 10^{-11}$ mol/cm^2-s, $C_{eq} = 2 \times 10^{-6}$ mol/cm^3 and $D = 10^{-6}$ cm^2/s is assumed. In addition, the length (i.e., spacing) between all conduits in the grid is assumed to be 100 m, whereas the initial diameter of all segments is considered as 0.010 cm.

5.3 Results and Discussion

A sample plane view extract of the observed potentiometric head field is shown in Figure 20, and the associated contour map is shown in Figure 21. Here, flow moves in the southeast direction. For simulation however, flow is allowed to enter from the left side and exit the right side, and the top and bottom edges are considered to be no flux boundaries. In addition, the head values at the boundaries are fixed throughout the simulation. Figure 22 shows the same potentiometric head field as a surface. Figure 23 shows the conduit segments within the network, represented by their diameter thickness. Here, the initial conduit diameter is defined as 0.010 cm. For this run, the karst network evolution model is simulated for laminar flow only and stops once turbulent flow begins to occur in a conduit.

Figure 24 shows the evolved head field after the simulation ends, which would occur after 390 yrs. From the figure it can be seen that the head field experiences a general increase in potentiometric head, which is also observed in the contour map in Figure 25. As dissolution is propagating across the network, the conduit segments at the entrance of the network are enlarged more than the conduit segments at the end of the network. At the entrance, the head loss across the larger conduit segments are reduced, which explains the increase in potentiometric head, particularly near the entrance. The head field in Figure 24 matches the head surface in Figure 26. This behavior further continues along the northern portion of the network, and makes it way downstream, resulting in an emerging preferential flow pattern along the southeast direction (see also Figure 27). Since turbulent flow sets in at t = 390 yrs, the simulation is terminated, and the flow pattern has not been fully developed along the entire network. However, the emerging preferential flow path can be indicated by the thicker conduit segments shown in Figure 27. Thicker lines indicate larger conduit segments, suggesting that the flow passes along the upper portion of the network before heading downwards at some angle. One observation as to why the upper portion of the network develops faster than the lower portion is due to the gradient configuration. The gradient along the longitudinal direction is greater than the gradient along the transverse direction. The longitudinal gradient has a greater influence on the preferential flow path evolution, while the transverse gradient has a lesser influence. The flow rate associated with the end of the simulation was computed for each conduit segment and is displayed in Figure 28. Thinner and thicker segments indicate smaller and larger flow rate values, respectively. As can be seen, the dynamic evolution of potentiometric head as a result of karst dissolution can induce flow rates to change directions, which can eventually induce backflow to occur in conduits. From

the figure, the black color segments indicate flow moving in the right direction or in the downward direction. The red color segments indicate flow moving in the left direction, or in the upward direction. These flow rate values are more apparent from Figure 26.

5.3.1 Broader impacts

Karst dissolution not only leads to the formation of emerging networks but can also induce backflow within these networks. Backflow or reversals in karst springs can potentially have negative consequences regarding the quality of groundwater resources (Gulley et al., 2011). For example, surface water consisting of nutrients from surface sediments may enter karst aquifers, which could degrade fresh groundwater resources. Nitrate loading in particular has been observed in Silver Springs and could adversely affect ecosystems (Phelps, 2004; Quinlan et al., 2007). Furthermore, spring reversals can introduce water with certain chemical compositions, thereby altering the aquifer geochemistry (Gulley et al., 2011). As a result, calcite dissolution would be impacted, which would then impact karst conduit network formation. In addition, dynamic temporal changes in climate (e.g., precipitation, streamflow) may further influence flow patterns in karst aquifers, propagating more backflow (Joigneaux, 2011). In essence, not only can simulating karst conduit networks indicate preferential flow paths but can also provide information regarding conduit discharges and their flow directions. The understanding of karst conduit network generation, as well as the knowledge of local climate conditions in a given spring can further improve the knowledge of how these distinct processes interact with each other and the impacts they have on the state of the karst aquifer.

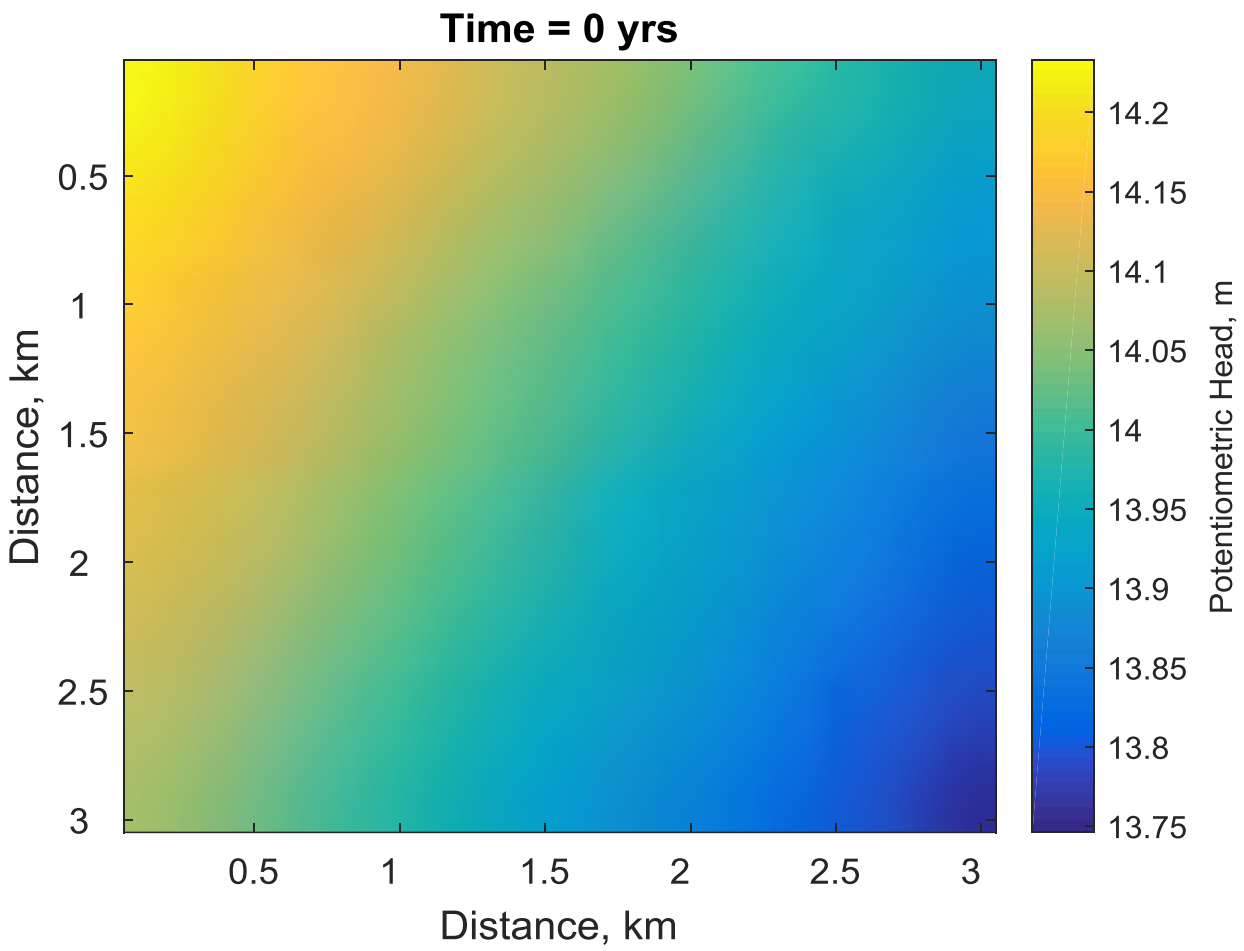

Figure 20 – Sample plot of observed potentiometric head within the Silver Springs springshed.

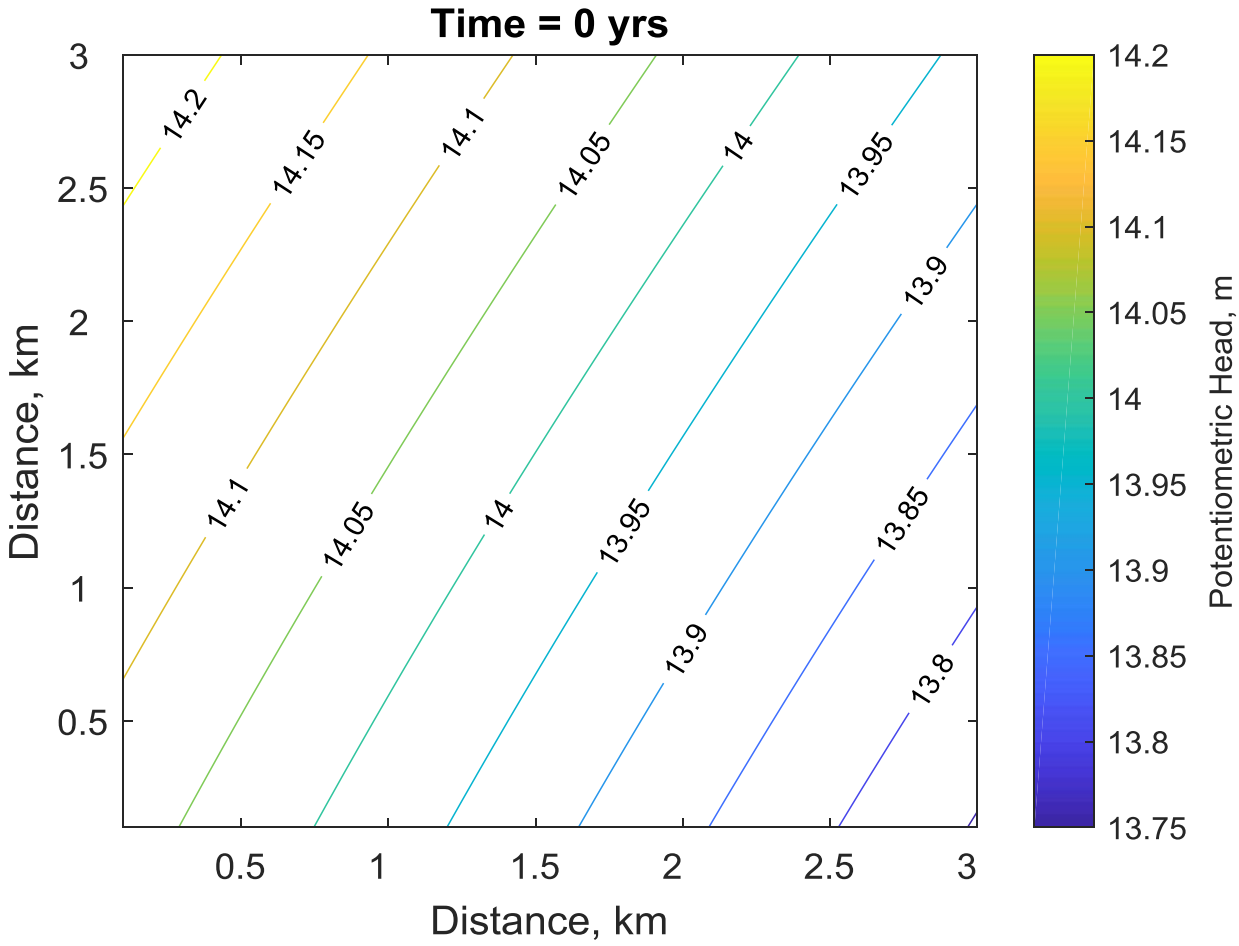

Figure 21 – Contour plot of initial potentiometric head seen in Figure 20.

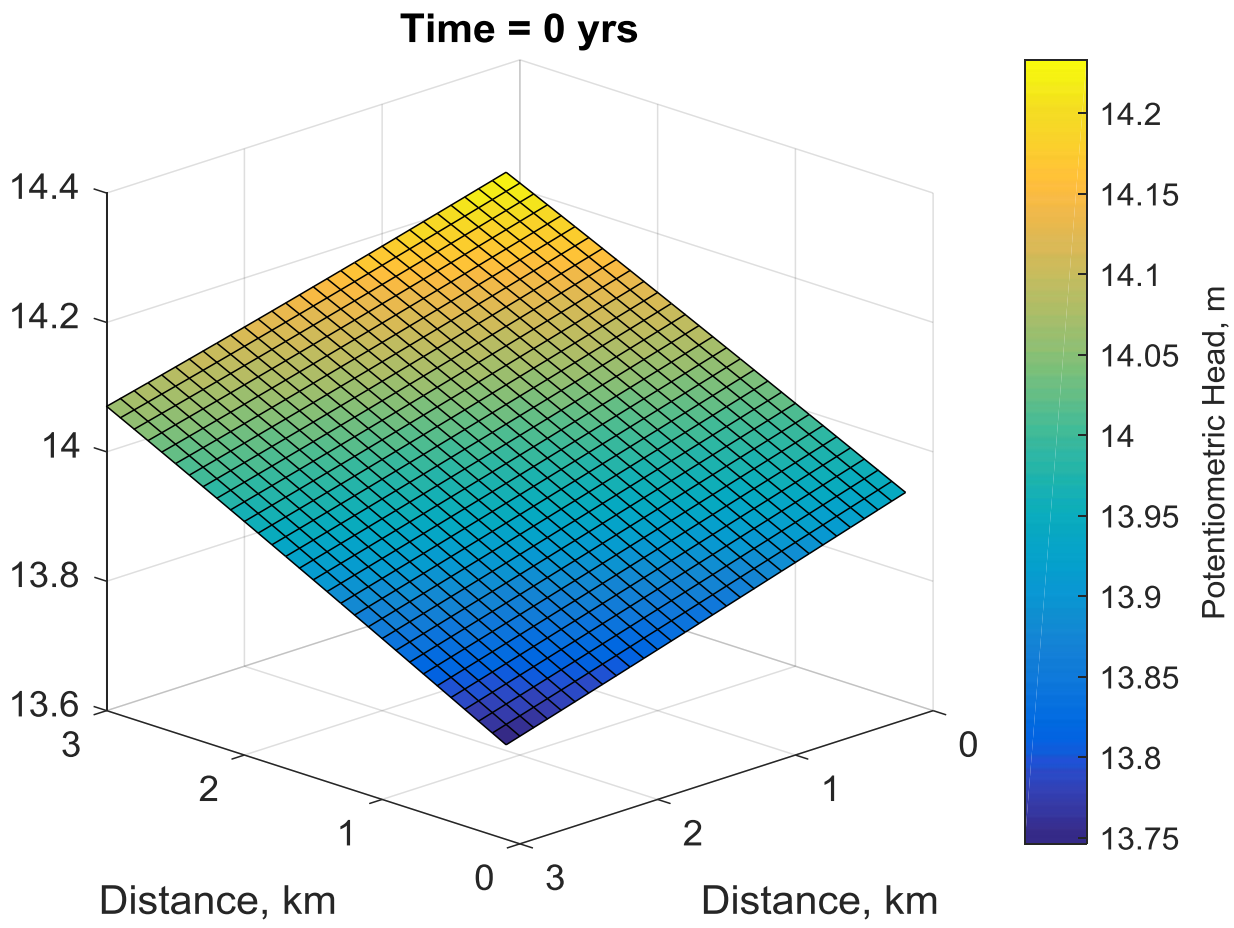

Figure 22 – Surface view of the observed (hence, time = 0) potentiometric head field shown in Figure 20.

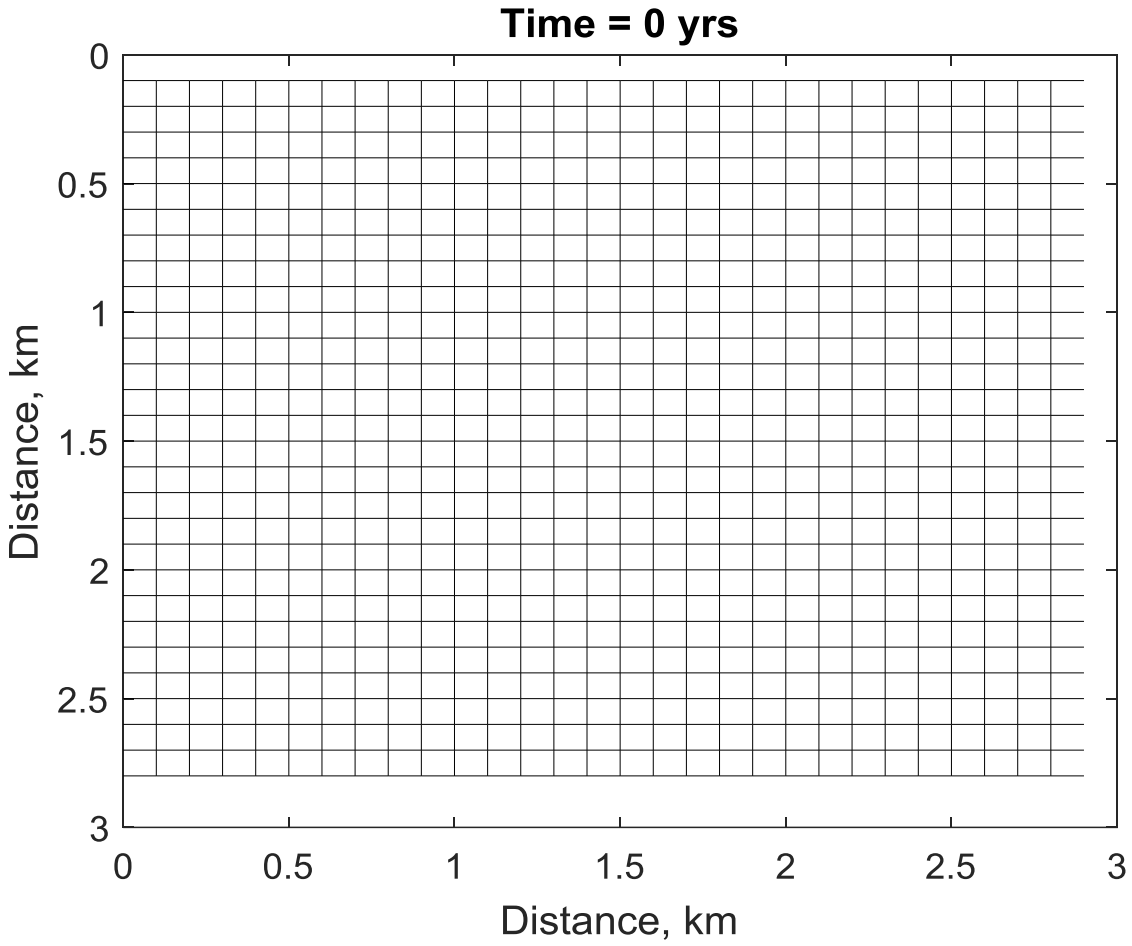

Figure 23 – Initial conduit network with initial diameter of 0.010 cm for all segments.

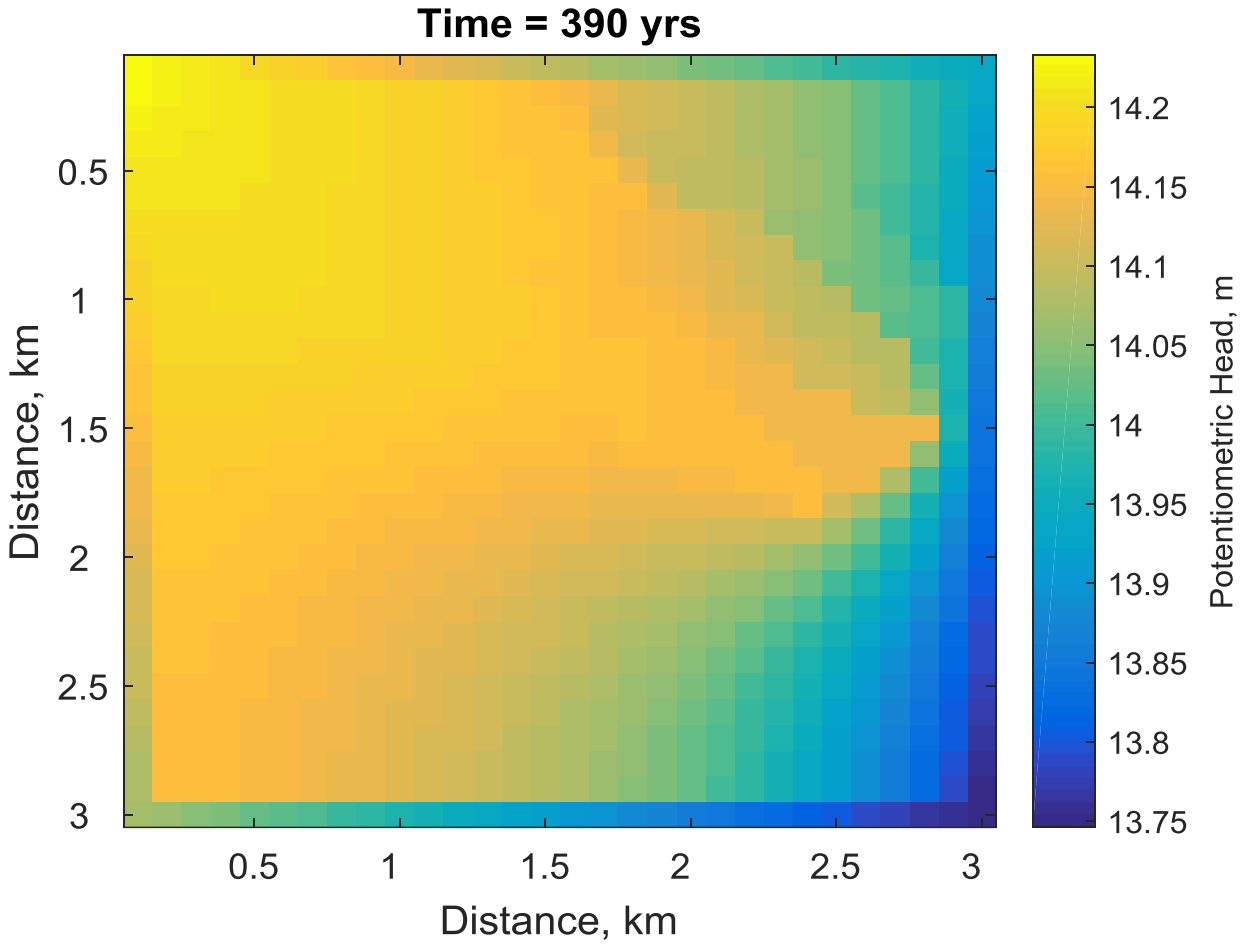

Figure 24 – Potentiometric head field at the onset of turbulent flow.

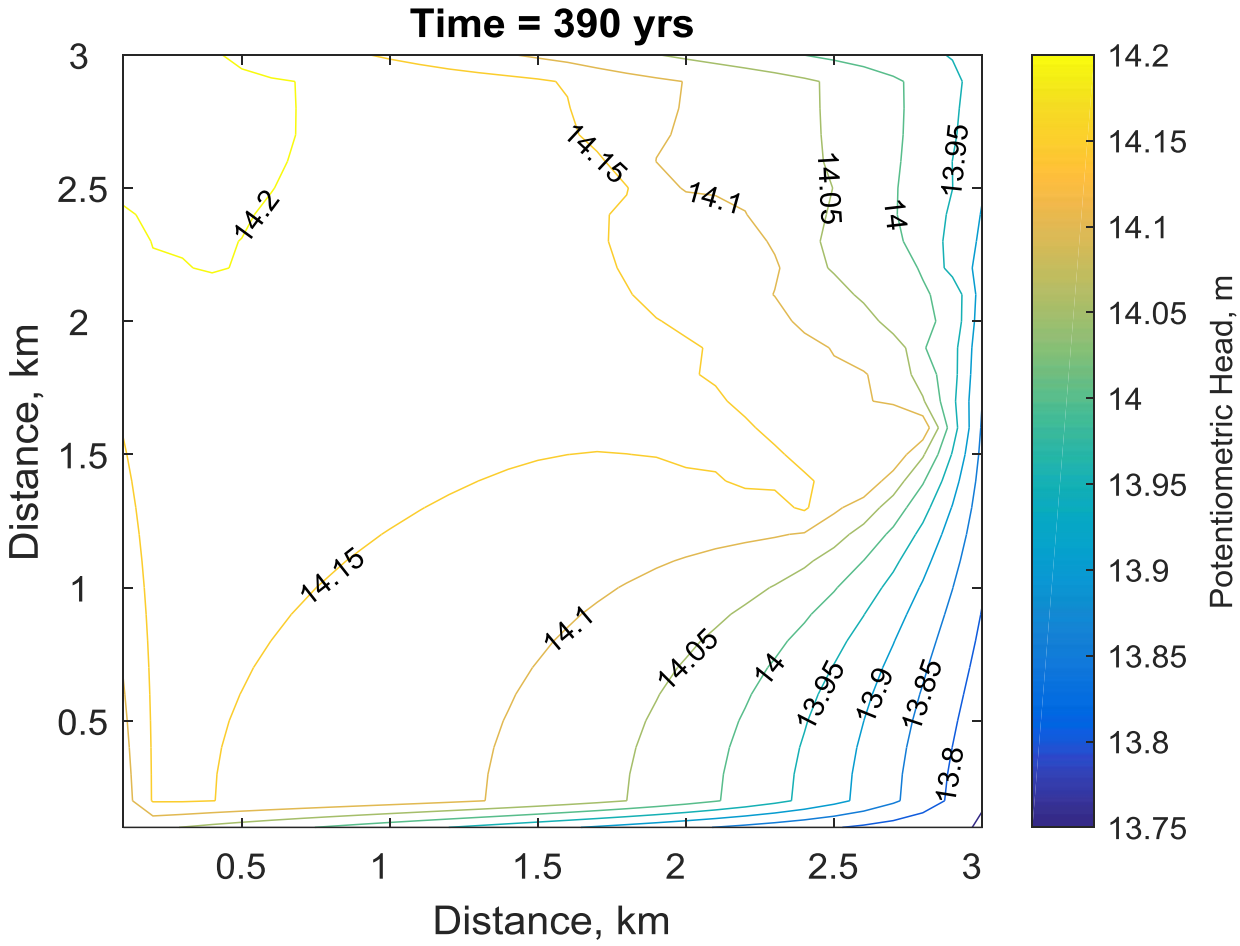

Figure 25 – Contour plot of potentiometric head at the end of simulation (see Figure 24).

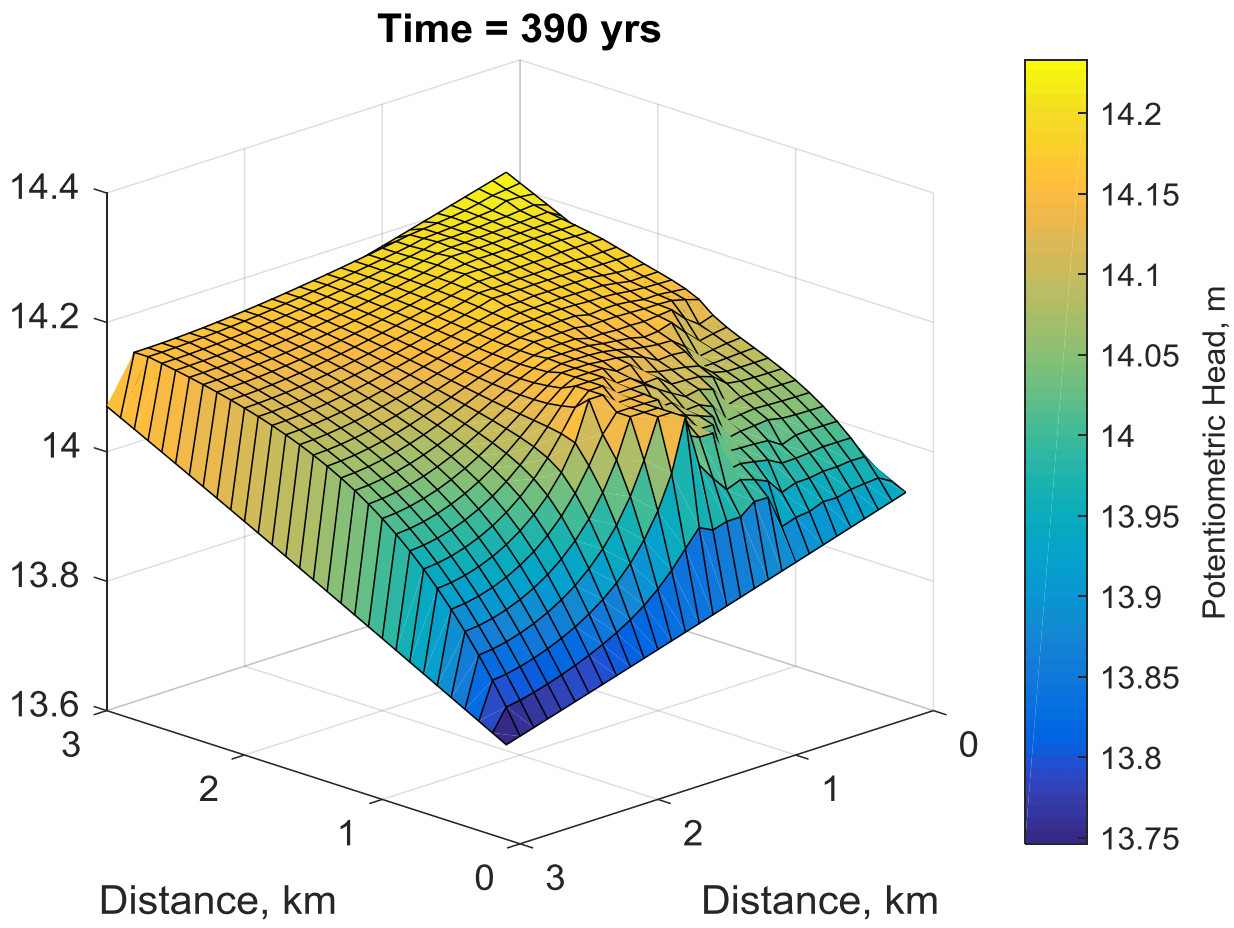

Figure 26 – Surface view of potentiometric head of the simulated karst network at the onset of turbulent flow. Note the nonlinear behavior of the head surface as a result of non-uniform conduit network.

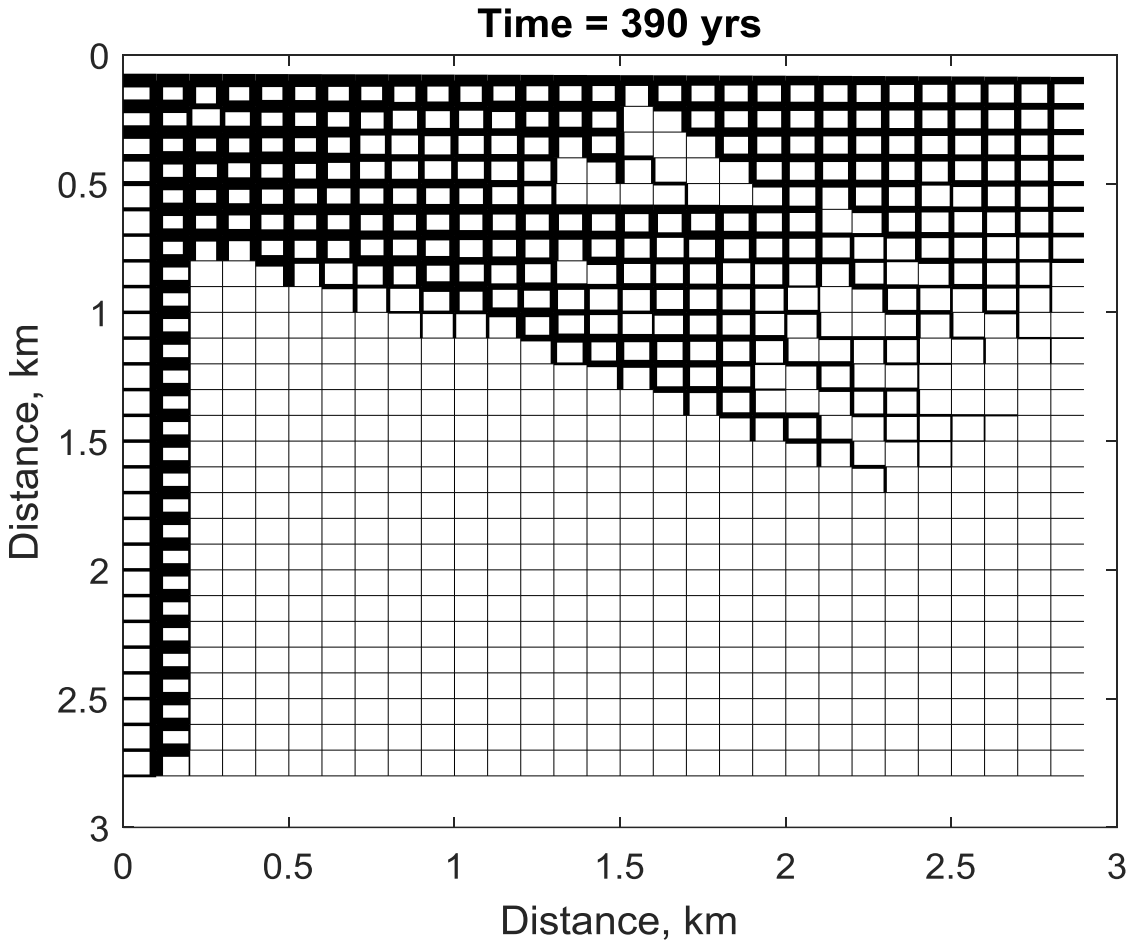

Figure 27 – Diameter thickness of the karst network at the onset of turbulent flow. Based on aquifer conditions, preferential flow paths begin to emerge. Thinner and thicker segments indicate smaller and larger conduits respectively.

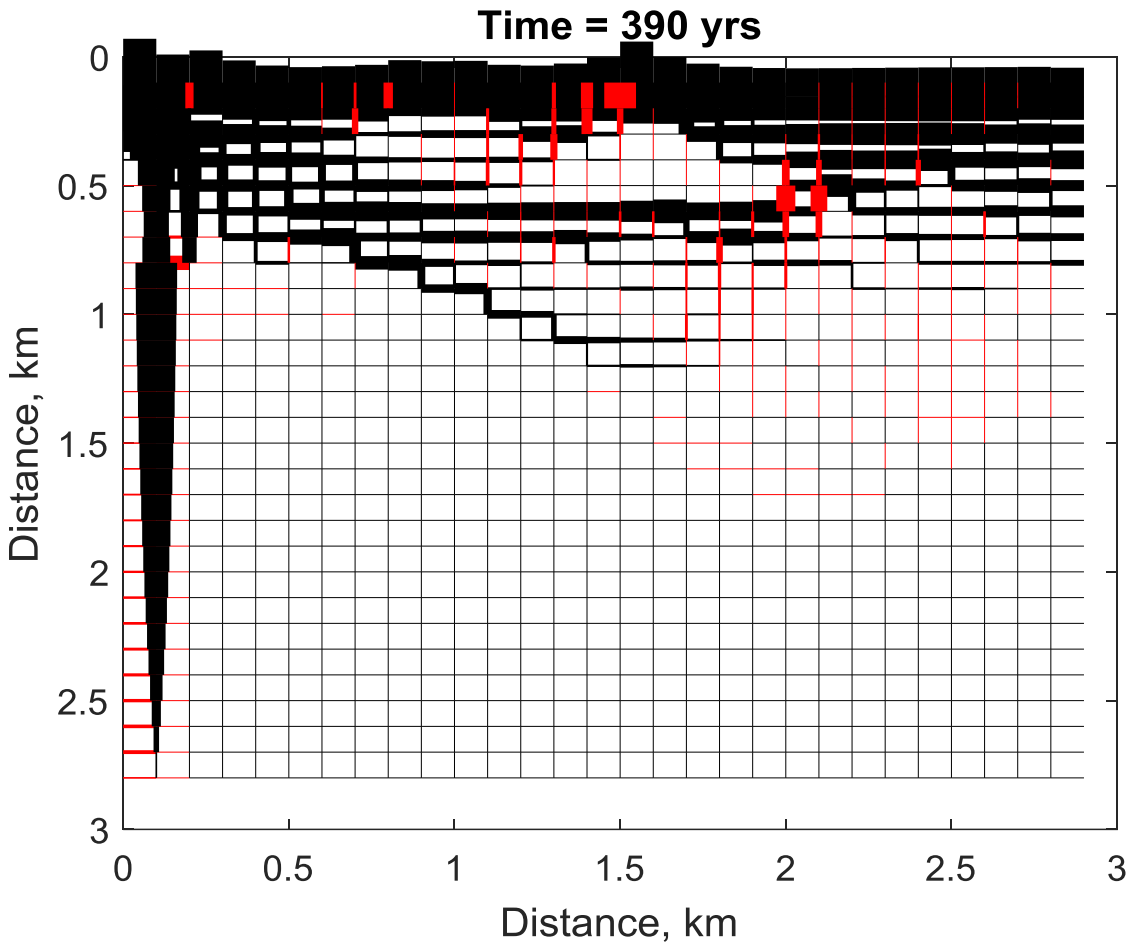

Figure 28 – Flow rate thickness at the end of simulation. Thinner and thicker segments indicate smaller and larger flow rates respectively. The black color indicates the positive direction (right and down directions), whereas the red color indicates the negative direction (left and up directions).

5.4 Conclusion

As a case study, a karst conduit network evolution model was applied to the Silver Springs springshed in central Florida. Using observed well data on potentiometric head, a head field was constructed via kriging which was used as the basis for conduit network evolution. The applied head field, along with initial assumptions on aquifer chemistry and fracture geometry, resulted in a unique realization of an early karst conduit network. From here, preferential flow patterns began to emerge, and flow patterns were slowly defined. Interestingly, the studied potentiometric head field evolved in such a way that induced flow to change directions, which is a key aspect to monitor in karst network simulation. As discussed, these changes may have certain implications on karst aquifers. Nutrient loading could infiltrate into springs, contaminating groundwater. Temporal climate changes can further instigate backflow into karst conduit networks, potentially adding additional nutrient loadings into aquifers, which would be adverse for ecosystems.

For an area such as central Florida that is susceptible to both sinkhole formations and anthropogenic activities (i.e., groundwater withdrawals), a sound understanding of the interaction of aquifer hydraulics and chemistry, and also local climate processes is essential for maintaining water quality and resources.

CHAPER 6: CONCLUSION

6.1 General conclusions

Karst systems in Florida is unique to its hydraulic and chemistry properties pertaining to the Floridan aquifer, and one can see how important it is to understand the nature of the Floridan aquifer from a hydrologic and chemistry standpoint in order to accurately understand and model processes such as contaminant transport, and karst dissolution. Given that Florida is subjected to sinkholes (Figure 1), an accurate understanding of aquifer properties, as well as knowledge of adsorption capacity of certain minerals as a potential pollutant adsorbent (Jambor and Dutrizac, 1998; Sajih et al., 2014, Sandhu et al., 2018), can pave the way towards modeling contaminant transport and determining implications to drinking water quality. The adsorption process shows potential in reducing radioactivity levels in contaminant plumes; however it may not be always efficient, depending on geographic setting, for instance. More adsorption data for several minerals may lead to improved models and observations regarding plume transport, as well as decision making.

The presence of karst aquifers may influence physical processes, such as solute transport, differently. To improve knowledge of karst dissolution in natural aquifers, karst dissolution models, based on dissolution concepts and experiments obtained from eariler studies (Dreybrodt, 1990; Palmer, 1991) can effectively model flow patterns and conduit profile changes as a function of time. Moreover, karst dissolution models can simulate changes in hydraulic head over time, and conduit ages can be extracted based on head profiles for certain fractures. This karst model was applied to the Silver Springs basin in Florida, and was able to reproduce head

profiles for extracted fractures mapped out in previous studies (Vernon, 1951; Florea and Vacher, 2006a) better than models assuming one-dimensional groundwater flow with leakage. Interestingly, the karst model predicted conduit ages that were for the most part reasonable to prior reports of aquifer age in the Silver Springs region (40 Myrs). Moreover, flow rates show increases over time, due to continuous dissolution. This implies that at some point, although it may take some time, flow rates would eventually become turbulent and may adversely affect natural processes. Although observations are specific to hydrologic basins, such as Silver Springs, this type of analysis can be applied in any natural setting, which may lead to unique, but meaningful results.

In fact, karst dissolution is governed by several parameters, making this physical process complex and dynamic. Calcium aggressive water reacts with the limestone rock, causing it to dissolve as water flows through fractures in aquifers. Water continues to dissolve the limestone rock until it is saturated, in doing so causing the fracture to grow in size, especially at the fracture entrance. This induces flow rates to increase, which then drive the dissolution process again. This feedback mechanism shows the strong linkage between chemistry dissolution and hydraulic flow patterns that govern karst evolution.

Furthermore, most individual parameters show a power law behavior with breakthrough time, suggesting some influence in the overall process. Notably, the initial conduit size (i.e., diameter) has the most influence out of the parameters tested on karst dissolution, while the kinetic rate and the diffusion coefficient did not appear to show some influence. It has also been observed that some parameters are directly and inversely proportional to breakthrough time. Results are consistent with prior simulations and can certainly improve knowledge of karst

features as better decision making and overall water resources management continues to be refined.

A case study was carried out on simulating karst conduit network evolution, based on observed potentiometric head well data. Here, the head field domain, as well as the initial conditions on aquifer chemistry and fracture geometry resulted in an emerging karst conduit network. Potentiometric head values monitored over time suggest conduit flow rates change in downslope direction. Characterizing the conduit evolution also revealed preferential flow paths, which show similar behavior with the flow rate values. From the results, backflow in conduits occurs, which could have implications on karst aquifers. An improved understanding of karst network generation and basin climate can contribute to better management of water resources.

6.2 Future research

As an extension to this research, simulating contaminant migration in the presence of both conduits and soil rock would be interesting to explore if the migration would travel further distances in less time, as opposed to assuming homogenous soil conditions. Perhaps this could be a more accurate way of characterizing plume migrations.

In addition, the karst evolution model could be expanded to simulate both laminar and turbulent flow. For added complexity, using a triangular irregular network (TIN) to represent conduits oriented in different directions could be employed to simulate network evolution. At the same time, processes such as recharge and infiltration can be incorporated with the model. The network evolution can then be further studied to observe its response to different natural processes and settings.

LIST OF REFERENCES

Abed-Elmdoust, A., Miri, M.-A., and Singh, A. (2016), Reorganization of river networks under changing spatiotemporal precipitation patterns: An optimal channel network approach. *Water Resour. Res.* 52(11), 8845-8860. doi:10.1002/2015WR018391.

Abed-Elmdoust, A., Singh, A., and Yang, Z. L. (2017), Emergent spectral properties of river network topology: an optimal channel network approach. *Nat. Sci. Rep.* 7(1), 11486.

Almeida, R. M. R., Lauria, D. C., Ferreira, A. C., and Sracek, O. (2004), Groundwater radon, radium and uranium concentration in Região dos Lagos, Rio de Janeiro State, Brazil. *J. Environ. Radioactiv.* 73, 323-334.

Andre, B. J., and Rajaram, H. (2005), Dissolution of limestone fractures by cooling waters: Early development of hypogene karst systems. *Water Resour. Res.* 41, W01015.

Appelo, C. A. J., and Postma, D. (2015), *Geochemistry, groundwater and pollution*. CRC Press.

Ardaman and Associates, Inc. (AAI) (2017), Zone of Capture Evaluation – Second Update, Consent Order OGC No. 16-1356, New Wales Phosphogypsum Stack System, Mosaic Fertilizer, LLC, Polk County, Florida. Report, File Number 16-13-0122A.

Baird, R. B., Easton A. D. and Rice, E. W. (2017), *Standard Methods for Examination of Water and Wastewater*. American Public Health Assn.

Burnett, W. C., and Elzerman, A. W. (2001), Nuclide migration and the environmental radiochemistry of Florida phosphogypsum. *J. Environ. Radioactiv.* 54, 27-51.

Chen, M. A., and Kocar, B. D. (2018), Radium sorption to iron (hydr)oxides, pyrite, and montmorillonite: implications for mobility. *Environ. Sci. Technol.* 52, 4023-4030.

Clemens, T., Huckinghaus, D., Sauter, M., Liedl, R., and Teutsch, G. (1996), A combined continuum and discrete network reactive transport model for the simulation of karst development. *Calibration and Reliability in Groundwater Modelling*, IAHS Publication, no. 237. IAHS, Colorado, 309-318.

Clifford, D., Vijjeswarapu, W., and Subramonian, S. (1988), Evaluating various adsorbents and membranes for removing radium from groundwater. *J. Am. Water Works Ass.* 80(4), 94-104.

Cross, H. (1936), Analysis of flow in networks of conduits or conductors. University of Illinois Bulletin, 286.

Dausmann, A. M., Doherty, J., Langevin, C. D., and Dixon, J. (2010), Hypothesis testing of buoyant plume migration using a highly parameterized variable-density groundwater model at a site in Florida, USA. *Hydrogeol J*. 18, 147-160.

de Rooij, R., and Graham, W. (2017), Generation of complex karstic conduit networks with a hydrochemical model. *Water Resour. Res.* 53(8), 6993-7011.

Dreybrodt, W. (1990), The role of dissolution kinetics in the development of karst aquifers in limestone: A model simulation of karst evolution. *J. Geol.* 98(5), 639-655.

Dreybrodt, W. (1996), Principles of early development of karst conduits under natural and man-made conditions revealed by mathematical analysis of numerical models. *Water Resour. Res.* 32(9), 2923-2935.

Dreybrodt, W., and Gabrovsek, F. (2000), Dynamics of the evolution of a single karst conduit. In: *Speleogenesis: Evolution of karst aquifers.* Hunstville: Natl. Speleol. Soc., 184-193.

Dreybrodt, W., and Gabrovsek, F. (2003), Basic processes and mechanisms governing the evolution of karst. *Speleogenesis and Evolution of Karst Aquifers*, 1(1), 1-26.

Dzombak, D. A., and Morel, F. M. M. (1990), *Surface complexation modeling: Hydrous Ferric Oxide*. Wiley-Interscience.

Floir. (2010), Review of the 2010 sinkhole data call. Florida Office of Insurance Regulation.

Florea, L. J., and Vacher, H. L. (2006a), Morphologic features of conduits and aquifer response in the unconfined Floridan Aquifer System, West Central Florida, *The 12th Symposium on the Geology of the Bahamas and other Carbonate Regions*. 32-44.

Florea, L. J., and Vacher, H. L. (2006b), Springflow Hydrographs: Eogenetic vs. Telogenetic Karst. Groundwater, 44(3), 352-361.

Florea, L. J., and Vacher, H. L. (2007), Eogenetic karst hydrology: Insights from the 2004 hurricanes, peninsular Florida. *Groundwater*, 45(4), 439-446.

Florea, L. J., Budd, D. A., and Brinkman, R. B. (2009), Caves and karst of West-Central Florida. *Caves and Karst of America*, 189-196.

Florea, L. J., Hashimoto, T., Kelley, K. Miller, D., and Mrykalo, R. (2003), Karst geomorphology and relation to the phreatic surface: Briar Cave, Marion County, Florida. *Karst Stud. West Cent. Fla.* 1, 9-19.

Florida Department of Environmental Protection. (2017), New Wales Process Water Characteristics, Active Stack (2003-2011): Supporting Wastewater Permit Application Tabulation. Lake Wales, FL.

Ford, D. C., and Williams, P. W. (2007), *Karst Hydrogeology and Geomorphology*. (Wiley, Chichester).

Fuleihan, N. F., Cameron, J. E., and Henry, J. F. (1997), The hole story: How a sinkhole in a phosphogypsum pile was explored and remediated. In: Beck B. F., Stephenson J.B. (eds) Proceedings of the 6th multidisciplinary conference on sinkholes and the engineering and environmental impacts of karst, the engineering geology and hydrogeology of karst terranes. Balkema, Rotterdam, 363-369.

Gabrovsek, F. (2007), On denudations rates in karst. *Acta. Carsologica*. 36(1), 7-13.

Gelhar, L. (1986), Stochastic subsurface hydrology from theory to applications. *Water Resour. Res.* 22, 135S-145S.

Ghasemizadeh, R., Yu, X., Butscher, C., Padilla, I. Y. and Alshawabkeh, A. (2006), Improved regional groundwater flow modeling using drainage features: a case study of the central northern karst aquifer system of Puerto Rico (USA). Hydrogeol. J. 24, 1463-1478.

Gonneea, M. E., Charette, M. A., Liu, Q., Herrera-Silveira, J. A., and Morales-Ojeda, S. M. (2014), Trace element geochemistry of groundwater in a karst subterranean estuary (Yucatán Peninsula, México). *Geochim. Cosmochim. Ac.* 132, 31-49.

Groves, C. G., and Howard, A. D. (1994), Early development of karst systems 1. Preferential flow path enlargement under laminar flow. *Water Resour. Res.* 30(10), 2837-2846.

Grundl, T., and Cape, M. (2006), Geochemical factors controlling radium activity in a sandstone aquifer. *Groundwater*. 44, 518-527.

Gulley, J., Martin, J. B., Screation, E. J., and Moore, P. J. (2011), River reversals into karst springs: A model for cave enlargement in eogenetic karst aquifers. *Geol. Soc. Am. Bull.* 123 (3-4), 457-467. https://doi.org/10.1130/B30254.1.

Halley, R. B., Schmoker, J. W. (1983), High porosity Cenozoic rocks of South Florida: progressive loss of porosity with depth. *Am. Assoc. Petrol. Geol. Bull.* 67, 191-200.

Hanna, R. B., and Rajaram, H. (1998), Influence of aperture variability on dissolutional growth of fissures in karst formations. *Water Resour. Res.* 34(11), 2843-2853.

Hooshyar, M., Singh, A., and Wang, D. (2017), Hydrologic controls on junction angle of river networks. *Water Resour. Res.* 53(5), https://doi.org/10.1002/2016WR020267.

Hooshyar, M., Singh, A., and Wang, D. (2019), Interbasin and intrabasin competitions control drainage network density. *Geophys. Res. Lett.* 46, https://doi.org/10.1029/2018GL081020.

Howard, A. D., and Groves, C. G. (1995), Early development of karst systems 2. Turbulent flow. *Water Resour. Res.* 31(1), 19-26.

Hull, C. D. and Burnett, W. C. (1996), Radiochemistry of Florida phosphogypsum. *J. Environ. Radioactiv.* 32(3), 213-238.

Jambor, J. L., and Dutrizac, J. E. (1998), Occurrence and constitution of natural and synthetic ferrihydrite, a widespread iron oxyhydroxide, *Chem. Rev.* 98, 2549−2585.

Joigneaux, E. et al., (2011), Impact of climate change on groundwater point discharge: backflooding of karstic springs (Loiret, France), *Hydrol. Earth Syst. Sci.* 15, 2459-2470.

Jones, M. J. *et al.* (2011), Reactions of radium and barium with the surfaces of carbonates minerals. *Appl. Geochem.* 26, 1231-1238.

Kaufmann, G. (2009), Modelling karst geomorphology on different time scales. *Geomorphology*, 106, 62-77.

Kaufmann, G. (2016), Modelling karst aquifer evolution in fractured, porous rock. *J. Hydrol.* 543, 796-807.

Kaufmann, G., and Braun, J. (1999), Karst aquifer evolution in fractured rocks. *Water Resour. Res.* 35(11), 3223-3238.

Kaufmann, G., Gabrovsek, F., and Romanov, D. (2016), Deep conduit flow in karst aquifers revisited. *Water Resour. Res.* 50, 4821-4836.

Kitadinis, P. K. (1997), *Introduction to geostatistics: applications in hydrogeology*. (Cambridge University Press, Cambridge).

Kuniansky, E. L., Bellino J. C., and Dixon, J. F. (2012), Transmissivity of the Upper Florida aquifer in Florida and parts of Georgia, South Carolina, and Alabama. U.S. Geological Survey Scientific Investigations Map 3204.

Langmuir, D., and Reese, A. C. (1985), The thermodynamic properties of radium. *Geochim. Cosmochim. Ac.* 49, 1593-1601.

Langston, A. L., Screaton, E. J., Martin, J. B., and Bailly-Comte, V. (2012), Interactions of diffuse and focused allogenic recharge in an eogenetic karst aquifer (Florida, USA). *Hydrogeol. J.* 20, 767-781.

Lauria, D. C., Almeida, R. M. R., and Sracek, O. (2004), Behavior of radium, thorium and uranium in groundwater near the Buena Lagoon in the Coastal Zone of the State of Rio de Janeiro, Brazil. *Environ. Geol.* 47, 11-19.

Marella, R. L. (1999), Water withdrawls, use, discharge, and trends in Florida, 1995. *Water Resources Investigations Report* 99-4002.

Mays, L. W. (2011), *Water Resources Engineering*. (John Wiley, New Jersey).

McCartan, L., Duerr, A. D., and Hawkins, R. M. (1988), Magnesium-rich clay minerals in tertiary carbonate rocks of southwestern Florida. Proceedings, 1988 USGS Workshop on the Geology and Geohydrology of the Atlantic Coastal Plain. 121-128.

Miller, J. A. (1990), Ground Water Atlas of the United States: Segment 6, Alabama, Florida, Georgia, South Carolina. No. 730-G. US Geological Survey.

Miller, R. L., and Sutcliffe, H. (1985). Occurrence of natural radium-226 radioactivity in groundwater of Sarasota, County, Florida. *Water Resources Investigations Report* 84-4237.

Mishra, S. P., and Tiwary, D. (1999), Ion exchangers in radioactive waste management. Part XI. Removal of barium and strontium ions from aqueous solutions by hydrous ferric oxide, *Appl. Radiat. Isotopes.* 51, 359-366.

Moore, P. J., Martin. J. B., Screaton, E. J., and Neuhoff, P. S. (2010), Conduit enlargement in an eogenetic karst aquifer, *J. Hydrol.* 393, 143-155.

Myers, S. (2016), *Control of Metal-Release and Tuberculation in a Silica-Laden Groundwater Distribution System on the Volcanic Island of Lana'i*, Master's Thesis, University of Central Florida, Orlando, Florida.

Navarro, A., and Carbonell, M. (2008), Assessment of groundwater contamination caused by uncontrolled dumping in old gravel quarries in the Besòs aquifer (Barcelona, Spain). *Environ. Geochem. Hlth.* 30, 273-289.

Newton, J. G. (1986), Development of sinkholes resulting from man's activities in the eastern United States. *U.S. Geological Survey Circular* 968, 54 p.

Nitzsche, O., and Merkel, B. (1999), Reactive transport modeling of uranium 238 and radium 226 in groundwater of the Königstein uranium mine, Germany. *Hydrogeol. J.* 7, 423-430.

O'Donnell, C. (2016), Mosaic plant sinkhole dumps 215 million gallons of reprocessed water into Floridan Aquifer. *Tampa Bay Times.* *http://www.tampabay.com/news/environment/water/mosaic-plant-sinkhole-dumps-215-million-gallons-of-reprocessed-water-into/2293845*

Palmer, A. N. (1991), Origin and morphology of limestone caves, *Geol. Soc. Am. Bull.* 103, 1-21.

Pardo-Igúzquiza, E., Dowd, P. A., Xu, C., and Durán-Valsero, J. J. (2012), Stochastic simulation of karst conduit networks. *Adv. Water Resour.* 35, 141-150.

Parkhurst, D. L., and Appelo, C. A. J. (1999), User's guide to PHREEQC (Version 2): A computer program for speciation, batch-reaction, one-dimensional transport, and inverse geochemical calculations. *Water-Resources Investigations Report* 99-4529, 1-312.

Parkhurst, D. L. and Appelo, C. A. J. (2013), Description of input and examples for PHREEQC version 3—A computer program for speciation, batch-reaction, one-dimensional transport, and inverse geochemical calculations: *U.S. Geological Survey Techniques and Methods*, book 6, chap. A43, (497 p).

Perne, M., Convington, M., and Gabrovsek, F. (2014), Evolution of karst conduit networks in transition from pressurized flow to free-surface flow. *Hydrol. Earth Syst. Sc.* 18, 4617-4633.

Phelps, G. G. (1994), Hydrogeology, water quality, and potential for contamination of the upper Floridan aquifer in the Silver Springs ground-water basin, central Marion County, Florida, *Water-Resources Investigations Report 92-4159*.

Quinlan, E. et al., (2008), Primary producers and nutrient loading in Silver Springs, FL, USA, *Aquat. Bot.* 88, 247-255. doi:10.1016/j.aquabot.2007.11.003.

Rodríguez-Iturbe, I., and Rinaldo, A. (2001), *Fractal river basins: Chance and self-organization*. (Cambridge University Press, New York).

Romanov, D., Gabrovsek, F., and Dreybrodt, W. (2004), Modeling the evolution of karst aquifers and speleogenesis. The step from 1-dimensional to 2-dimensional modeling domains. *Speleogenesis and Evolution of Karst Aquifers*, 2(1), 1-26.

Ronayne, J. M. (2013), Influence of conduit network geometry on solute transport in karst aquifers with a permeable matrix. *Adv. Water Resour.* 56, 27-34.

Rutherford, P. M., Dudas, M. J., and Arocena, J. M. (1995), Radioactivity and elemental composition of phosphogypsum produced from three phosphate rock sources. *Waste Manage. Res.* 13, 407-423. https://doi.org/10.1016/S0734-242X(05)80021-7.

Rutherford, P. M., Dudas, M. J., and Samek, R. A. (1994), Environmental impacts of phosphogypsum. *Sci. Total Environ.* 149(1-2). 1-38.

Sajih, M. *et al.* (2014), Adsorption of radium and barium on goethite and ferrihydrite: A kinetic and surface complexation modelling study. *Geochim. Cosmochim. Ac.* 146, 150-163.

Sandhu, D., Singh, A., Fan, N., Wang, D., and Duranceau, S. (2016), Hydro-geomorphic response of Everglades to changing climate and anthropogenic activities. *J. Hydrol.* 543, 861-872.

Sandhu, D. et al., (2018), Fate and transport of radioactive gypsum stack water entering the Floridan aquifer due to a sinkhole collapse. *Sci. Rep.* 8, 11439.

SENES Consultants Limited. (1987), An analysis of the major environmental and health concerns of phosphogypsum tailings in Canada and methods for their reduction. The Ontario Ministry of the Environment, Alberta Environment, Canada.

Sepúlveda, N. (2009), Analysis of methods to estimate spring flows in a karst aquifer. *Groundwater*, 47(3), 337-349.

Shoemaker, W. B. *et al*. (2004), Comparison of estimated areas contributing recharge to selected springs in north-central Florida by using multiple ground-water flow models. US Geol. Surv. Open File Rep 03-448.

Shoemaker, W. B., Cunningham, K. J., Kuniansky, E. L., and Dixon, J. (2008), Effects of turbulence on hydraulic heads and parameter sensitivities in preferential groundwater flow layers. *Water Resour. Res.* 44, W03501. https://doi.org/10.1029/2007WR006601.

Siemers, J., and Dreybrodt, W. (1998), Early development of karst aquifers on percolation networks of fractures in limestone. *Water Resour. Res.* 34(3), 409-419.

Sinclair, W. C. (1982), Sinkhole development resulting from ground-water withdrawal in the Tampa area, Florida. *U.S. Geological Survey Water-Resources Investigations Report* 81-50, 19 p.

Spechler, R. M., and Kroening, S. E. (2007), Hydrology of Polk County, Florida. *Scientific Investigations Report* 2006-5320. https://doi.org/10.3133/sir20065320.

Swamee, P. K., and Swamee, N. (2007), Full-range pipe-flow equations. *J. Hydraul. Res.* 45(6), 841-843.

Swarzenski, P., Reich, C., Kroeger, K. D., and Baskaran, M. (2007), Ra and Rn isotopes as natural tracers of submarine groundwater discharge in Tampa Bay, Florida. *Mar. Chem.* 104, 69-84.

Szabo, Z., DePaul, V. T., Fischer, J. M., Kraemer, T. F., and Jacobsen, E. (2012), Occurrence and geochemistry of radium in water from principal drinking-water aquifer systems of the United States. *Appl. Geochem.* 27, 729-752.

Tahsin, S., Medeiros, S., and Singh, A. (2016), Resilience of coastal wetlands to extreme hydrologic events in Apalachicola Bay. *Geophys. Res. Lett.* 43, 7529-7537.

Tahsin, S., Medeiros, S., and Singh, A. (2018), Assessing the resilience of coastal wetlands to extreme hydrologic events using vegetation indices: A review. *Remote Sens.* 10(9), 1390. https://doi.org/10.3390/rs10091390.

Thyne, G. D. (2007), *PHREEQC S Course Manual*. (Science Based Solutions LLC).

Tihansky, A. (1999), Sinkholes, west-central Florida. Land subsidence in the United States: US Geological Survey Circular 1182, 121-140.

Turner, D. R. (1993), Mechanistic approaches to radionuclide sorption modeling. Center for Nuclear Waste Regulatory Analyses, San Antonio, Texas, USA.

Vernon, R. O. (1951), Geology of citrus and levy counties, Florida. Tallahassee, FL: Florida Geological Survey.

White, W. B. (2002), Karst hydrology: recent developments and open questions. Engineering Geology, 65, 85-105.

White, W. B. (2007), Groundwater flow in karstic aquifers. In: J.W., Delleur. *The Handbook of Groundwater Engineering*. (CRC Press, Boca Raton).

Williams, L. J., and Kuniansky, E. L. (2015), Revised hydrogeologic framework of the Floridan aquifer system in Florida and parts of Georgia, Alabama, and South Carolina. US. Geol. Surv. Prof. Pap., 1807.

Wilson, W. L., and Beck, B. F. (1992), Hydrogeologic Factors Affecting New Sinkhole Development in the Orlando Area, Florida. *Groundwater*, 30(6), 918-930. https://doi.org/10.1111/j.1745-6584.1992.tb01575.x.

Xu, Z., Bassett, S. W., Hu, B., and Dyer, S. B. (2016), Long distance seawater intrusion through a karst conduit network in the Woodville Karst Plain, Florida. *Sci. Rep.* 6, 32235

Yobbi, D. K. (1996), Simulation of subsurface storage and recovery of treated effluent injected in a saline aquifer, St. Petersburg, Florida. *Water-Resources Investigations Report*, 95-4271, 1-29.

Zhu, C., and Anderson, G. (2002), *Environmental Applications of Geochemical Modeling.* Cambridge University Press.

Zhu, C., Hu, F. Q., and Burden, D. S. (2001), Multi-component reactive transport modeling of natural attenuation of an acid groundwater plume at a uranium mill tailings site. *J. Contam. Hydrol.* 52, 85-108.